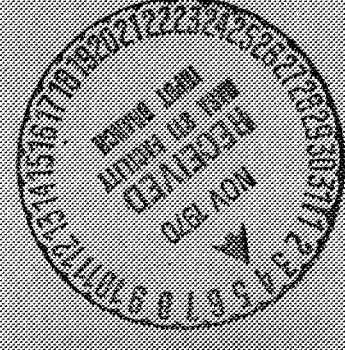
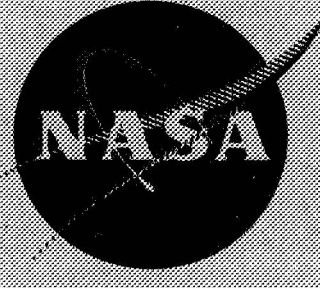


N70-18739

**CASE FILE
COPY**

**NASA CR-72600
UARL H910666-15**



KINETIC FLOW PERFORMANCE IN NOZZLES

**FINAL REPORT
December 5, 1969**

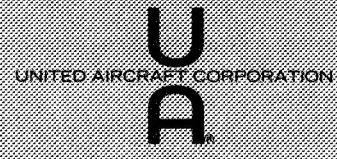
V.J. SARLI, L.S. BENDER, L.D. ACETO, and W.G. BURWELL

prepared for

NATIONAL AERONAUTICS AND SPACE ADMINISTRATION

CONTRACT NAS 3-11225

United Aircraft Research Laboratories



EAST HARTFORD, CONNECTICUT 06108

NOTICE

This report was prepared as an account of Government-sponsored work. Neither the United States, nor the National Aeronautics and Space Administration (NASA), nor any person acting on behalf of NASA:

- A.) Makes any warranty or representation, expressed or implied, with respect to the accuracy, completeness, or usefulness of the information contained in this report, or that the use of any information, apparatus, method, or process disclosed in this report may not infringe privately-owned rights; or
- B.) Assumes any liabilities with respect to the use of, or for damages resulting from the use of, any information, apparatus, method or process disclosed in this report.

As used above, "person acting on behalf of NASA" includes any employee, or contractor of NASA, or employee of such contractor, to the extent that such employee or contractor of NASA, or employee of such contractor prepares, disseminates, or provides access to any information pursuant to his employment or contract with NASA, or his employment with such contractor.

Requests for copies of this report should be referred to

National Aeronautics and Space Administration
Scientific and Technical Information Facility
P. O. Box 33
College Park, Maryland 20740

**NASA CR-72600
UARL H910666-15**

FINAL REPORT

KINETIC FLOW PERFORMANCE IN NOZZLES

by

V.J. SARLI, L.S. BENDER, L.D. ACETO, and W.G. BURWELL

United Aircraft Research Laboratories



EAST HARTFORD, CONNECTICUT 06108

prepared for

NATIONAL AERONAUTICS AND SPACE ADMINISTRATION

December 5, 1969

CONTRACT NAS 3-11225

**NASA Lewis Research Center
Cleveland, Ohio
P. N. Herr, Project Manager
Advanced Rocket Technology Branch**

FOREWORD

This work was performed by United Aircraft Research Laboratories for the National Aeronautics and Space Administration under Contract NAS 3-11225 initiated June 6, 1968.

Included among those who cooperated in performance of the work under Contract NAS 3-11225 were Dr. V. J. Sarli, Program Manager; Dr. W. G. Burwell, Chief, Kinetics and Thermal Sciences Section, Mr. L. S. Bender and Mr. R. Roback of the UARL and Mr. T. F. Zupnik and Mr. L. Aceto, Scientific Staff of Pratt & Whitney Aircraft Division of United Aircraft Corporation.

This work was conducted under program management of the NASA Lewis Research Center, Cleveland, Ohio, and the Project Manager was Mr. P. N. Herr.

This document was unclassified in its entirety.

ABSTRACT

Kinetic Flow Performance in Nozzles

by

V. J. Sarli, L. S. Bender,
L. D. Aceto and W. G. Burwell

Analytical investigations have been performed with the primary objectives of correlating experimental engine performance data for four space-storable propellant combinations, $\text{CH}_4\text{-Flox}$, $\text{CH}_4\text{-OF}_2$, $\text{B}_2\text{H}_6\text{-OF}_2$ and $\text{B}_2\text{H}_6\text{-Flox}$; determining the deliverable performance of the tripropellant combination, $\text{H}_2\text{-F}_2\text{-Li}$; and assembling existing kinetic performance calculation procedures into a handbook for the propulsion engineer and vehicle designer to use. Summarized in this report are correlations of analytically-predicted and experimentally-measured engine performance results for the four space-storable propellant combinations and preliminary estimates of possible performance losses associated with two-phase, nonequilibrium nozzle flow of the combustion products of the tripropellant combination, $\text{H}_2\text{-F}_2\text{-Li}$. Presented in a separate document entitled "NASA Kinetic Performance Handbook" are self-consistent kinetic performance and aerodynamic degradation charts to permit rapid evaluation of deliverable performance for four propellant combinations, $\text{H}_2\text{-F}_2$, $\text{H}_2\text{-O}_2$, Aerozine 50- N_2O_4 and $\text{CH}_4\text{-Flox}$, over a wide range of operating conditions and for different nozzle geometries and engine sizes.

KINETIC FLOW PERFORMANCE IN NOZZLES

Final Report
 June 6, 1968 - December 5, 1969
 Contract NAS 3-11225

TABLE OF CONTENTS

	<u>Page</u>
SUMMARY	1
CONCLUSIONS	3
INTRODUCTION	5
BACKGROUND INFORMATION - SUMMARY OF PREVIOUS RELATED EFFECTS	7
SPACE-STORABLE PERFORMANCE DATA CORRELATION	9
Space-Storable Nozzle Test Data	10
Performance Analysis	13
Comparison of Calculated and Delivered Performance	18
KINETIC PERFORMANCE CHARTS	19
TRIPROPELLANT PERFORMANCE ANALYSIS	21
Equilibrium Thermodynamics	21
Chemical Kinetic Loss	25
Change of Phase Loss	25
Divergence Loss	27
Viscous Boundary Layer Loss	27
Net Loss and Calculated Predicted Performance	27
REFERENCES	29
LIST OF SYMBOLS	32
APPENDIX - DISTRIBUTION LIST	33
TABLES (2)	43-44
FIGURES	

KINETIC FLOW PERFORMANCE IN NOZZLES

Final Report
June 6, 1968 - December 5, 1969
Contract NAS 3-11225

SUMMARY

Analytical investigations performed during the first year of effort under Contract NAS 3-11225 are described in this report. These investigations have been directed primarily toward correlating engine test data for four space-storable propellant combinations, estimating the deliverable performance of the tripropellant combination, H_2-F_2-Li , and assembling existing kinetic performance calculation procedures into a handbook for the propulsion engineer and vehicle designer to use.

Direct comparisons are presented of analytically-predicted and experimentally-measured performance results for the CH_4-Flox , CH_4-OF_2 , $B_2H_6-OF_2$ and B_2H_6-Flox propellant combinations. The data cover a wide range of mixture stoichiometries and include operations at nominal combustion chamber pressures of 50 and 100 psia with four conical and bell nozzle configurations. These data were obtained from experimental rocket engine test firings performed at the P&WA Florida Research and Development Center, under Contract NAS 3-10294, and by the Rocketdyne Division of North American Rockwell under Contract NASw-1229. Generally successful correlation of these data has been achieved when accounting was made of losses due to boundary layer friction, heat transfer, divergence, transonic region flow nonuniformities, combustion inefficiency, and the lack of chemical recombination during nozzle expansion. The correlations point out, however, that uncertainties associated with the performance of the injector/combustor combination are reflected and amplified in terms of the nozzle performance and that systematic errors may be prevalent in the reported engine performance data. Of additional importance has been the need to establish effective reaction mechanisms and rate constants to provide a consistent fit of experimental data throughout the mixture ratio and chamber pressure ranges.

Analytical results are also presented to characterize the aerodynamic and kinetic losses and to estimate the net performance of the H_2-F_2-Li tripropellant combination for wide ranges of operating conditions. This tripropellant combination has, in addition to the common aerodynamic and chemical kinetic losses, potential losses attributable to finite-rate condensation and the lack of equilibration between the gaseous, liquid and solid phases of one of the primary combustion products, lithium fluoride. The analysis developed to handle these processes provides for the

separation of the loss mechanisms and computation of each loss parametrically as a function of combustion chamber operating variables, mixture stoichiometry, and nozzle area ratio. The dominant loss mechanisms are found to be due to finite-rate chemistry and condensation. However, under some conditions the additional two-phase losses may become substantial. The condensation losses, as presented are conservative, and indications are they may be significantly less depending upon the actual rate of nucleation in the expanding nozzle flow.

A brief discussion is also made herein of existing kinetic performance calculation procedures which can be employed to provide a rapid estimate of the deliverable performance of high energy liquid propellant systems over wide ranges of operating conditions, nozzle geometries and engine sizes. The compilation of these procedures in the form of charts to permit interpolation of aerodynamic and kinetic performance losses for the H_2-F_2 , H_2-O_2 , Aerozine 50- N_2O_4 and CH_4 -Flox propellant combinations appears in a separate document entitled "NASA Kinetic Performance Handbook". The information in this document allows estimations of deliverable performance of each propellant combination to be made as a function of chamber pressure, oxidizer-fuel ratio, engine thrust, nozzle exit area ratio, nozzle contour and reaction rate constants pertinent to that combination. The procedures and kinetic rate data employed to make these estimates are consistent with those recommended by the ICRPG Performance Standardization Working Group.

CONCLUSIONS

1. Effective reaction mechanisms have been established to permit analysis of the nonequilibrium expansion of the combustion products from four space-storable propellant combinations: methane-flox, methane-oxygen difluoride, diborane-flox and diborane-oxygen difluoride.
2. Analytical procedures developed to correlate hydrogen-fluorine-rocket engine test data can be extended to predict and extrapolate the deliverable performance of space-storable propellant combinations.
3. Correlation of a large body of rocket engine test data for the above-mentioned space-storable propellant combinations has been achieved. Agreement between predicted and measured performance results was within $\pm 2.0\%$ for approximately 80% of the available engine test data. This agreement is somewhat less favorable than was the case for the correlation of hydrogen-fluorine engine test data previously analyzed by this Contractor.
4. Combustion efficiency and heat transfer effects for the space-storable propellants considered herein are most appropriately established by empirical means, as was the case for the hydrogen-fluorine propellant system.
5. Correlations to establish the effective combustion efficiencies associated with engine tests of the above-mentioned space-storable propellants are quite similar to those developed for the hydrogen-fluorine propellant system, again suggesting that a significant interdependence exists between apparent combustion chamber inefficiencies and nozzle performance degradations.
6. Most noticeable disagreement between predicted and measured performance results occurs at low oxidizer-fuel ratios for the four space-storable propellants investigated, as was the case with hydrogen-fluorine results. Generally, for low oxidizer-fuel ratios, the measured engine performance was higher than could reasonably be predicted from theoretical considerations.
7. Simplified performance charts can be used to estimate the deliverable performance of high-energy liquid rocket propellants over wide ranges of operating conditions and configurations within $\pm 1\%$ relative to results from accepted standard machine calculation procedures. Compilations of such charts for the H_2-O_2 , H_2-F_2 , CH_4 -Flox (82.6% F_2) and Aerozine 50- N_2O_4 propellants combinations are included in a separate document entitled "NASA Kinetic Performance Handbook".
8. Significant performance losses may appear in engine tests involving the cryogenic tripropellant, hydrogen-fluorine-lithium. Aside from possible combustion inefficiencies, these losses may derive primarily from an inability to form gaseous lithium fluoride and/or the lack of equilibrium condensation of liquid lithium fluoride in the expansion nozzle.

9. Considerable uncertainty exists in the kinetic data required to establish the rate of formation of gaseous lithium and the rate of nucleation of liquid lithium fluoride.
10. Two-phase flow losses due to thermal or velocity disequilibrium between the gaseous, liquid and solid phases of lithium fluoride do not appear to be of sizable magnitude at the anticipated operating conditions of the cryogenic tripropellant system.

INTRODUCTION

Categorically, space-storable propellants such as methane-flox (CH_4 -Flox) and diborane-oxygen difluoride (B_2H_6 - OF_2) are of increasing interest in the future mission planning of NASA, while high energy cryogenic combinations such as hydrogen-oxygen (H_2 - O_2) and hydrogen-fluoride (H_2 - F_2) continue to be of importance. The characteristics of the space storables which contribute to the potential operational advantages of these propellants include (1) space storability using only insulating materials and heat shields, (2) ease of handling, (3) potential high I_{sp} performance, (4) high density, and (5) hypergolic ignition. The types of fuels which fall into the family of long term space storables include the low molecular weight-hydrocarbons, - - e.g., methane (CH_4), propane (C_3H_8), butene - 1 (C_4H_8) - - hydrazine (N_2H_4) and the reactive compound, diborane (B_2H_6). The oxidizers being considered for use with these fuels include fluorine, fluorine-oxygen mixtures (flox) and the compound, oxygen difluoride (OF_2). Comparisons of the maximum theoretical performance of various combinations of the space-storable systems with the common cryogenic systems (H_2 - O_2 and H_2 - F_2) are given in Ref. 1 for limited range of variables - - viz. a chamber pressure near 100 psia ($6.895 \times 10^5 \text{ N/m}^2$) and expansion ratio of 40. These comparisons indicate that space storables fall generally within the performance range of 380 to 435 seconds (3727 to 4266 N-sec/kg) in contrast to the 450 to 475 second range (4410 to 4655 N-sec/kg) of the common cryogenics.

Whereas the performance of the more energetic H_2 - F_2 cryogenic combination was demonstrated some time ago (e.g. Refs. 2 and 3) and accurate predictions have been made of H_2 - F_2 engine performance over wide ranges of operating conditions (Ref.4), experimental programs are only now establishing (Refs. 5, 6 and 7) the performance capability of several attractive space-storable combinations, including CH_4 -Flox (Contract NAS 3-10294 and NASw-1229) and B_2H_6 - OF_2 (Contract NASw-1229). In addition, mission studies directed toward defining the performance potential of systems employing these propellants are also currently in progress (e.g. Ref. 8) and should be helpful in selecting the most appropriate combination for any particular application. However, neither the experimental programs nor the systems studies have shown that the deliverable performance of space-storable propellants can be predicted accurately or extrapolated to conditions or configurations other than those employed in the limited test programs.

Previous experience by this Contractor (Refs. 4, 9 and 10) has indicated that reliable prediction of nonequilibrium performance can be made, provided that accurate and complete kinetic data are available and that appropriate accounting can be made of influences imposed by inefficient combustion and nozzle aerodynamics. Specifically, under Contract NASw-1293, a methodology and refined techniques were established for predicting, correlating and extrapolating the performance of high energy liquid propellant combinations including space-storable combinations. It is in consequence of this work that the analytical investigation described herein was undertaken to

correlate experimental engine performance data for the four most extensively studied space-storable propellant combinations, $\text{CH}_4\text{-Flox}$, $\text{CH}_4\text{-OF}_2$, $\text{B}_2\text{H}_6\text{-OF}_2$ and $\text{B}_2\text{H}_6\text{-Flox}$; to estimate the deliverable performance of the cryogenic tripropellant combination, $\text{H}_2\text{-F}_2\text{-Li}$; and to assemble existing simplified kinetic performance calculation procedures into a handbook for the propulsion engineer and vehicle designer to use.

BACKGROUND INFORMATION - SUMMARY OF PREVIOUS RELATED EFFORTS

The United Aircraft Research Laboratories was selected under Contracts NASw-366, NAS 3-2572, NASw-1293 and NAS 3-11225 to investigate nonequilibrium flow processes in high expansion ratio nozzles and to develop improved techniques for predicting the performance of rocket engines utilizing high energy space-storable propellants. A variety of nonequilibrium processes were investigated for a number of propellant combinations under Contract NASw-366, and it was confirmed that nonequilibrium chemistry would be a significant factor in limiting the theoretical performance of all the propellants considered at typical rocket conditions.

Three machine computational programs were developed in connection with Contract NASw-366 to treat nonequilibrium flows of reacting gas mixtures in both one-dimensional and two-dimensional or axisymmetric exhaust nozzles. The machine programs for constructing two-dimensional or axisymmetric flows with finite chemical kinetics consist of a "performance deck" which can be used to evaluate the performance of a prescribed nozzle contour and a "design deck" which can be used in the determination of an optimum nozzle contour. The studies reported under Contract NASw-366 demonstrated that the one-dimensional and two-dimensional machine computation programs for reactive gas flows can predict experimental measurements of nozzle flow properties when the kinetics of the reactions occurring in the system are known.

Contract NAS3-2572 was undertaken as a follow-on effort to Contract NASw-366 and involved the application of the machine computation programs mentioned above to investigate selected problems associated with chemical nonequilibrium nozzle flows. These problems included establishment of the sensitivity of performance to reaction rates and nozzle scale. A primary result of this investigation was a demonstration of the extreme importance of particular 3-body recombination reactions, such as $H + H + M \rightleftharpoons H_2 + M$, in limiting H_2-O_2 and Aerozine 50- N_2O_4 system performance. In addition, the feasibility of employing a "modified" sudden-freezing analysis to calculate nonequilibrium nozzle performance was also demonstrated.

Under Contract NASw-1293 an investigation was performed to determine the effect of chemical nonequilibrium flow on the performance of H_2-F_2 rocket nozzles and to correlate a variety of H_2-F_2 engine test data obtained by NASA, the Rocketdyne Division of NAA and the P&WA Florida Research and Development Center. Specifically, the work included (a) establishment of a realistic recombination mechanism applicable to the combustion products of H_2-F_2 , (b) determination of reaction rate constants for this mechanism based on data appearing in the literature and on theoretical calculations carried out by this Contractor, (c) parametric calculations to indicate the effects of individual reactions on overall performance for a range of oxidizer-fuel ratios at two combustion chamber pressures, (d) analysis of engine test data obtained in several different engine/nozzle configurations operated at four pressure levels between $P_c = 50$ psia and $P_c = 300$ psia over a range of mixture ratios, and (e) calculations

of the effects of nozzle scale and configuration and combustion inefficiency on H_2-F_2 engine performance. Generally successful correlation of these data was achieved when accounting was made of losses due to boundary layer friction, divergence, transonic region flow nonuniformities, combustion inefficiency, heat transfer and the lack of chemical recombination during nozzle expansion. The correlations point out, however, that inefficient injector/combustor performance can substantially alter the thrust developed in any particular nozzle, thereby introducing a variable uncertainty in theoretical predictions made without consideration of the performance of the associated combustion system. In addition, these correlations pointed out that uncertainties may also arise due to systematic errors prevalent in reported engine performance data. Such uncertainties may be as great as 2 percent and were observed in a substantial block of test data acquired during early phases of the Rocketdyne test program.

The correlation of experimental and analytical performance results led to the establishment of a kinetic mechanism and reaction rate data for analytical investigations of the H_2-F_2 propellant system such as studies of the effect of nozzle scale and contour on performance. These studies indicated that well-defined optimum conical and contoured (i.e. truncated perfect) nozzles are not established when consideration is given to performance penalties associated only with nonequilibrium and aerodynamic effects during nozzle expansion. Some additional parameter related to the mission requirement imposed on the engine, (e.g. stage velocity increment) must be specified in order to obtain well-defined optimum contoured and conical nozzles.

Under Contract NAS 3-11225, analytical investigations have been performed with the primary objectives of correlating experimental engine performance data for four space storable propellant combinations, CH_4-Flox , CH_4-OF_2 , $B_2H_6-OF_2$ and B_2H_6-Flox ; determining the deliverable performance of the tripropellant combination, H_2-F_2-Li ; and assembling existing kinetic performance calculation procedures into a handbook for the propulsion engineer and vehicle designer to use. Summarized in this report are correlations of analytically-predicted and experimentally-measured engine performance results for the four space storable propellant combinations and preliminary estimates of possible performance losses associated with two-phase, non-equilibrium nozzle flow of the combustion products of the tripropellant combination, H_2-F_2-Li . Presented in a separate document entitled "NASA Kinetic Performance Handbook" (NASA CR-72601) are kinetic performance and aerodynamic degradation charts to permit rapid evaluation of deliverable performance for four propellant combinations, H_2-F_2 , H_2-O_2 , Aerozine 50- N_2O_4 and CH_4-Flox , over a wide range of operating conditions and for different nozzle geometries and engine sizes.

SPACE-STORABLE PERFORMANCE DATA
CORRELATION

As has been stated previously, the most extensively studied space-storable propellant combinations are the CH_4 -Flox, CH_4 - OF_2 , B_2H_6 - OF_2 and B_2H_6 -Flox combinations (Refs. 6 and 7), although some engine data have been reported (Ref. 5) for C_3H_8 -Flox and C_4H_8 -Flox propellants. The test data obtained during each reported study were generated in a variety of engine configurations including uncooled, transpiration-cooled, and regeneratively-cooled thrust chambers. In the case of the Flox oxidizers, most testing was performed with an "optimized" mixture of fluorine and oxygen corresponding to that mixture which would provide the maximum theoretical shifting-equilibrium performance for the particular fuel being tested.

The delivered performance which can be achieved with a specific propellant combination in a rocket engine is considerably less than the theoretical performance based on shifting-equilibrium flow expansion. Therefore, in order to predict performance and correlate the delivered performance of the engine, a determination must be made of several "losses" encountered in testing, but not accounted for in theoretical, one-dimensional, shifting-equilibrium performance calculations. These losses include those due to combustion inefficiency, exit flow divergence, transonic region flow nonuniformity, external heat transfer and boundary layer friction as well as finite-rate nozzle recombination. The various losses can be calculated "a priori" (e.g. exit flow divergence) or can be measured experimentally (e.g. heat transfer) during engine tests.

The loss reported as combustion inefficiency from engine tests is established indirectly from measured and derived variables such as propellant weight flow and chamber pressure. During engine tests any degradation resulting from temperature variations or nonuniform distribution of oxidizer and fuel is not accountable using present test measurement techniques and its effect is, therefore, included as part of the derived combustion efficiency, i.e. characteristic velocity efficiency. However, the combustion efficiency utilized to establish the desired correlation of delivered performance and analytically-predicted performance is distinguished from the derived values in that the former is essentially an impulse efficiency determined from calculations which are dependent on reaction rate data used (i.e. the nonequilibrium loss calculated therefrom) and the accountable aerodynamic degradations. The resulting "effective" combustion efficiency is related to the derived values through a semi-empirical correlation. Such a correlation has been useful when a wide range of engine test data and operating conditions are available for the propellant system being considered (Ref. 4).

The nonequilibrium loss can only be calculated if reliable reaction kinetic data are available for the propellant combinations of interest. Such data are only partially available for the recombination reactions of $\text{CH}_4\text{-Flox}$, $\text{CH}_4\text{-OF}_2$, and $\text{B}_2\text{H}_6\text{-Flox}$, $\text{B}_2\text{H}_6\text{-OF}_2$. However, the data in the literature include most of the important reactions and some of third bodies necessary to be treated in nonequilibrium flow analysis. The important reactions are the hydrogen recombination, hydrogen-fluoride recombination and hydrogen-oxygen recombination reactions. Therefore, it is possible that the role which kinetics play in limiting engine/nozzle performance can be established by correlating the engine test data of the four mentioned propellant combinations with analytical results. Some adjustments in reaction rate constants and mechanism will be made to accommodate the range of test data so that, in the final analysis, the engine performance data influence strongly the extent that the rates are altered from theory or literature values. Previous experience with correlation of $\text{H}_2\text{-F}_2$ engine test data (Ref. 4) has indicated that the combustion inefficiency and recombination losses represent major sources of performance degradations, and care must be exercised to avoid assigning losses due to combustion inefficiency (or any unaccountable loss) to lack of recombination.

During the present investigation data for four space propellant combinations in four nozzle contours have been made available for correlation. The range of data should be sufficient to enable a partition for the nonequilibrium loss and loss due to combustion inefficiency. As in the correlation of $\text{H}_2\text{-F}_2$ engine test data (Ref. 4), the partition is performed by an iterative scheme based on adjustment of reaction rates and combustion inefficiency to yield a single correlation technique that results in minimum deviation between delivered performance from engine tests and analytically-predicted performance.

Space-Storable Nozzle Test Data

The performance data to be correlated consist of $\text{CH}_4\text{-Flox}$ (82.6% F_2) test results obtained by P&WA-FRDC under contract NAS 3-10294 (Ref. 6) and by Rocketdyne under contract NASw-1229 (Ref. 7). Additional performance data obtained by Rocketdyne include those for the space-storable combinations: $\text{CH}_4\text{-Flox}$ (70.4% F_2), $\text{CH}_4\text{-OF}_2$, $\text{B}_2\text{H}_6\text{-Flox}$ (70.4% F_2), $\text{B}_2\text{H}_6\text{-OF}_2$.

Methane Fuel Performance Data

A summary of $\text{CH}_4\text{-Flox}$ (82.6% F_2) delivered performance data from engine firings performed by P&WA-FRDC is presented in Figs. 1 and 2 and by Rocketdyne in Figs. 3 and 4. The engine test firings were performed at chamber pressures of 100 psia ($6.895 \times 10^5 \text{ N/m}^2$) utilizing two nozzle contours, a bell type and 15 deg conical nozzle. P&WA-FRDC utilized a modified RL-10 nozzle with an expansion area ratio of 40 in

contrast to the Rocketdyne 70 percent bell with an expansion area ratio of 60. The RL-10 nozzle contour is characterized by a sharp nozzle throat with a throat radius $r_t = 0.249$ ft (0.0759 m); the 70% bell includes a throat of small curvature, e.g. throat radius of curvature to throat radius, $r_c/r_t = 0.3905$, with throat radius, $r_t = 0.175$ ft (0.0533 m). Slight differences exist between the two 15 deg conical nozzles with the P&WA-FRDC nozzle characterized by a sharp-cornered throat and the Rocketdyne nozzle characterized by long throat, $r_c/r_t = 3.635$. The expansion area ratio and throat radius in each case is the same as that of the corresponding contoured nozzle. Also a triplet injector type was utilized for the performance data considered in this analysis.

Figures 1 and 2 illustrate the effect of O/F ratio on the delivered performance, (I_{sp}) vac, and the corresponding characteristic velocity efficiency derived from measured data obtained by FRDC in uncooled altitude engine firings. Also included in these figures for comparison are the maximum theoretical, one-dimension, shifting-equilibrium and frozen performance curves. Similar information is included in Figs. 3 and 4 from engine firings performed and reported by Rocketdyne. Although differences in results for the similar nozzle contours are small, major differences appear in the performance data reported for corresponding nozzle types in the two series of data, (e.g. compare results shown in Figs. 1 and 3, 2 and 4). The levels of delivered performance from Rocketdyne tests are higher than those from P&WA-FRDC engine tests by as much as 10 sec (98 N-sec/kg) near an O/F ratio of 5 and about 5 seconds (49 N-sec/kg) on average. The P&WA-FRDC data indicate a distinct drop in delivered performance and combustion efficiency with O/F ratio in contrast to the flat trend of the Rocketdyne data. Although the differences in performance level for each nozzle type are in part a direct result of the nozzle expansion ratios (A/A_{min} equal 40 for FRDC and 60 for Rocketdyne nozzles) and throat geometries, they are not consistent with the large differences in combustion efficiency reported for the altitude tests (98% vs 92%). Preliminary inspection indicates that P&WA-FRDC characteristic velocity efficiencies are low for the reported level of performance relative to the Rocketdyne data. This fact is supported in part by sea level test results obtained during the course of the FRDC engine tests in which case characteristic velocity efficiencies of 95% have been reported (Ref. 6).

The level of performance reported for the Rocketdyne 70% bell nozzle is similar to that reported for the 15 deg conical nozzle; cf. Figs. 3 and 4. The 70% bell performance is, however, unaccountably high in view of its sharp throat geometry relative to the long throat of the conical nozzle. That this is the case is shown in theoretical nonequilibrium flow calculations (to be discussed subsequently) and in comparisons of the data for the RL-10 contour and 15 deg conical nozzle of P&WA-FRDC; cf. Figs. 1 and 2.

Additional performance data have been obtained by Rocketdyne utilizing methane fuel and two other oxidizers: (1) a Flox mixture containing 70.4% fluorine, and (2) its composition equivalent, the chemical compound, OF_2 . The test firings were performed for the same conditions of pressure and range of O/F ratios as in the previous Rocketdyne engine firings. The nozzle configuration for the additional test series was that of the long-throat 15 deg conical nozzle. The variation of delivered performance and derived characteristic velocity efficiency with O/F ratio are illustrated in Figs. 5 and 6. On average the delivered performance for OF_2/CH_4 oxidizer fuel combination (Fig. 6) is slightly higher than that of the Flox (70.4% F_2)/ CH_4 combination (Fig. 5). The combination yielding the higher average performance is accompanied by correspondingly high characteristic velocity efficiency masking the conclusion that the higher performance is due solely to the differences in heat of formation between OF_2 and the equivalent composition Flox combination (Ref. 11). Analysis and correlation of the engine test performance and calculated delivered performance are presented in a subsequent section.

Diborane Fuel Performance Data

A summary of the B_2H_6 -Flox (70.4% F_2) and B_2H_6 - OF_2 engine test data from firings performed by Rocketdyne is presented in Figs. 7 through 11. Figures 7 through 11 illustrate the variation of delivered performance and characteristic velocity efficiency derived from engine test data for the 70% bell nozzle and long-throat 15 deg conical nozzle described in a previous section.

Preliminary comparison of these data indicates that the effect of nozzle contour on delivered performance is a noticeable one (cf. Figs. 7 and 8, Figs. 9 and 10). The delivered performance for each of the propellant combinations is slightly higher in the 15 deg conical nozzle. This is contrary to the Rocketdyne results reported for the CH_4 -Flox (82.6% F_2) combination for which the effect of nozzle contour did not appear (cf. Figs. 3 and 4). The higher level of performance for the 15 deg conical nozzle is a direct result of the long throat vs the sharper throat contour employed with the 70% bell.

Comparison of the delivered performance shown in Figs. 7 and 9 illustrates that no noticeable change in delivered performance occurs in the 15 deg conical nozzle as a result of using the compound OF_2 as oxidizer instead of the equivalent composition Flox mixture. However, a higher level of delivered performance is evident for the OF_2 oxidizer when the comparison is made for the results obtained in the 70% bell nozzle (cf. Figs. 8 and 10).

Additional test data for Flox (70.4% F_2) with the conical nozzle at a nominal chamber pressure of 50 psia ($3.448 \times 10^5 \text{ N/m}^2$) are illustrated in Fig. 11. At a given O/F ratio the delivered performance is distinctly less than the performance

illustrated in Fig. 7 for the higher pressure of 100 psia ($6.895 \times 10^5 \text{ N/m}^2$). The trend is consistent with theory.

Performance Analysis

The correlation of the engine test data with calculated performance requires that the several losses encountered in engine test data be established in order that the theoretical, one-dimensional, shifting-equilibrium performance can be appropriately degraded to permit direct comparison with the delivered performance. These losses include aerodynamic losses and kinetic losses. In addition, the individual performance data measurements must be corrected by the corresponding combustion inefficiency experienced during engine test. The aerodynamic losses which include effects due to exit flow divergence, wall friction, throat flow nonuniformities and heat transfer can be established using the techniques reported previously (Ref. 4) for the analysis and correlation of $\text{H}_2\text{-F}_2$ engine test data. Use of these techniques implies that the actual nonequilibrium flow process in a non-one-dimensional nozzle can be treated by separate analyses of the kinetics and divergence losses. During the course of the previous investigation (Ref. 4) calculations were performed to establish that the two-dimensional (axisymmetric) nonequilibrium performance can be accurately represented by the separate treatment of each loss. The investigation also indicated that the wall friction losses are sensitive to the gas model utilized (equilibrium-, nonequilibrium-, or frozen-flow). On the basis of the exhaustive analysis performed previously for the $\text{H}_2\text{-F}_2$ propellant combination, the two-dimensional frozen-flow gas model has been selected to establish frictional drag as well as divergence loss for the space-storable propellant combinations.

Aerodynamic Losses

The results of calculations of divergence and frictional drag losses for the propellants, nozzles, and pressure combinations are illustrated in Figs. 12 through 22. The divergence loss calculations are based on a comparison of calculated axisymmetric and one-dimensional frozen-flow performance and the frictional losses were calculated utilizing the boundary layer procedures developed by Bartz (Ref. 12) with the adiabatic wall option employing, as input information, axisymmetric frozen-flow properties.

In addition to the frictional drag and divergence losses, a small degradation in performance is experienced as a result of the convergent-transonic section loss which accounts for nonuniform transonic flow and for frictional drag loss in the subsonic portion of the nozzle. This loss amounts to approximately 0.5% of equilibrium performance and its calculations is discussed in the Ref. 4 report. The degradation in performance resulting from throat property nonuniformity and subsonic losses is indicated in the figures as the transonic loss (cf. Figs. 12 through 22).

The effect of heat transfer on performance for the appropriate propellant, nozzle and pressure combinations is also shown in Figs. 12-22. The performance losses correspond to the values derived from engine test data and were obtained directly from Ref. 6 for the P&WA-FRDC engine tests and Ref. 7 for the Rocketdyne engine test data.

Nonequilibrium Chemistry Loss

The one-dimensional, nonequilibrium chemistry loss associated with each propellant, nozzle and pressure combination can be calculated only if reliable reaction kinetic data are available for the mechanism which adequately describes the chemical processes taking place during the nozzle expansion. The reaction mechanism which describes fully these processes can become quite involved and complex if it is necessary to consider all the potential reactions between the species present. In a separate investigation of reaction mechanisms and rates performed for the Theoretical Methods Committee of the Interagency Chemical Rocket Propulsion Group (ICRPG) it has been shown that the B_2H_6 -Flox propellant combination involves at least sixteen (16) gaseous species and as many as fifty (50) reactions, while the CH_4 -Flox propellant combination involves at least twelve (12) species which can be related by twenty-three (23) reactions when all third bodies are considered as equally efficient in promoting recombination reactions (Ref. 13). The number of reactions is substantially higher if particular third-body efficiencies must be identified for the propellant combinations. Figures 23 through 26 illustrate some of the significant product species encountered in equilibrium analysis of CH_4 -Flox (82.6% F_2) and B_2H_6 - OF_2 propellant combination. The species are the same for Flox (70% F_2), Flox (82.6% F_2) and OF_2 oxidizers. Analyses performed during the course of this investigation have indicated that the reaction mechanism which describes the recombination of H_2 - F_2 combustion products represents the most important block of reactions for the CH_4 -Flox (82.6% F_2) propellant combination. This fact was also established in Ref. 1 with the additional probability that, at high O/F ratios, the water recombination reactions must also be considered as part of the energy recovery mechanism, especially as the oxygen content in the Flox mixture is increased (as, for example, in Flox (70% F_2)). For the B_2H_6 -Flox and OF_2 propellant combinations the reaction mechanism which describes the recombination of H_2 - O_2 combustion products represents the most important block of reactions.

The reactions contributing significantly to the recovery of energy during recombination processes are usually limited to three-body reactions. Many other reactions, such as bimolecular exchange reactions, occur in the full mechanism, but these can usually be neglected as secondary in establishing the nonequilibrium performance of the propellant combinations (Refs. 1, 4 and 13). Although the bimolecular reactions are important to the production of selected species for the three-body energetic reactions, their influence on propulsion performance is felt indirectly and only as long as the conditions are present in the nozzle for the three-body recombination reactions to occur at the minimum critical rate (i.e., the rate corresponding to "freezing" of the chemistry). With the view of reducing the mechanisms to a tolerable number of reactions it was concluded that only three-body reactions should be con-

sidered for the complex combination of species possible for the CH_4 and B_2H_6 fuels when combined with F_2 and O_2 bearing oxidizers. The mechanisms, therefore, have been limited to the principal recombination reactions:



where M represents significant 3rd bodies unique to the propellant combination. For the CH_4 -Flox ($-\text{OF}_2$) propellant combinations the third bodies include H, H_2 , HF, CO_2 , CO and H_2O . For B_2H_6 -Flox ($-\text{OF}_2$) propellant combinations the third bodies include H, H_2 , HF, BOF, BF and H_2O .

It should be pointed out that no provisions are included in the reaction mechanism for the possible condensation of carbon or boron oxide compounds or the direct reactions of carbon or boron containing species (e.g., CO or BO). It has been required during this investigation to limit the effort to the principal goal of correlating engine test data and this can be accomplished within the accuracy of the data by the 18 reaction system suggested above.

Table 1 summarizes the reaction rate constants of the recombination reactions that make up the mechanism for the CH_4 -Flox ($-\text{OF}_2$) and B_2H_6 -Flox ($-\text{OF}_2$) combustion products. The rate constants for the hydrogen and hydrogen-fluorine recombination reactions along with the third-body efficiencies of H, H_2 and HF are consistent with values appearing in the literature. These rates have been selected as representative of the most reliable data available at this time (Ref. 14 and 15).

The rates for the water recombination reaction:



have been established from analysis of the experiments of Schott and Bird (Ref. 16) along with the dependent hydrogen recombination rate:



as established in Ref. 14 (see, e.g., Ref. 17). The effect of H_2O as the third body for H_2O recombination reaction is about 20 times that of argon by comparison of the rate established from Ref. 17 and experimentally measured values in flame studies reported in Refs. 18 and 19.

The third-body efficiencies for H, H_2 , HF, CO_2 , CO, H_2O , BOF and BF relative to argon for reactions not cited in literature have been estimated, and have not been verified experimentally.

The CH_4 -Flox ($-\text{OF}_2$) and B_2H_6 -Flox ($-\text{OF}$) nonequilibrium losses based on the reaction rate constants of Table 1 for the engine test conditions and nozzle considered in this investigation are shown in Figs. 12-22 (kinetic loss). In actuality the nonequilibrium losses illustrated in Figs. 12-22 represent the results of several iterations between rates and combustion inefficiency (discussed below) to achieve the desired goal of correlation of engine test data with calculated performance results. These iterations have required the rates of Table 1 to be multiplied by the factor 2 in the final correlation. The performance losses computed in this section and illustrated in Figs. 12 to 22 as additive effects yield the predicted performance for each of the propellant combinations and the nozzle contours for the situation of 100 percent combustion efficiency.

Combustion Efficiency Correction

The combustion efficiency correction remains to be accounted for before a direct comparison of predicted and delivered performance can be achieved. The combustion efficiency correction cannot be determined "a priori" and, therefore, cannot be conveniently treated as a degradation factor across the oxidizer-fuel range, as were the aerodynamic and nonequilibrium performance losses.

It was pointed out previously that inconsistencies in delivered performance and combustion efficiency exist not only between the two sets of data as reported by Rocketdyne and FRDC, but also among the individual sets (e.g., the data from the Rocketdyne 15 deg conical and 70 percent bell nozzles). These inconsistencies have resulted in unsatisfactory direct correlation and comparison of the data; the differences in vacuum specific impulse performance, after accounting for aerodynamic and nonequilibrium degradation, do not correspond to the wide variations in the combustion efficiencies. A reasonable approach in such circumstances has been to estimate an effective combustion efficiency and to correlate it with the characteristic velocity efficiency established from measured data. This technique was successful in the correlation of H_2 - F_2 engine test data for which a large mass of data for a wide range of nozzle configurations and operating conditions was available from independent tests (Ref. 4). The technique allows effective averaging of the unaccountable losses for the engine tests and relates the loss to the apparent combustion efficiency (characteristic velocity efficiency) established from measured data.

The effective combustion efficiency for each CH_4 -Flox ($-\text{OF}_2$) and B_2H_6 -Flox ($-\text{OF}_2$) performance data point was evaluated after accounting for aerodynamic and nonequilibrium degradation from the difference between the analytically predicted performance with no combustor loss (Figs. 12 to 22) and the actual delivered performance (Figs. 1-12). This difference includes the degradation due to combustion inefficiency, as well as possible degradations resulting from striation of the oxidizer and fuel, condensation effects experienced in the nozzle and any other unaccountable

phenomena experienced in the real injector-combustor-nozzle system. The combination of these individual evaluations of effective combustion efficiency and combustion efficiency from measured data can be used to establish a smooth line correlation, so that a one-to-one relationship exists between the effective and measured efficiency values. The effective combustion efficiency is a combustion-induced impulse efficiency expressed as a fraction of the maximum theoretical (one-dimensional, shifting-equilibrium) vacuum specific impulse.

Figures 27 and 28 illustrate the comparison of effective combustion efficiency, η_c^{*E} , with the measured characteristic velocity efficiency, η_c^* , for the CH_4 -Flox ($-\text{OF}_2$) and B_2H_6 -Flox ($-\text{OF}_2$) combinations, respectively. The symbols refer to the individual data points reported from test firings for the propellant combinations and nozzle configurations as listed in each figure. It is apparent from Figs. 27 and 28 that some of the test points indicate an effective combustion efficiency in excess of 100%. These unreasonable values of efficiency are a direct result of the corresponding delivered performance values falling above the predicted values. Although this discrepancy can be eliminated by increasing the values of the predicted performance (e.g., by increasing the reaction rate constants), the overall correlation would be altered so that the desired comparison of predicted and measured performance would be degraded for a large number of data points and test series. The present B_2H_6 - OF_2 data available are treated as being equal in quality.

Figure 29 illustrates the comparison of effective combustion efficiency with the characteristic velocity efficiency established from measured data for both the CH_4 and B_2H_6 fuel systems being considered in this investigation. In each of Figs. 27, 28 and 29 a smooth line is shown which represents the mean variation of effective combustion efficiency, η_c^{*E} , with the experimentally evaluated characteristic velocity efficiency, η_c^* .

These figures illustrate that the characteristic velocity efficiencies for uncooled altitude tests reported by P&WA-FRDC are low for the corresponding reported delivered performance data. From the correlation curves the level of the characteristic velocity efficiency as reported in sea level tests (Ref. 6) more nearly reflects the level of the effective combustion efficiency consistent with the reported delivered performance. The same figures point up that the Rocketdyne delivered performance data, in many instances, are high even for the high level of characteristic velocity efficiency reported. However, the indicated correlation curve for the effective combustion efficiency tends to smooth out these inconsistencies and makes possible correction of delivered performance to permit comparison of these data with calculated performance results (100 percent combustion efficiency). Specifically, the individual data points are corrected for combustion inefficiency to reflect delivered performance for 100 percent combustor efficiency by adding to the delivered performance that fraction of the theoretical equilibrium specific impulse suggested by the effective combustion efficiency, η_c^{*E} , correlation.

Comparison of Calculated and Delivered Performance

Figures 12 through 22 illustrate the comparison of calculated performance and delivered performance for the 100 percent efficient combustor based on the effective combustion efficiency curve of Fig. 29. The symbols in each of the figures represent the delivered performance of the individual test firings after adjusting the performance by the averaged effective combustion efficiency to reflect 100% efficient combustion. The comparison of the analytically-predicted and measured performance results indicates reasonable overall agreement.

The correlation of the engine test data with calculated delivered performance is somewhat better for the B_2H_6 propellant than for the CH_4 propellant. Specific attention should be called first to Fig. 15 for which case the predicted performance is considerably lower than that reported from engine tests, and then to Figs. 16 and 17 for which the reverse is apparent. In the former case the delivered performance was previously reported to be inconsistently high relative to the other CH_4 -Flox (82.6% F_2) data (cf. Fig. 4). In the latter case the characteristic velocity efficiency was reported inconsistently high (by almost 2%) relative to the other test data obtained by Rocketdyne. The high characteristic velocity efficiency, Figs. 5 and 6, resulted in no additional correction of delivered performance in order to reflect 100% efficient combustion, whereas, only a slight amount of correction would have been required to improve the correlation.

Figures 30-32 illustrate, in summary form, the comparisons achieved between engine test performance corrected to 100% combustion efficiency and the analytically-predicted performance expressed as percent deviation from predicted performance. Fig. 30 illustrates the comparison for CH_4 -Flox (- OF_2) engine tests, Fig. 31 for the B_2H_6 -Flox (- OF) engine tests, and Fig. 32 for the combined results. From Fig. 32 it can be established that 80 percent of the engine test data, involving 5 propellants, 4 nozzles, and 2 pressures, have been correlated within ± 2.0 percent over a wide range of oxidizer-fuel ratios.

KINETIC PERFORMANCE CHARTS

The evolution of techniques for predicting liquid rocket propellant nozzle performance has progressed to the point where the propulsion specialist is faced by an overabundance of machine calculation programs as well as a surplus of procedures to tie these various programs together. For example, exact numerical procedures are now available (Refs. 20 and 21) which solve simultaneously the chemical kinetic and gas dynamic equations pertinent to two-dimensional and axisymmetric flow fields, such as those encountered in the supersonic portions of typical expansion nozzles. Such numerical procedures are usually lengthy, and all require access to high-speed digital computation machines involving considerable effort and expense to obtain predictions of nonequilibrium nozzle performance.

The need is clearly evident for a simple, direct procedure for the rapid estimation of the delivered performance of rocket nozzles for a variety of propellant systems over broad ranges of such parameters as combustion chamber pressure, O/F ratio, nozzle-contour and scale, and reaction rate constants. Such a procedure must largely be graphic in nature and present the results of machine calculations in a form which permits interpolation of the various possible performance losses (e.g. kinetic, frictional drag and divergence losses) over the broad ranges of conditions and configurations. Such a method should also present sufficient data so as not to become obsolete with the revision of such parameters as reaction rate constants.

In order to maintain the necessary simplicity and degree of flexibility required of such a method, a procedure has been developed and verified which presumes that the various component losses (viz. kinetic, viscous and divergence loss) in an expansion nozzle can be deducted from the theoretical, one-dimensional shifting-equilibrium performance of the nozzle, neglecting any coupling effects which may actually occur in the flow system. This approach has been shown to give results of good accuracy (Ref. 4) and is in accordance with the recommendations of the ICRPG Performance Standardization Working Group (Ref. 22).

Using this procedure a series of performance estimation graphs has been prepared for four propellant combinations typical of current earth-storable, space-storable and cryogenic systems (viz. aeroxine 50-N₂O₄, CH₄-O₂ (17.4%)-F₂ (82.6%), H₂-O₂ and H₂-F₂). The graphs have been assembled in the form of a handbook (Ref. 23) so as to enable the propulsion engineer and vehicle designer to make rapid estimates of the deliverable performance of these propellants over broad ranges of conditions and nozzle configurations. The conditions assumed generally encompass a range of O/F ratios surrounding the optimum mixture ratio for each propellant and include combustion chamber pressures between 100 and 1000 psia. The configurations assumed include both conical and bell nozzle contours for values of nozzle exit area ratio between 20 and 100, and for nominal thrust levels between 100 and 1,000,000 pounds.

Presented in this handbook are self-consistent kinetic performance and aerodynamic degradation charts which are sufficiently general to permit user-supplied nozzle area ratio gradients to be employed to estimate the nonequilibrium performance of virtually any nozzle. Additionally, sufficient information is included to enable estimation of the effect on kinetic performance loss of variations in reaction rate constants relative to the values used in the handbook.

The above flexibility in nozzle and rate selection arises from the method of nonequilibrium performance prediction adopted, a modified sudden-freezing criterion for multi-reaction systems (Refs. 24, 25, 26). This approximation to the full-kinetic process has been found to produce results of good accuracy when calibrated against one-dimensional, full-kinetic results for each propellant combination (Ref. 4).

Previous investigations have shown the effects of flow divergence and nozzle curvature to be reliably estimated by performing axisymmetric flow calculations assuming a chemically-frozen gas flow model. The divergence loss charts which appear in the handbook were prepared using this flow model and are presented for both conical and bell nozzles. Boundary layer losses have been estimated using the modified Bartz turbulent boundary layer program (Ref. 12) using an adiabatic nozzle wall and are likewise presented for the conical and bell nozzles. No effect of wall heat transfer was considered.

Due to the lack of sensitivity of transonic flow loss to variations in throat contour when the subsonic convergent angle and throat radius of curvature are moderate, the transonic loss is assumed constant at 1/2% of frozen vacuum specific impulse. The user is cautioned to maintain moderate convergence angles in the subsonic portion (less than 25 deg) and sufficiently large r_c/r_t values (>1.0) in order to prevent transonic flow losses from becoming excessive.

Every attempt has been made to maintain performance prediction accuracy within $\pm 1\%$ of the performance predicted by the full-kinetic axisymmetric machine program recommended by the ICRPG (Ref. 22). Specific breakdown of calculation accuracies are:

Kinetic loss $\pm 1/2\%$
Divergence loss $\pm 1/4\%$
Boundary layer loss $\pm 1/4\%$

For further description of the methods employed, and for sample calculations using these methods, the reader is referred to the "NASA Kinetic Performance Handbook", NASA CR-72601 (Ref. 23).

TRIPROPELLANT PERFORMANCE ANALYSIS

The interest in the tripropellant, H_2-F_2-Li is based on the high energy released by the combustion of fluorine with the light metal lithium, coupled with the desirable low molecular weight hydrogen as a working fluid. The combination offers a theoretical specific impulse (vacuum) between 540 (5292 N-sec/kg) and 565 sec (5540 N-sec/kg) for 30% H_2 addition (Figs. 33 and 34). However, this complex system introduces certain potential loss characteristics, e.g., condensation, drop size effects, chemistry and change of phase interactions, that must be evaluated in order to predict overall performance. The approach used herein to predict performance is essentially that employed previously in this report, extended to consider the condensation mechanism. No attempt has been made to consider the effect of injector design or to include the sequential injection of propellant components. The propellants were considered homogeneously mixed and reacted to the equilibrium state defined at the chamber conditions. The independence of each of the loss mechanisms is assumed, based upon the previous studies (Ref. 4) which have indicated the interaction to be minimal.

The following discussion is divided to cover these six factors:

1. Equilibrium thermodynamics
2. Chemical kinetic loss
3. Change of phase loss
4. Divergence loss
5. Viscous boundary layer loss

Equilibrium Thermodynamics

All analyses were made with reference to the maximum theoretically available performance based upon the chamber conditions. These results serve as the upper bound for all net performance. The H_2 dilution was varied over the range bounded by 20 and 40 percent H_2 by weight. The mass ratio of Li to F_2 was set at its stoichiometric proportion (2.74). The propellants were also expanded with the composition held constant (frozen-flow) at the chamber equilibrium composition. This defined the bound to the maximum total chemical and condensation loss. Two sets of propellant input conditions were assumed: (1) liquid lithium (960°R), liquid fluorine (153°R), and gaseous hydrogen (537°R); and (2) solid lithium (37°R), liquid fluorine (153°R), and liquid hydrogen (37°R).

Li(l)-F₂(l)-H₂(g)

The shifting-equilibrium calculations for Li(l)-F₂(l) in stoichiometric proportions of 2.74 at a chamber pressure of 500 psia (3.447×10^6 N/m²) indicate that

the maximum theoretical performance is 542 sec (5312 N-sec/kg), which occurs near 32% H₂ dilution for an exit area ratio of 60. The same condition expanded to an area ratio of 200 to 1 produces a maximum of 564 sec (5528 N-sec/kg) at 30% H₂ (Figs. 33 and 34). Figures 33 and 34 illustrate that the levels remain approximately the same exit area ratios, with the effect of pressure producing only a slight shift in the maximum point toward lower percent dilutions. These results are noteworthy in that there is no practical change in the equilibrium results as a function of chamber pressure with these inlet conditions.

Li(s)-F₂(l)-H₂(l)

Figures 35-46 illustrate the effect of H₂ diluent on the equilibrium and frozen performance for Li(s)-F₂(l)-H₂(l) at chamber pressures of 500, 750, and 1000 psia, expanded to 60 to 200 area ratios. The equilibrium optimum $I_{sp_{vac}} = 544$ sec (5330 N-sec/kg) at $P_c = 500$ psia (3.447×10^6 N/m²) occurs at approximately 25 percent H₂ for an area ratio of 200.

The optimum point shifts with nozzle expansion ratio and the conditions of the initial constituents. A reduction of expansion area ratio to 60 increases the optimum point to approximately 30% H₂. A comparison of the results for the two sets of input propellant conditions indicates a shift in optimal performance to a higher H₂ concentration with the higher constituent enthalpy; i.e., Li(l)-H₂(g).

Figures 37 and 38 illustrate typical variations of equilibrium composition with area ratio for selected operating conditions. Typically, the H-atom concentration is seen to fall off dramatically in the throat region for the pressure involved in this investigation. The indications are that equilibrium exists between the H atom and the H₂ molecule. However, the magnitude of the net energy in this exchange is negligible relative to the entire system, since the highest concentration of H is several orders of magnitude less than that of the H₂ and the other predominant products. The implication is that the major thermochemical effects are controlled by the lithium and fluorine containing species.

Condensation Effects

The full nonequilibrium model includes the consideration of both the chemistry and condensation phenomena. This model implies that the gas is homogeneously accelerated to a freezing area ratio where the chemistry and condensation is stopped and expansion continued with no further change in the composition, i.e., condensation and chemical nonequilibrium are so coupled that the freezing of the recombination reactions results in immediate cessation of condensation.

Figures 39-45 illustrate the nonequilibrium performance for selected propellant combinations and operating conditions for this gas model. The full nonequilibrium

model is designated by nonequilibrium with condensation. The difference between the value of specific impulse at a freezing area ratio and the equilibrium value is due to the lack of recombination and condensation resulting in nonequilibrium degradation.

To demonstrate the significance of the condensation phenomena, calculations were made with condensation suppressed. This model is one that accelerates the flow such that condensation cannot take place, but chemical equilibrium can be maintained. The physical realization of the model is abstract; however, the results serve to indicate the magnitude of the contribution made by condensation. The nonequilibrium performance with condensation suppressed is also illustrated in Figs. 39-45. Typically, for chamber conditions: $P_c = 500$ psia, 30% H_2 , $Li(l)-F_2(l)-H_2(g)$ a thrust contribution due to condensation of 26.5 sec (259.7 N-sec/kg) at an area ratio of 60 is indicated, out of a total difference between equilibrium and frozen of 58.4 sec (572 N-sec/kg) (cf., Fig. 45).

The same chamber conditions expanded to a 200 to 1 area ratio indicates a loss due to the lack of condensation of 32.9 sec (322 N-sec/kg) out of a maximum loss of 70.4 sec (690 N-sec/kg) (cf., Fig. 40).

Separation of Condensation and Recombination Losses

There is a history of analysis associated with the assessment of losses due to the lack of recombination (Ref. 4). The concept of freezing area ratio is used to establish the losses that are incurred by retarding kinetics in any section of the expansion process. The chemical kinetics and change of phase dynamics are treated in similar manners. Both phenomena influence performance via heat release to the working media; the chemistry by way of recombination and the change of phase by way of liquification and solification. Finite-rate chemistry limits the recombination of species and the resulting available energy to the expansion process.

The condensation process is controlled by two phenomena (1) nucleation; i.e. the generation of sites for the continuing condensation and (2) droplet growth.

The composition of a typical $Li-F_2-H_2$ propellant combination indicates that a substantial portion of the constituents are in the form of LiF at the onset of condensation such that the conversion in phase is not limited by the production of LiF from reactants. This indicates that the separation of the recombination and condensation zones may be possible (cf., Figs. 37 and 38).

The two models, one with condensation allowed and the other with condensation suppressed, provide a means of assessing the contributions made to performance by condensation and recombination on an individual basis.

Figures 39-45 present the variation of the theoretical nonequilibrium performance of the two models with arbitrary freezing area ratios. One model considers that condensation and chemical equilibrium are so coupled that freezing the recombination reactions simultaneously suppresses the condensation. The alternative model maintains that the condensation cannot occur throughout the expansion (this implies an extremely slow nucleation rate), but that equilibrium chemistry can be obtained up to an arbitrary area ratio (freezing area ratio) and subsequently expanded with no further recombination (frozen flow). The combination of the two allows the generation of curves representing the potential loss incurred as a result of lack of recombination or condensation with arbitrary freezing area ratio (cf., Figs. 46-52).

Note that while the term freezing area ratio can be applied to the chemical loss, it is a misnomer for the condensation loss. There, the meaning is "that area ratio at which condensation has ceased" in the same sense that recombination does.

The Effect of Freezing Area Ratio

The maximum chemical loss attained by freezing anywhere between the combustion chamber and the throat is approximately 47 sec (460 N-sec/kg) (cf., Fig. 51). The explanation for the insensitivity of the loss to freezing between chamber and throat is that at these temperatures there is only a limited amount of recombination taking place. In the throat region, the changes are rapid and the chemical effect becomes pronounced. From Fig. 41, the supersonic section between the throat and an area ratio of 2 displays a decrease in loss from 47 sec (460 N-sec/kg) to 21 sec (206 N-sec/kg) attributable to chemical kinetics. At an area ratio of 4, the loss is reduced to 13 sec (128 N-sec/kg), and then to zero at the exit of 200:1. This characteristic is typical of H_2 dilutions from 20% to 30%.

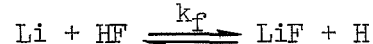
The change of phase phenomena is an inherently important factor in the expansion of this flow system. At a dilution of 20% H_2 , no condensed LiF is formed in the ideal combustion chamber, while at 30% dilution about 2% of the total mass, which is 10% of the total LiF, is condensed (cf., Fig. 53). The condensation increases through the equilibrium expansion until half of all the LiF condensed is condensed at an area ratio 1.6 for 30% H_2 diluent, with condensation appearing at an area ratio 3.5 for 20% dilution. The LiF in 30% H_2 dilution case is entirely converted to solid at area ratio of 10, while for the 20% H_2 case, 70% of the LiF is formed as solid at an area ratio of 60.

Figure 54 illustrates the influence of initial constituent state ($Li(l)$, $F_2(l)$, $H_2(g)$ vs $Li(s)$, $F_2(l)$, $H_2(l)$), in the condensation profile through the nozzle expansion. The lower enthalpy propellant combination ($Li(s)$, $F_2(l)$, $H_2(l)$) displays earlier condensation in general.

The condensation mechanism contributes significantly to the performance (cf., Fig. 19). The critical region again is the area immediately downstream of the throat. The loss obtained by suppressing condensation anywhere between the chamber and the throat is 25 sec (245 N-sec/kg). Again, the explanation is in the temperature levels. Between an area ratio of 1 and 3, the loss drops from 25 sec (245 N-sec/kg) to 11.5 sec (113 N-sec/kg), while at an area ratio of 6 the loss has dropped to 6 sec (59 N-sec/kg), and then to zero at 200:1. Similar condensation effects are displayed in Figs. 46-52 for a selected set of operating conditions.

Chemical Kinetic Loss

A review of the system composition and the energies associated with each of the elements present indicates that in the high expansion regions of the nozzle the important controlling reaction is the two-body reaction



A secondary reaction involving the recombination of H atoms ($2\text{H} + \text{H} \rightleftharpoons \text{H}_2 + \text{H}$) is of minor importance for the tripropellant system due to the extremely low concentration of H atoms. Expansion made with this reaction frozen confirm this conclusion.

The lack of chemical kinetic data prompted the use of an estimated rate for the similar reaction



$$k_f = 6.35 \times 10^9 T^{\frac{1}{2}} e^{-6750/T}, \text{ ft}^3/\text{lbs-mol-sec}, T\text{-}^\circ\text{R}$$

(as reported in Ref 13) for the reaction



Calculations were made to determine the loss that could be obtained solely due to nonequilibrium chemistry by means of the Bray-like analysis (cf., Ref. 24), utilizing the bimolecular reaction as the rate controlling reaction. The results of these nonequilibrium calculations are detailed in Table 2 along with the other important degradations encountered for the tripropellant system.

Change of Phase Loss

The losses due to formation of condensed phase are instituted by two mechanisms. The most direct loss is the departure from equilibrium produced by the condensation rate process being unable to follow the changes imposed by the nozzles accelerations.

Hence, rather than maintaining the liquid-gas or liquid-solid prescribed by equilibrium, a supercooled condition is created. The energy normally released to the gas is inhibited and the performance reduced.

It is impossible to assess at which point cessation of condensation occurs, if it occurs at all, because of the lack of nucleation rate data and the lack of methods to calculate combined nonequilibrium chemical and condensation phenomena; the value listed should be treated as an estimate of the maximum possible loss. The condensation of LiF, however, is likely to continue beyond the point of chemical freezing since a large fraction of the Li and F exists as LiF or Li_2F_2 . The condensation phenomena, therefore, can occur independently of the chemical phenomena. Even when this does not occur in a continuous manner, it is possible that condensation shock will occur before the nozzle exit in large expansion ratio nozzles. In either case the condensation losses will be considerably reduced from the values listed in the table. Calculations have been performed to indicate that losses due to cessation of condensation are considerably reduced if the cessation occurs only slightly downstream of the chemical freezing point (cf., Figs. 46-52). The nonequilibrium condensation loss listed in Table 2 has been established from Figs. 46-52 using the same freezing point as determined from chemical nonequilibrium analysis.

There is an additional loss produced by condensation; the condensation is in the form of particles (liquid or solid) and maintenance of thermodynamic equilibrium is a function of the particle size (surface area) and the surrounding media. In most cases there will be lags established between the particles and the gas. That is, the temperatures and velocities of the particles and gas will differ. The particle lag losses calculated for selected propellant combinations, particle sizes, and operating conditions are illustrated in Figs. 55 and 59. The maximum potential lag losses (independent of nozzle and particle size) are calculated by assuming the extreme conditions of no heat transfer from condensed phase to gas and no acceleration of the condensed phase from the indicated area ratio to the exhaust. The condensed phase concentration is fixed at the equilibrium concentration for the conditions and area ratio listed on the figure.

The actual calculated losses depicted in Figs. 55-59 were established by allowing heat transfer and acceleration to occur from the indicated area ratio. Upstream of the indicated area ratio the system was assumed to be in equilibrium. This approach was chosen because machine programs are not available for analysis of particle flow in which the mass fraction of the particle is continually changing.

Analysis of the 100 pound (444.8 N) thrust nozzle with 50 micron diameter particles indicates that the maximum loss is 2.4% of the equilibrium performance, (cf., Fig. 59). This loss, however, is strongly dependent on the particle size, and thrust level (nozzle size). The thrust level influences the loss via the larger

accelerations necessary for the smaller nozzles. Large accelerations produce lags which are responsible for the additional losses. For example, while the 100 pound (444.8 N) thrust nozzle generates 2.4% loss based on equilibrium, Fig. 56 indicates that the 10,000 pound (444.8×10^2 N) thrust nozzle produces a negligible loss for the same 50 micron particles.

Increasing the particle size decreases the surface area for the fixed amount of mass, decreasing the accelerating force on the particle and increasing the lag. The result is larger losses for larger particles. Figure 56 displays a maximum actual calculated loss of 2.4% for 200 micron particles while also indicating no loss for 50 micron particles.

The column identified as the additional 2-phase flow loss (Table 2) lists the maximum degradations encountered as a result of thermal and velocity lags suffered by particles of the indicated size (50 and 200 microns). These values were obtained by using the maximum actual calculated loss values in Figs. 55-59.

Divergence Loss

Analysis of the conical nozzle divergence loss indicates that this loss is in the range of 1.5 to 1.8% for A/A_{MIN} of 60 to 200. The mean value for standard exit area ratios is suitably defined by the cosine law.

The bell nozzles behave in a manner consistent with the results demonstrated in previous studies reviewed in this report. The divergence loss rises abruptly in the expansion section near the throat to a maximum specified by the radius of curvature of the throat and the final exit area ratio. The loss subsequently decreases in an exponential fashion to zero at the perfect nozzle design area ratio. The typical divergence for truncated perfect nozzles commonly used is between 1.25% and 2.2%.

Viscous Boundary Layer Loss

The boundary layer loss has a range of 1%-2% for the 100-10,000 pound thrust nozzle ($4.448 \times 10^2 - 4.448 \times 10^4$ N).

Net Loss and Calculated Predicted Performance

The net delivered performance of a nozzle can be viewed as the theoretical equilibrium values less the sum of all kinetic and aerodynamic losses. Table 2 contains the losses evaluated for a specified range of conditions for thrust level and particle size. From this table, some general guidelines may be established.

The net losses listed in Table 2 for a wide range of pressures, thrust levels, expansion ratios, and particle sizes for several conditions of propellant and diluent H₂ combinations indicate that the potential performance degradation can vary from approximately 26 to 68 sec (255-677 N-sec/kg). The calculated delivered performance established from the range of net losses and maximum theoretical performance is between 487.4 sec (4777 N-sec/kg) and 520.2 sec (5098 N-sec/kg), the former for Li(s)-F₂(l)-H₂(l) in a 100 lbs thrust (4.448 N) nozzle with an assumed particle size of 50 microns, and the latter for Li(l)-F₂(l)-H₂(g) in a 10,000 lbs thrust nozzle (4.448 x 10⁴ N) also with an assumed particle size of 50 microns. The delivered performance would be reduced approximately by an additional 10 seconds with an assumed particle size of 200 microns.

The condensation loss may be reduced by an abrupt, but delayed condensation (shock) liberating energy at a point where subsequent thermal and kinetic losses are minimal. The net result would be a decrease in condensation loss, but no significant increase in the additional two-phase loss.

REFERENCES

1. Bittker, D. A.: Nonequilibrium Calculations of Methane-Fluorine-Oxygen and Butene-1-Fluorine Oxygen Rocket Performance, NASA TN D-4991, January 1969.
2. Bailey, T. E. and W. R. Munk: Hydrogen-Fluorine Propulsion System. Contract No. NASw-754, Final Report P&WA FR-1585, 1966, NASA Report No. 72074.
3. Waldman, B. J., and E. B. Shuster: Fluorine-Hydrogen Performance Evaluation Phase I, Part II: Nozzle Performance Analysis and Demonstration. Contract No. NASw-1229, Final Report NAA Rocketdyne R-6636-2, April 1967, NASA Report No. CR-72038.
4. Sarli, V. J., W. G. Burwell, L. S. Bender, T. F. Zupnik and L. D. Aceto: Investigation of Nonequilibrium Flow Effects in Hydrogen-Fluorine Rocket Nozzles (U), Second Annual Technical Report, Contract NASw-1293, NASA CR-72347, December 1967.
5. Masters, A. I.: Investigation of Light Hydrocarbon Fuels with Fluorine-Oxygen Mixtures as Liquid Rocket Propellants, Final Report NASA CR-72147, September 1967.
6. Masters, A. I.: Investigation of Light Hydrocarbon Fuels with Fluorine-Oxygen Mixtures as Liquid Rocket Propellants, Final Report, NASA CR-72425, November 1968.
7. Fluorine-Hydrogen Performance Evaluation; Phase II: Space Storable Propellant Performance Demonstration, Contract NASw-1229, NASA CR-72542, Rocketdyne R-6636-3, April 1969.
8. Lockheed Missiles and Space Company: Phase II Propellant Selection for Unmanned Spacecraft Propulsion Systems, Mid-Term Status Letter No. 4, Contract NASw-1644, January 1969.
9. Sarli, V. J., W. G. Burwell and T. F. Zupnik: Investigation of Nonequilibrium Flow Effects in Hydrogen-Fluorine Rocket Nozzles. NASA Report CR-72162, Contract NASw-1293, First Annual Technical Report, September 1966.
10. Bailey, T. E., W. G. Burwell and V. J. Sarli; Experimental and Analytical Investigation of Chemical Nonequilibrium Losses in Fluorine-Hydrogen Rocket Engines (U). Paper presented at the 9th Liquid Propulsion Symposium held October 25-27, 1967, in St. Louis, Missouri.

REFERENCES
(cont.)

11. King, R. C. and G. T. Armstrong: "Constant Pressure Flame Calorimetry with Fluorine, II Heat of Formation of Oxygen Difluoride", Journal of Research of the National Bureau of Standards, A. Physics and Chemistry, Vol. 72A, No. 2, March-April 1968.
12. Elliot, D. G., D. R. Bartz and S. Silver: Calculation of Turbulent Boundary Layer Growth and Heat Transfer in Axisymmetric Nozzles. Jet Propulsion Laboratories Report TR No. 32-387, February 1963.
13. Cherry, S. S. and L. J. Van Nice: Screening of Reaction Rates, Phase II Final Report, TRW Systems Group, Report No. 08832-6002-T000, Redondo Beach, California, December 6, 1967.
14. Jacobs, T. A., R. R. Giedt and N. Cohen, "Kinetics of Hydrogen Halides in Shock Waves. II. A New Measurement of the Hydrogen Dissociation Rate", Journal of Chem. Phys., Vol. 47, No. 1 (1967).
15. Jacobs, T. A., R. R. Giedt and N. Cohen, "Kinetics of Decomposition of HF in Shock Waves", Journal of Chem. Phys., Vol. 43, No. 10 (1965).
16. Schott, G. L. and P. F. Bird, "Kinetic Studies of Hydroxyl Radicals in Shock Waves. IV. Recombination Rates in Rich Hydrogen-Oxygen Mixtures", Journal of Chem. Phys., Vol. 41, No. 9 (1964).
17. Bowman, C. T.: Application of Kinetics Calculations to the Interpretation of Shock Tube Data, Meeting of Combustion Institute, Western States Section, Berkeley, October 30, 1968.
18. Bulewize, E. M. and T. M. Sugden, "The Recombination of Hydrogen Atoms and Hydroxyl Radicals in Hydrogen Flame Gases", Trans. Faraday Soc., 54, 1855 (1958).
19. McAndrew, R. and R. Wheeler, "The Recombination of Atomic Hydrogen in Propane Flame Gases", J. Phys. Chem., 66, 229 (1962).
20. User's Manual for Chemical Kinetic Analysis (Deck 2). PWA-2888, Supplement 2, prepared under Air Force Contract No. AF 33(615)-3128, July 1966.
21. Axisymmetric Reacting Gas Nonequilibrium Performance Program. TRW Systems Report No. 02874-6004-R000, prepared under NASA Contract NAS 9-4358, March 8, 1967.
22. Pieper, J. L.: ICRPG Liquid Propellant Thrust Chamber Performance Evaluation Manual Central Propulsion Information Agency No. 178, September 1968.

REFERENCES
(cont.)

23. Bender, L. S., V. J. Sarli and W. G. Burwell: NASA Kinetic Performance Handbook, Contract NAS 3-11225, NASA CR- 72601, September 1969.
24. Sarli, V. J., W. G. Burwell and T. F. Zupnik: Investigation of Nonequilibrium Flow Effects in High Expansion Ratio Nozzles. Final Report Contract NAS3-2572, NASA CR-54221, December 1964.
25. Sarli, V. J., W. G. Burwell, R. Hofland, Jr. and T. F. Zupnik: Evaluation of the Bray Sudden-Freezing Criterion for Predicting Nonequilibrium Performance in Multireaction Rocket Nozzle Expansions. Presented at the AIAA Propulsion Joint Specialist Conference, Colorado Springs, Colorado, June 14-18, 1965. AIAA Paper No. 65-554.
26. Burwell, W. G., V. J. Sarli and T. F. Zupnik: Applicability of Sudden-Freezing Criteria in Analysis of Chemically-Complex Rocket Nozzle Expansions. Presented at 7th AGARD Colloquium on Recent Advances in Aerothermochemistry, Oslo, Norway, May 16-20, 1966. Also available as United Aircraft Corporation Research Laboratories Report UAR-E72, May 1966.

LIST OF SYMBOLS

A	Area
A_{min}	Minimum area
C^*	Characteristic velocity
$I_{sp_{vac}}$	Vacuum specific impulse
O/F	Oxidizer-fuel ratio
P_c	Chamber pressure
r	Radius
r_c	Throat radius of curvature
r_t	Throat radius
x	Axial distance
y	Radial distance
η_{c^*}	Combustion efficiency
η_{c^*E}	Effective combustion efficiency

APPENDIX I
 DISTRIBUTION LIST FOR FINAL REPORT
 (Contract NASA CR-72600)

<u>Addressee</u>	<u>No. of Copies</u>
National Aeronautics and Space Administration Lewis Research Center 21000 Brookpark Road Cleveland, Ohio 44135	
ATTN: Contracting Officer, MS 500-313	1
Liquid Rocket Tech. Branch, MS 500-209	8
Technical Report Control Office, MS 5-5	1
Technology Utilization Office, MS 3-16	1
AFSC Liaison Office, MS 4-1	2
Library	2
Office of Reliability & Quality Assurance, MS 500-203	1
D. L. Nored, MS 500-209	1
E. W. Conrad, MS 100-1	1
Carl Aukerman, MS 86-1	1
David Bittker, MS 6-1	1
National Aeronautics and Space Administration Washington, D. C. 20546	
ATTN: Code MT	1
Code RFX	2
Code RPL	2
Code SV	1
Scientific and Technical Information Facility P. O. Box 33 College Park, Maryland 20740	
ATTN: NASA Representative, Code CRT	6
National Aeronautics and Space Administration Ames Research Center Moffett Field, California 94035	
ATTN: Library	1
C. A. Syvertson	1
National Aeronautics and Space Administration Flight Research Center P. O. Box 273 Edwards, California 93523	
ATTN: Library	1

DISTRIBUTION LIST FOR FINAL REPORT
(Contract NASA CR-72600)

<u>Addressee</u>	<u>No. of Copies</u>
National Aeronautics and Space Administration Goddard Space Flight Center Greenbelt, Maryland 20771 ATTN: Library C. R. Gunn	1 1
National Aeronautics and Space Administration John F. Kennedy Space Center Cocoa Beach, Florida 32899 ATTN: Library	1
National Aeronautics and Space Administration Langley Research Center Langley Station Hampton, Virginia 23365 ATTN: Library R. L. Swain	1 1
National Aeronautics and Space Administration Manned Spacecraft Center Houston, Texas 77001 ATTN: Library	1
National Aeronautics and Space Administration George C. Marshall Space Flight Center Huntsville, Alabama 35812 ATTN: Library Keith Chandler, R-P&VE-PA	1 1
National Aeronautics and Space Administration Western Operations Office 150 Pico Boulevard Santa Monica, California 90406 ATTN: Library	1
Jet Propulsion Laboratory 4800 Oak Grove Drive Pasadena, California 91103 ATTN: Library D. Bartz	1 1

DISTRIBUTION LIST FOR FINAL REPORT
(Contract NASA CR-72600)

<u>Addressee</u>	<u>No. of Copies</u>
Office of the Director of Defense Research & Engineering Washington, D. C. 20301 ATTN: Dr. H. W. Shultz, Office of Asst. Dir. (Chem. Technology)	1
Defense Documentation Center Cameron Station Alexandria, Virginia 22314	1
Arnold Engineering Development Center Air Force Systems Command Tullahoma, Tennessee 37389 ATTN: AEOIM	1
Aeronautical Systems Division Air Force Systems Command Wright-Patterson Air Force Base Dayton, Ohio ATTN: D. L. Schmidt, Code ASRCNC-2	1
Air Force Rocket Propulsion Laboratory (RPR) Edwards, California 93523	1
Air Force Rocket Propulsion Laboratory (RPM) Edwards, California 93523	1
Air Force FTC Edwards Air Force Base, California 93523 ATTN: FTAT-2 Col. J. M. Silk	1 1
Air Force Office of Scientific Research Washington, D. C. 20333 ATTN: SREP, Dr. J. F. Masi	1
U. S. Army Missile Command Redstone Scientific Information Center Redstone Arsenal, Alabama 35808 ATTN: Chief, Document Section Dr. W. Wharton	1 1

DISTRIBUTION LIST FOR FINAL REPORT
(Contract NASA CR-72600)

<u>Addressee</u>	<u>No. of Copies</u>
Bureau of Naval Weapons Department of the Navy Washington, D. C. ATTN: J. Kay, Code RTMS-41	1
Commander U. S. Naval Ordnance Test Station China Lake, California 93557 ATTN: Code 45 Code 753 Code W. F. Thorm, Code 4562	1 1 1
Picatinny Arsenal Dover, New Jersey ATTN: I. Forsten, Chief Liquid Propulsion Laboratory	1
Martin Marietta Corporation Martin Division Baltimore 3, Maryland ATTN: John Calathes (3214)	1
McDonnell Aircraft Corporation P. O. Box 6101 Lambert Field, Missouri ATTN: R. A. Herzmark	1
North American Aviation, Incorporated Space & Information Systems Division 12214 Lakewood Boulevard Downey, California 90242 ATTN: Technical Information Center, D/096-722 (AJ01) H. Storms	1 1
Northrop Space Laboratories 1001 East Broadway Hawthorne, California ATTN: Dr. William Howard	1

DISTRIBUTION LIST FOR FINAL REPORT
(Contract BASA CR-72600).

<u>Addressee</u>	<u>No. of Copies</u>
Jet Propulsion Center Purdue University West Lafayette, Indiana 47907 ATTN: Security Librarian Dr. Bruce A. Reese, Dir.	1
Republic Aviation Corporation Farmingdale, Long Island New York ATTN: Dr. William O'Donnell	1
Rocket Research Corporation 520 South Portland Street Seattle, Washington, 98108	1
Rocketdyne Division of North American Aviation, Incorporated 6633 Canoga Avenue Canoga Park, California 91304 ATTEN: Library, Department 596-306	1
Rohm and Hass Company Redstone Arsenal Research Division Huntsville, Alabama 35808 ATTN: Librarian	1
Space-General Corporation 9200 East Flair Drive El Monte, California 91734 ATTN: C. E. Roth, Jr.	1
Stanford Research Institute 333 Ravenswood Avenue Menlo Park, California 94025 ATTN: Thor Smith	1
Thiokol Chemical Corporation Reaction Motors Division Denville, New Jersey 07834 ATTN: A. Sherman Librarian	1

DISTRIBUTION LIST FOR FINAL REPORT
(Contract NASA CR-72600)

<u>Addressee</u>	<u>No. of Copies</u>
TRW Systems, Incorporated 1 Space Park Redondo Beach, California 90200 ATTN: G. W. Elverum	1
STL Tech. Lib. Doc. Acquisitions	1
United Aircraft Corporation Pratt & Whitney Aircraft Division Florida Research & Development Center P. O. Box 2691 West Palm Beach, Florida 33402 ATTN: R. J. Coar	1
Library	1
United Aircraft Corporation United Technology Center P. O. Box 358 Sunnyvale, California 94088 ATTN: Librarian	1
Vought Astronautics Box 5907 Dallas 22, Texas ATTN: Warren C. Trent	1
Air Force Aero Propulsion Laboratory Research & Technology Division Air Force Systems Command United States Air Force Wright-Patterson AFB, Ohio 45433 ATTN: APRP (C. M. Donaldson)	1
Aerojet-General Corporation P. O. Box 296 Azusa, California 91703 ATTN: Librarian	1
Aerojet-General Corporation 11711 South Woodruff Avenue Downey, California 90241 ATTN: F. M. West, Chief Librarian	1

DISTRIBUTION LIST FOR FINAL REPORT
(Contract NASA CR-72600)

<u>Addressee</u>	<u>No. of Copies</u>
Aerojet-General Corporation P. O. Box 1947 Sacramento, California 95809 ATTN: Technical Library 2484-2015A Dr. C. M. Beighley D. T. Bedsole	 1 1 1
Aeronutronic Division of Philco Corporation Ford Road Newport Beach, California 92600 ATTN: Dr. L. H. Linder, Manager D. A. Carrison Technical Information Department	 1 1 1
Aerospace Corporation P. O. Box 95085 Los Angeles, California 90045 ATTN: J. G. Wilder, MS 2293 Library-Documents	 1 1
Astropower, Incorporated Subs. of Douglas Aircraft Company 2121 Campus Drive Newport Beach, California 92663 ATTN: Dr. George Moc, Director Research	 1
ARO, Incorporated Arnold Engineering Development Center Arnold AF Station, Tennessee 37389 ATTN: Dr. B. H. Goethert, Chief Scientist	 1
Atlantic Research Corporation Shirley Highway & Edsall Road Alexandria, Virginia 22314 ATTN: A. Scurlock Security Office for Library	 1 1
Battelle Memorial Institute 505 King Avenue Columbus, Ohio 43201 ATTN: Report Library, Room 6A	 1

DISTRIBUTION LIST FOR FINAL REPORT
(Contract NASA CR-72600)

<u>Addressee</u>	<u>No. of Copies</u>
Bell Aerosystems, Incorporated Box 1 Buffalo, New York 14205 ATTN: T. Reinhardt W. M. Smith	1 1
The Boeing Company Aero Space Division P. O. Box 3707 Seattle, Washington 98124 ATTN: Ruth E. Peerenboom (1190) J. D. Alexander	1 1
Chemical Propulsion Information Agency Applied Physics Laboratory 8621 Georgia Avenue Silver Spring, Maryland 20910	1
Chrysler Corporation Missile Division Warren, Michigan ATTN: John Gates	1
Curtiss-Wright Corporation Wright Aeronautical Division Woodridge, New Jersey ATTN: G. Kelley	1
Douglas Aircraft Company, Inc. Santa Monica Division 3000 Ocean Park Boulevard Santa Monica, California 90405 ATTN: J. L. Waisman R. W. Hallet G. W. Burge	1 1 1
Fairchild Stratos Corporation Aircraft Missiles Division Hagerstown, Maryland ATTN: J. S. Kerr	1

DISTRIBUTION LIST FOR FINAL REPORT
(Contract NASA CR-72600)

<u>Addressee</u>	<u>No. of Copies</u>
General Dynamics/Astronautics P. O. Box 1128 San Diego, California 92112 ATTN: F. Dore	1
Library & Information Services (128-00)	1
General Electric Company Re-Entry Systems Department P. O. Box 8555 Philadelphia, Pennsylvania 19101 ATTN: F. E. Shultz	1
Dr. E. S. Gantz	1
General Electric Company Flight Propulsion Laboratory Department Cincinnati, Ohio ATTN: D. Suichu	1
Grumman Aircraft Engineering Corporation Bethpage, Long Island New York ATTN: Joseph Gavin	1
IIT Research Institute Technology Center Chicago, Illinois 60616 ATTN: C. K. Hersh, Chemistry Division	1
Lockheed Missiles & Space Company P. O. Box 504 Sunnyvale, California ATTN: Y. C. Lee, Power Systems R&D	1
Technical Information Center	1
Lockheed Propulsion Company P. O. Box 111 Redlands, California 92374 ATTN: Miss Belle Berlad, Librarian	1

DISTRIBUTION LIST FOR FINAL REPORT
(Contract NASA CR-72600)

<u>Addressee</u>	<u>No. of Copies</u>
Lockheed Missiles & Space Company Propulsion Engineering Division (D.55-11) 1111 Lockheed Way Sunnyvale, California 94087	1
Marquardt Corporation 1655 Saticoy Street Box 2013 - South Annex Van Nuys, California 91404 ATTN: Librarian	1

Table 1

Summary of Elementary Reactions and Reaction
Rate Constants Employed
in CH₄-Flox (-OF₂) and B₂H₆-Flox (-OF₂) Mechanism

Reaction		Forward Rate: lbs-moles, ft ⁻³ , sec, °R
1	H + H + Ar \rightleftharpoons H ₂ + Ar	$k_f = 4.62 \times 10^{14} T^{-1}$
2	H + F + Ar \rightleftharpoons HF + Ar	$k_f = 1.155 \times 10^{15} T^{-1}$
3	H + OH + Ar \rightleftharpoons H ₂ O + Ar	$k_f = 7.85 \times 10^{15} T^{-1}$

Third Body Efficiencies Relative To Argon

Third Body	Reaction		
	1	2	3
H	20	1	3
H ₂	2.5	2.5	3
HF	2.5	2.5	3
CO ₂	2	2	10
CO	2	2	3
H ₂ O	2.5	2.5	20
BOF	2	2	10
BF	2	2	3

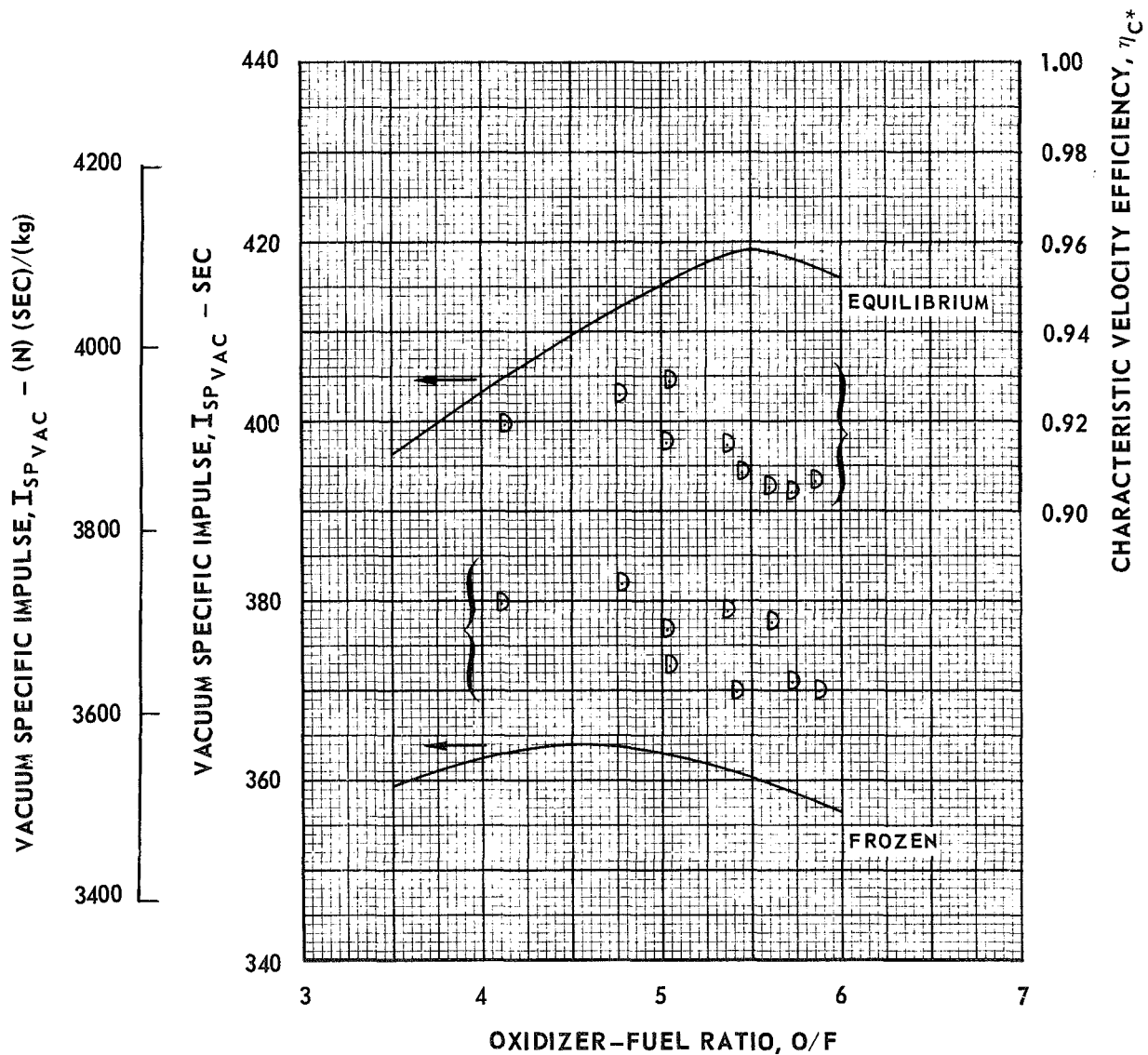
TABLE 2
SUMMARY OF RESULTS FOR
Li - F₂ - H₂

FUEL	P _c psia	THRUST psia	φ H ₂	(A/A _{MIN}) _{EXIT}	ISP EQ. I. M. sec	FROZ. IN sec	NON-EQUILIBRIUM LOSS CHEM sec	COND (MAX) sec	AERODYNAMIC LOSS DIV DRAG sec	TRANSONIC sec	ADDITIONAL 2 PHASE LOSS 50 microns 200 microns	NET LOSS 50 microns 200 microns sec
Li (s) - F ₂ (g) - H ₂ (g)	1000	100	25% ↓	60	521.0	472.0	13.8	4.2	7.1	8.0	10.9	58
	↓	↓	↓	200	545.4	484.0	19.5	9.0	7.25	9.7		
	10,000	10,000	25% ↓	60	521.0	472.0	9.0	1.0	7.1	5.2		
	↓	↓	↓	200	545.4	484.0	13.0	2.5	7.25	6.5		
Li (g) - F ₂ (g) - H ₂ (g)	500	100	20%	60	520.7	465.5	16.2	7.2	7.0	7.9		
	↓	↓	25%	60	533.0	472.0	18.0	11.0	7.1	8.0		
	↓	↓	30%	60	541.7	483.3	20.0	15.0	7.25	8.2		
	↓	↓	20%	200	547.7	475.8	24.5	12.5	7.1	9.5		
	↓	↓	25%	200	561.0	483.0	25.0	18.2	7.25	9.6		
	↓	↓	30%	200	564.6	494.2	24.2	20.0	7.4	9.8		
	10,000	10,000	20%	60	520.7	465.5	7.2	5.0	7.1	5.1	0	26.7
	↓	↓	25%	60	533.0	472.0	8.5	5.5	7.1	5.2	0	28.7
	↓	↓	30%	60	541.7	483.3	12.5	6.0	7.25	5.3	0	33.5
	↓	↓	20%	200	547.7	475.8	13.5	8.2	7.16	6.43	0	37.7
	↓	↓	25%	200	561.0	483.0	14.2	10.5	7.25	6.5	0	40.8
	↓	↓	30%	200	564.6	494.2	16.5	8.5	7.4	6.7	0	41.6
1000	100	25% ↓	60	536.5	479.3	11.5	11.2	7.2	8.1	13.5	67.9	
↓	↓	↓	200	562.0	492.0	16.5	18.2	7.4	9.8			
10,000	10,000	25% ↓	60	536.5	479.3	8.5	5.5	7.2	5.3	2.4		
↓	↓	↓	200	562.0	492.0	12.5	10.5	7.4	6.6	2.5		

EFFECT OF OXIDIZER-FUEL RATIO ON DELIVERED VACUUM SPECIFIC IMPULSE AND CHARACTERISTIC VELOCITY EFFICIENCY FOR 15 DEG CONICAL NOZZLE/TRIPLET INJECTOR EMPLOYED IN FRDC ENGINE FIRINGS

CH₄ (g) - FLOX (82.6% F₂)

$P_C = 100 \text{ PSIA } (6.895 \times 10^5 \text{ N/m}^2)$ $(A/A_{MIN})_{EXIT} = 40$
 $r_t = 0.249 \text{ FT } (0.076 \text{ m})$ $(r_c/r_t) \approx 0$

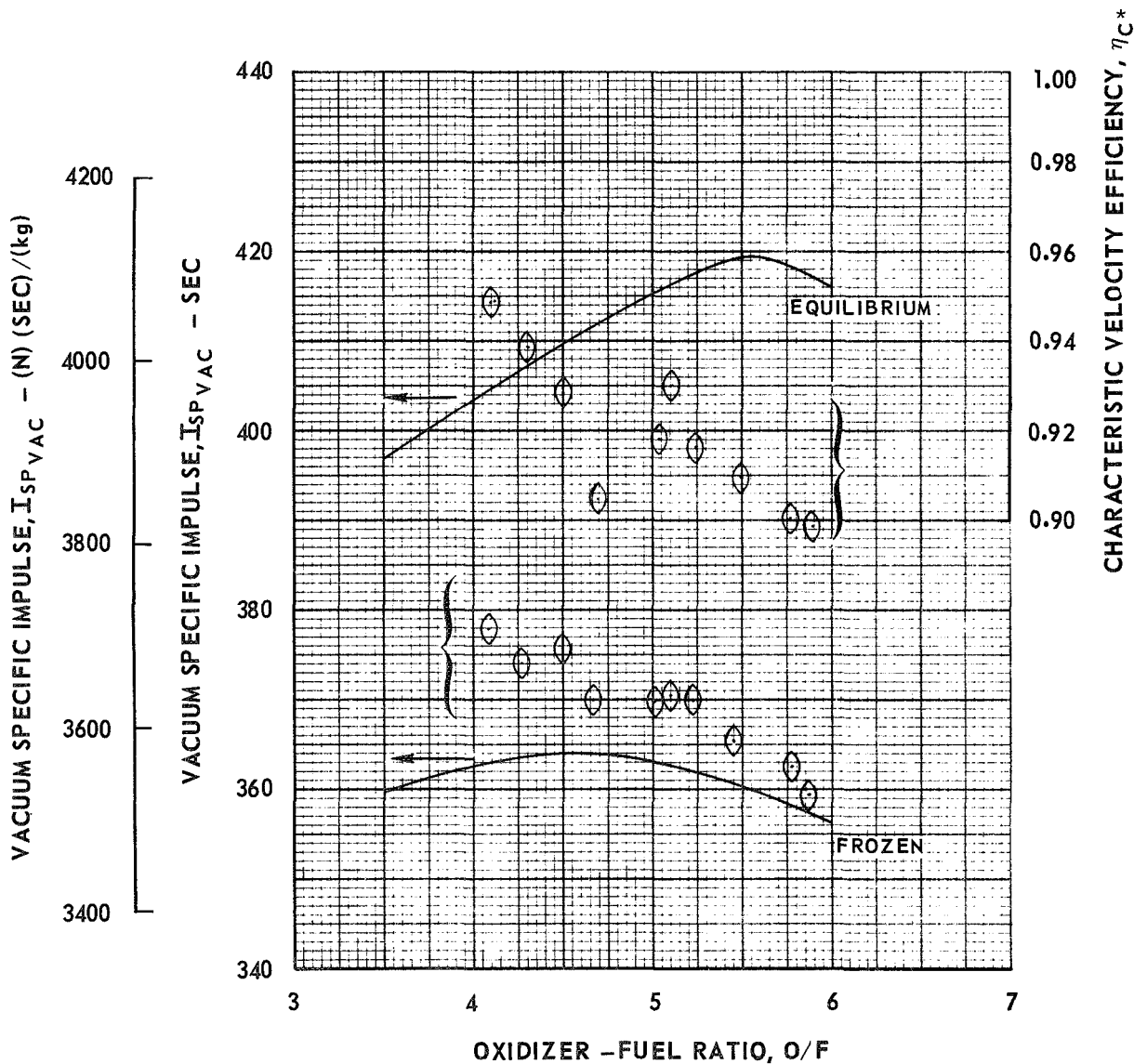


EFFECT OF OXIDIZER-FUEL RATIO ON DELIVERED VACUUM SPECIFIC IMPULSE AND CHARACTERISTIC VELOCITY EFFICIENCY FOR RL-10 NOZZLE/TRIPLET INJECTOR EMPLOYED IN FRDC ENGINE FIRINGS

CH₄ (g) - FLOX (82.6% F₂)

P_C = 100 PSIA (6.895 X 10⁵ N/m²) (A/A_{MIN})_{EXIT} = 40

r_t = 0.249 FT (0.076 m) (r_c / r_t) ≈ 0



EFFECT OF OXIDIZER-FUEL RATIO ON DELIVERED VACUUM SPECIFIC IMPULSE AND CHARACTERISTIC VELOCITY EFFICIENCY FOR 15 DEG CONICAL NOZZLE EMPLOYED IN ROCKETDYNE ENGINE FIRINGS

CH₄ (g) - FLOX (82.6% F₂)

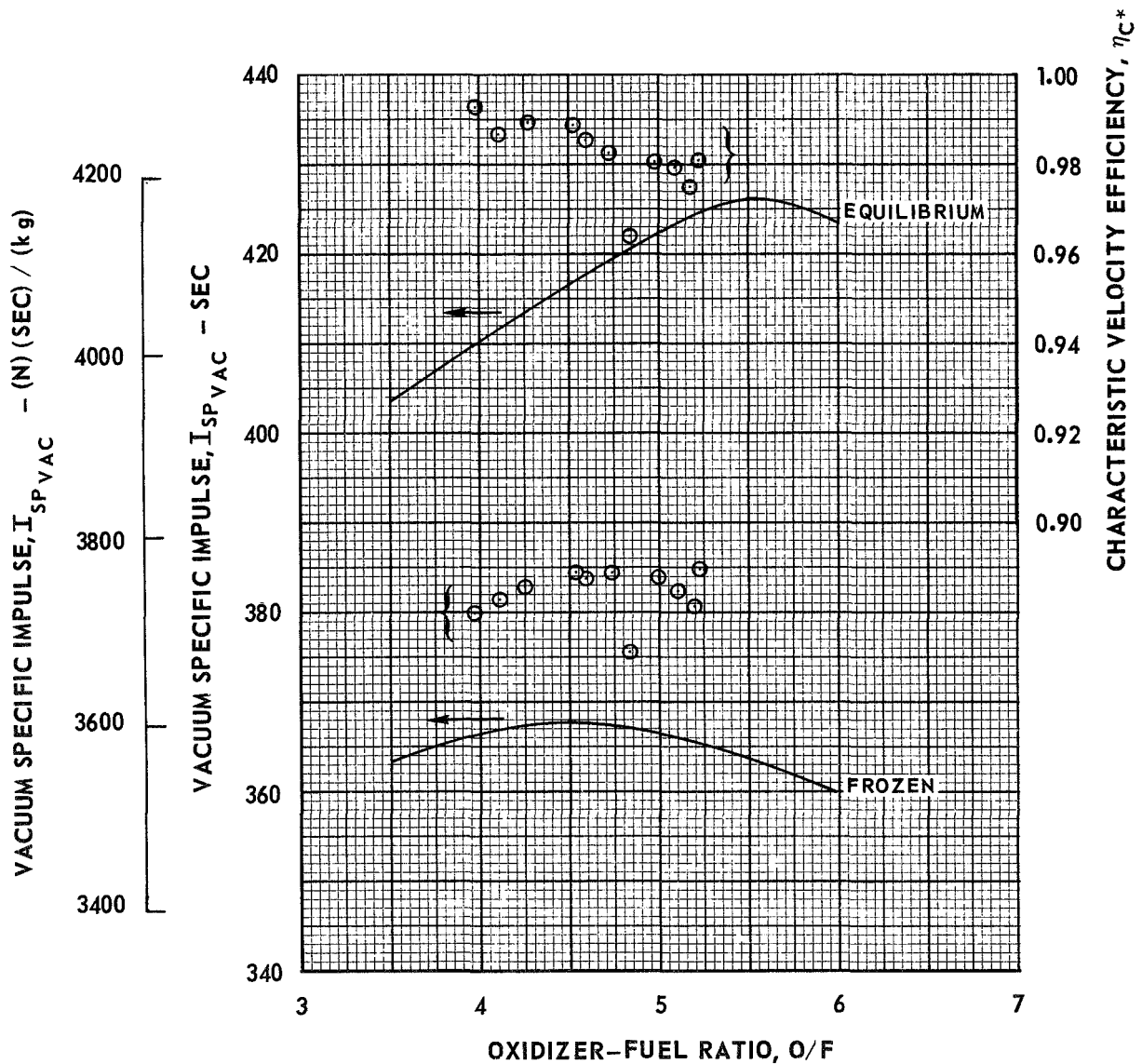
P_C = 100 PSIA (6.895 X 10⁵ N/m²)

(A/A_{MIN})_{EXIT} = 60

(r_c/r_t)_{DOWNSTREAM THROAT} = 3.635

(r_c/r_t)_{UPSTREAM THROAT} = 1.5

r_t = 0.175 FT (0.053 m)

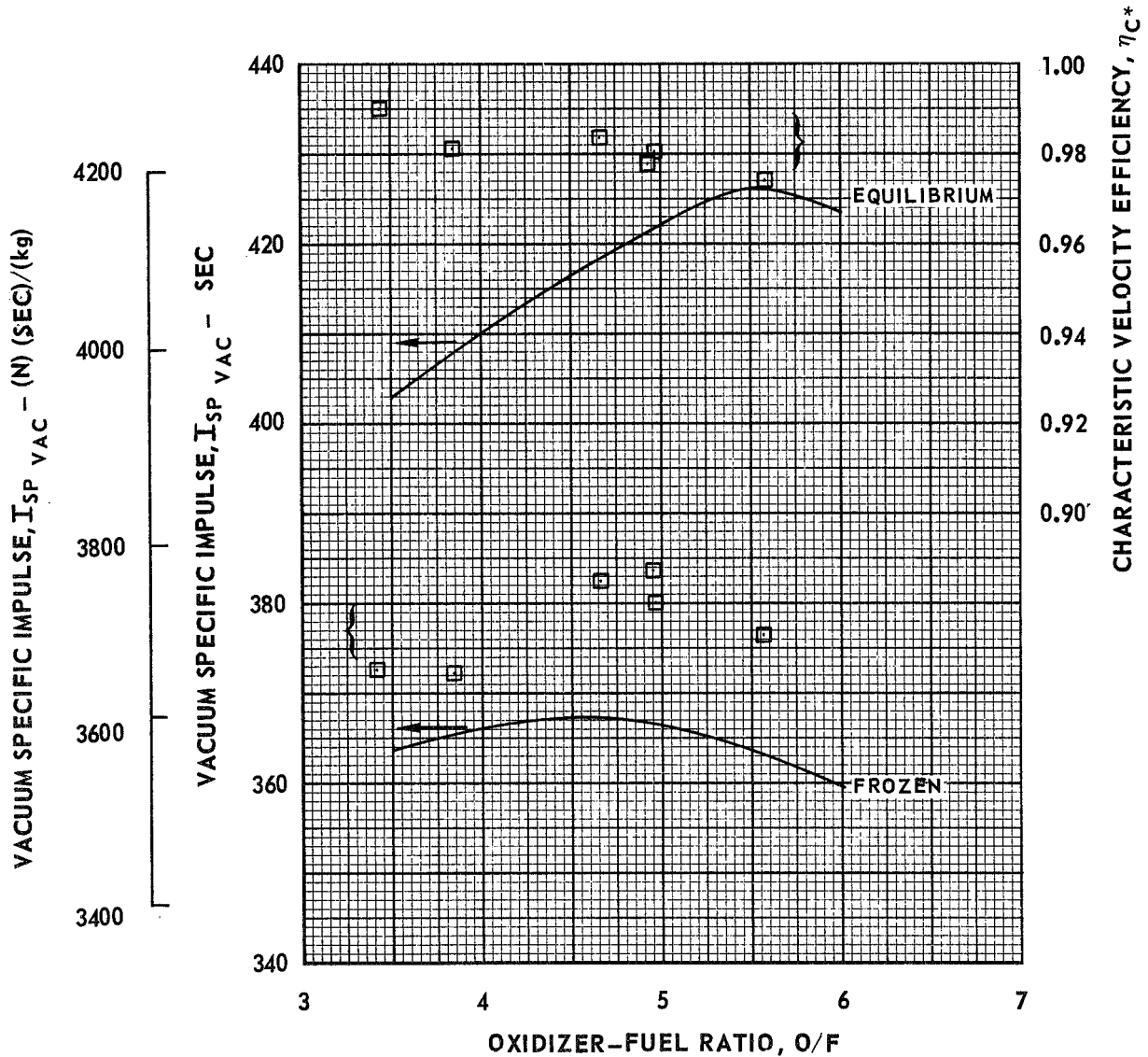


EFFECT OF OXIDIZER-FUEL RATIO ON DELIVERED VACUUM SPECIFIC IMPULSE AND CHARACTERISTIC VELOCITY EFFICIENCY FOR 70 PERCENT BELL CONTOUR EMPLOYED IN ROCKETDYNE ENGINE FIRINGS

CH₄ (g) - FLOX (82.6% F₂)

P_C = 100 PSIA (6.895 X 10⁵ N/m²) (A/A_{MIN})_{EXIT} = 60

(r_c/r_t)_{DOWNSTREAM THROAT} = 0.391 (r_c/r_t)_{UPSTREAM THROAT} = 1.5 r_t = 0.175 FT (0.053 m)



EFFECT OF OXIDIZER-FUEL RATIO ON DELIVERED VACUUM SPECIFIC IMPULSE AND CHARACTERISTIC VELOCITY EFFICIENCY FOR 15 DEGREE CONICAL NOZZLE EMPLOYED IN ROCKETDYNE ENGINE FIRINGS

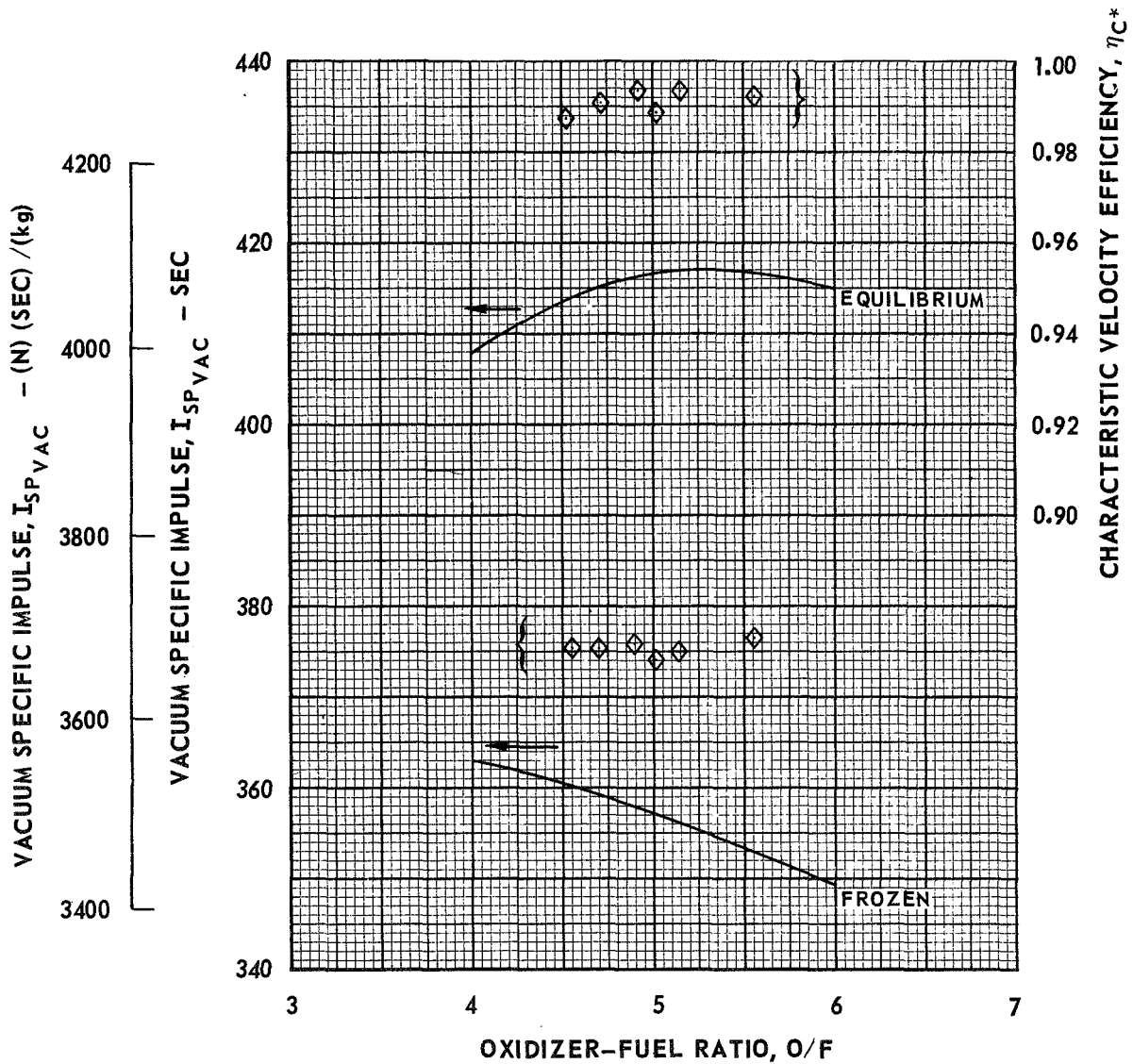
CH₄ (g) - FLOX (70.4% F₂)

P_C = 100 PSIA (6.895 X 10⁵ N/m²) (A/A_{MIN})_{EXIT} = 60

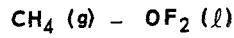
(r_c/r_t)_{DOWNSTREAM THROAT} = 3.635

(r_c/r_t)_{UPSTREAM THROAT} = 1.5

r_t = 0.175 FT (0.053 m)



EFFECT OF OXIDIZER-FUEL RATIO ON DELIVERED VACUUM SPECIFIC IMPULSE AND CHARACTERISTIC VELOCITY EFFICIENCY FOR 15 DEGREE CONICAL NOZZLE EMPLOYED IN ROCKETDYNE ENGINE FIRINGS

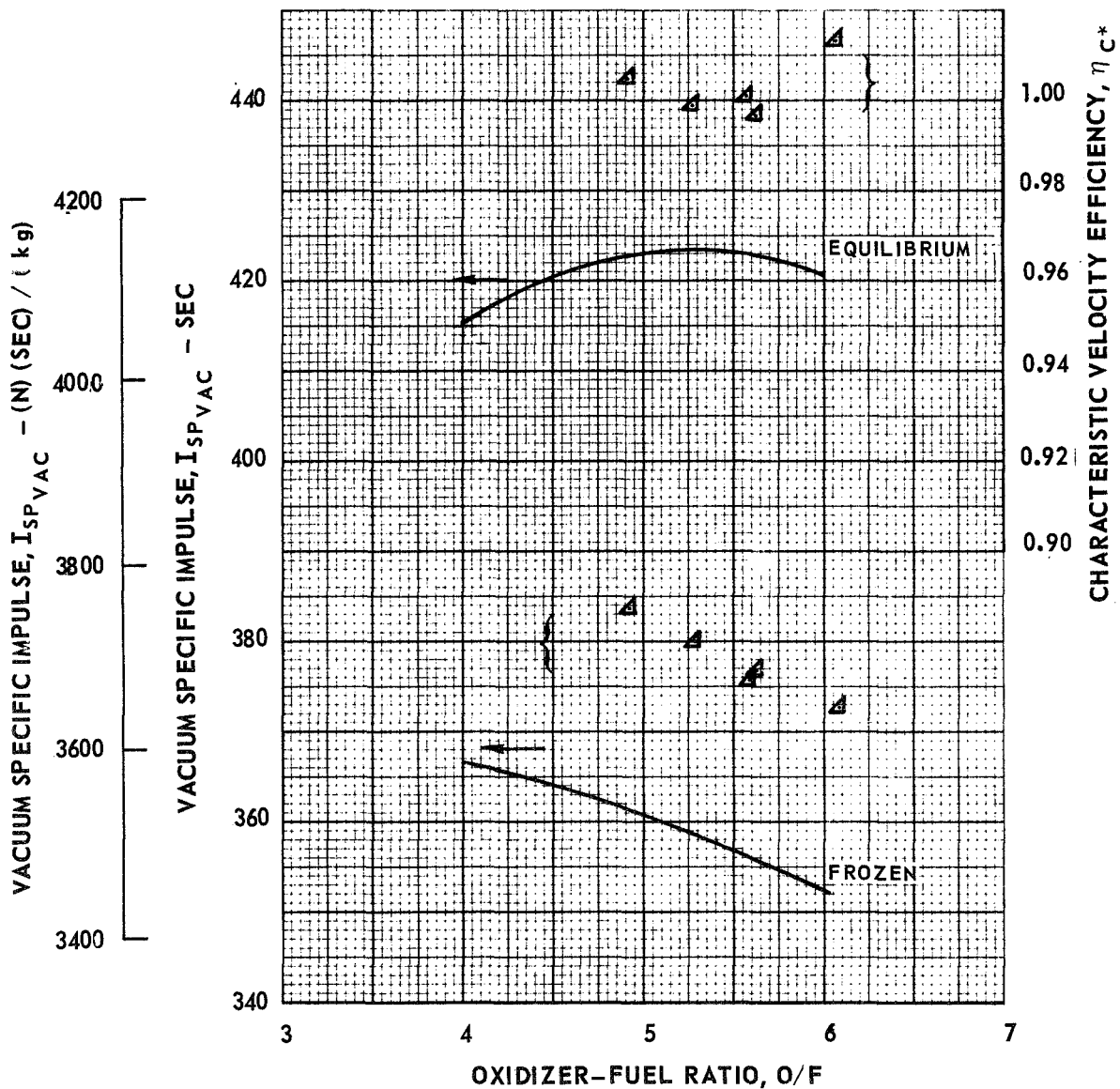


$P_C = 100 \text{ PSIA } (6.895 \times 10^5 \text{ N/m}^2) \quad (A/A_{MIN})_{EXIT} = 60$

$(r_c/r_t)_{DOWNSTREAM \ THROAT} = 3.635$

$(r_c/r_t)_{UPSTREAM \ THROAT} = 1.5$

$r_t = 0.175 \text{ FT } (0.053 \text{ m})$

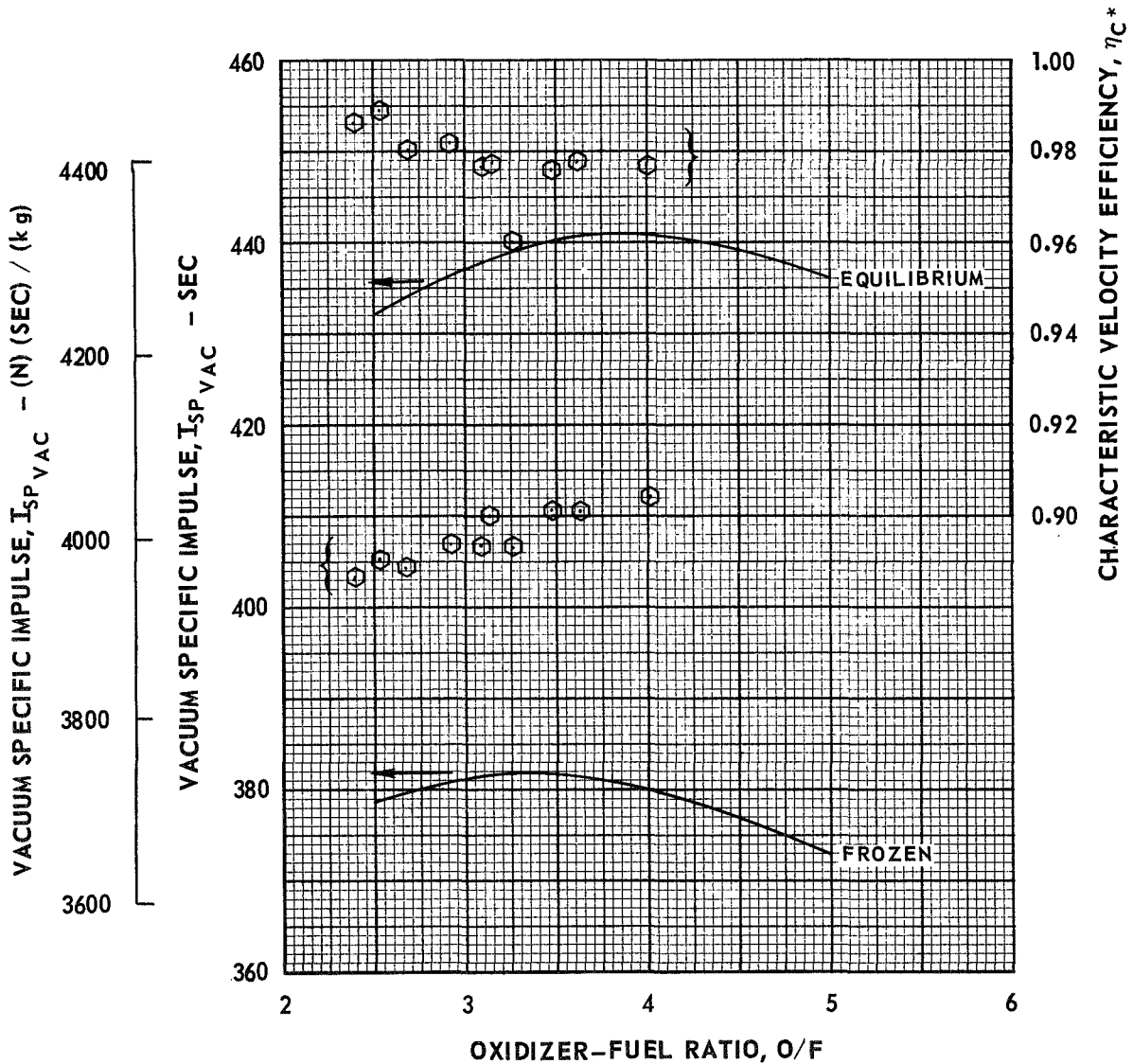


EFFECT OF OXIDIZER-FUEL RATIO ON DELIVERED VACUUM SPECIFIC IMPULSE AND CHARACTERISTIC VELOCITY EFFICIENCY FOR 15 DEGREE CONICAL NOZZLE EMPLOYED IN ROCKETDYNE FIRINGS

$B_2 H_6 (g) - FLOX (70.4\% F_2)$

$P_C = 100 \text{ PSIA } (6.895 \times 10^5 \text{ N/m}^2) \quad (A/A_{MIN})_{EXIT} = 60$

$(r_c/r_t)_{DOWNSTREAM \ THROAT} = 3.635 \quad (r_c/r_t)_{UPSTREAM \ THROAT} = 1.5 \quad r_t = 0.175 \text{ FT } (0.053 \text{ m})$

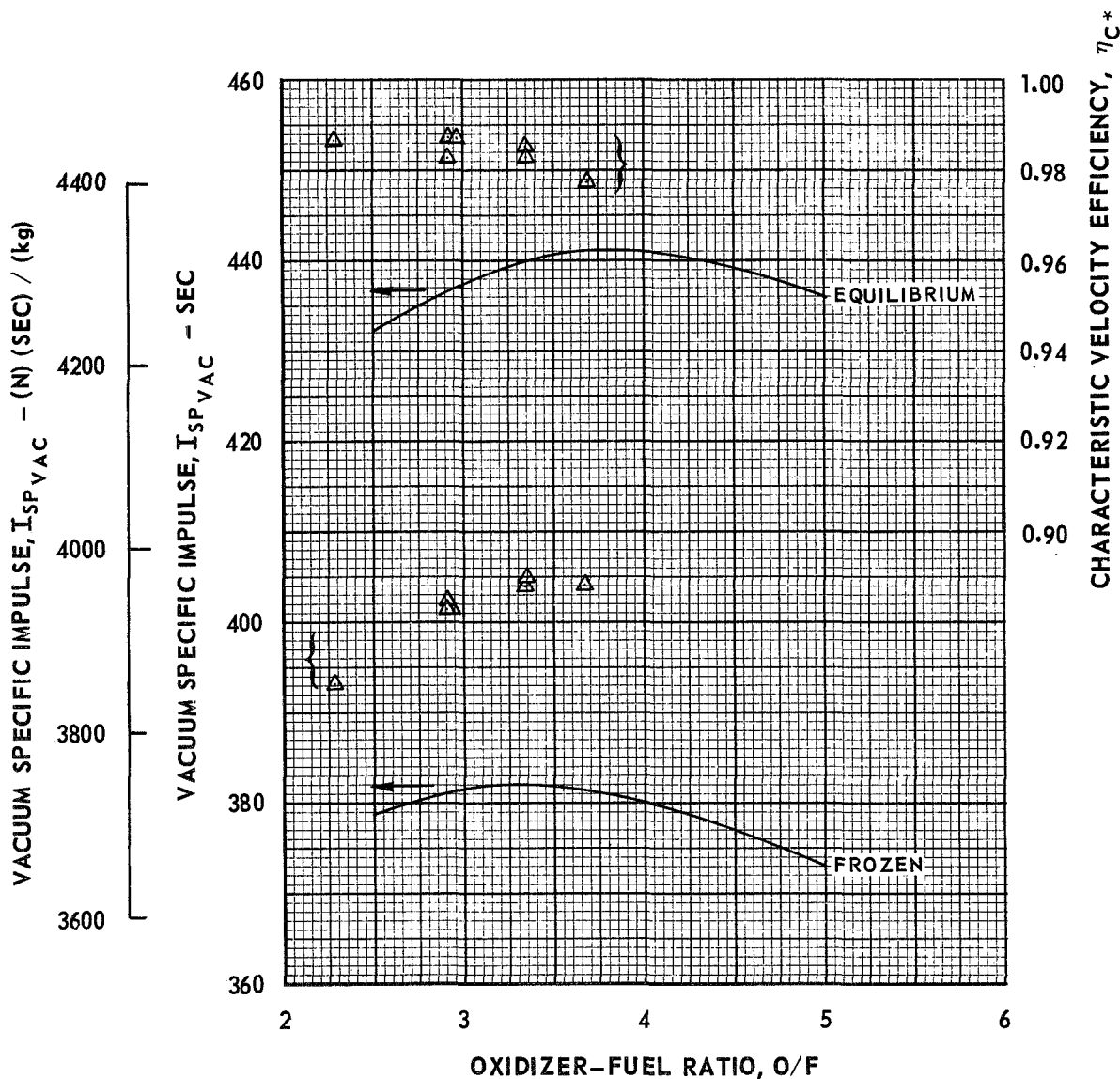


EFFECT OF OXIDIZER-FUEL RATIO ON DELIVERED VACUUM SPECIFIC IMPULSE AND CHARACTERISTIC VELOCITY EFFICIENCY FOR 70 PERCENT BELL CONTOUR EMPLOYED IN ROCKETDYNE ENGINE FIRINGS

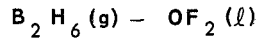
$B_2 H_6 (g) - FLOX (70.4\% F_2)$

$P_c = 100 \text{ PSIA } (6.895 \times 10^5 \text{ N/m}^2)$ $(A/A_{MIN})_{EXIT} = 60$

$(r_c/r_t)_{DOWNSTREAM \ THROAT} = 0.391$ $(r_c/r_t)_{UPSTREAM \ THROAT} = 1.5$ $r_t = 0.175 \text{ FT } (0.053 \text{ m})$

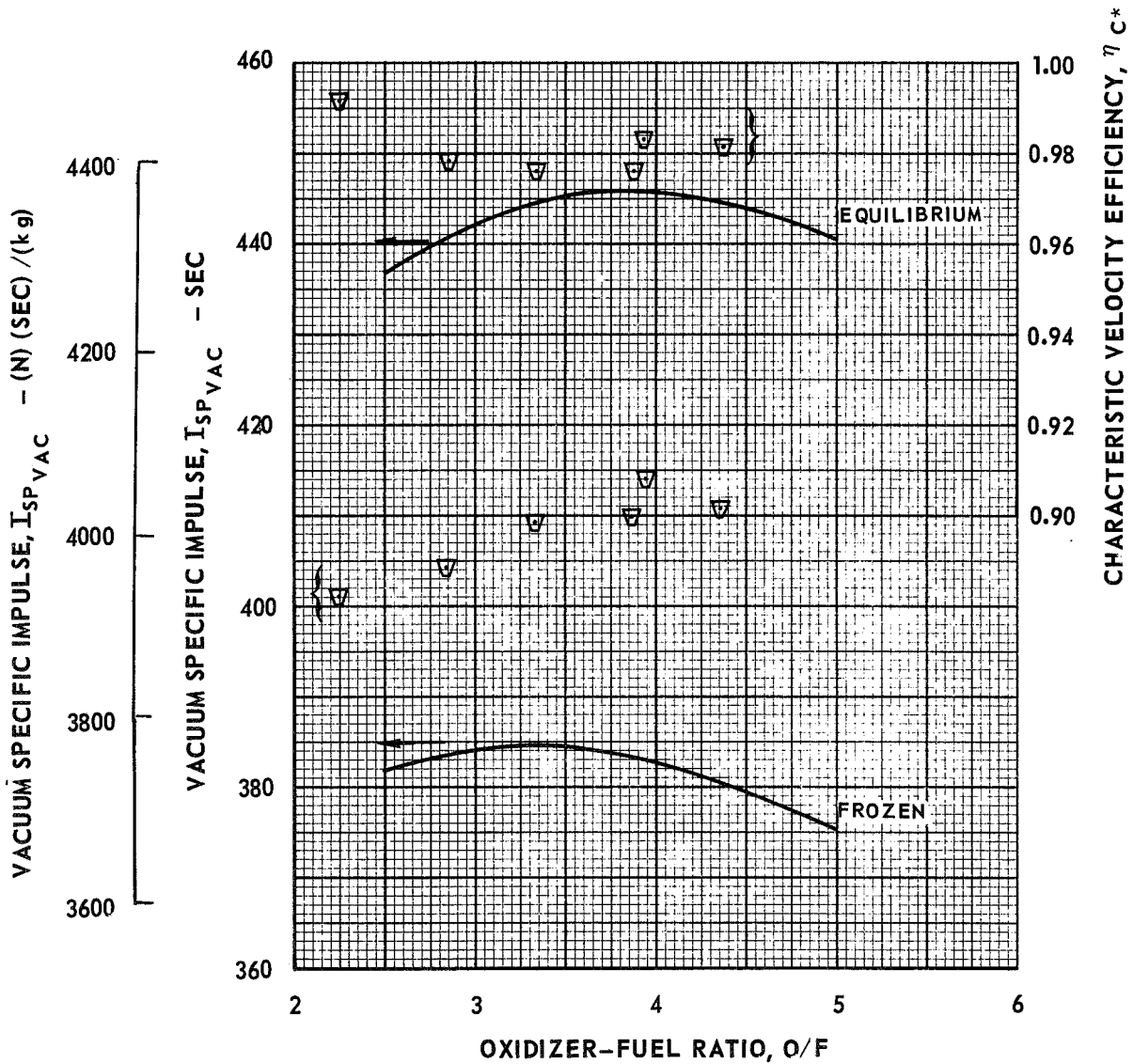


EFFECT OF OXIDIZER-FUEL RATIO ON DELIVERED VACUUM SPECIFIC IMPULSE AND CHARACTERISTIC VELOCITY EFFICIENCY FOR 15 DEGREE NOZZLE EMPLOYED IN ROCKETDYNE ENGINE FIRINGS

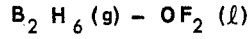


$P_c = 100 \text{ PSIA } (6.895 \times 10^5 \text{ N/m}^2) \quad (A/A_{MIN})_{EXIT} = 60$

$(r_c/r_t)_{DOWNSTREAM \ THROAT} = 3.635 \quad (r_c/r_t)_{UPSTREAM \ THROAT} = 1.5 \quad r_t = 0.175 (0.053 \text{ m})$

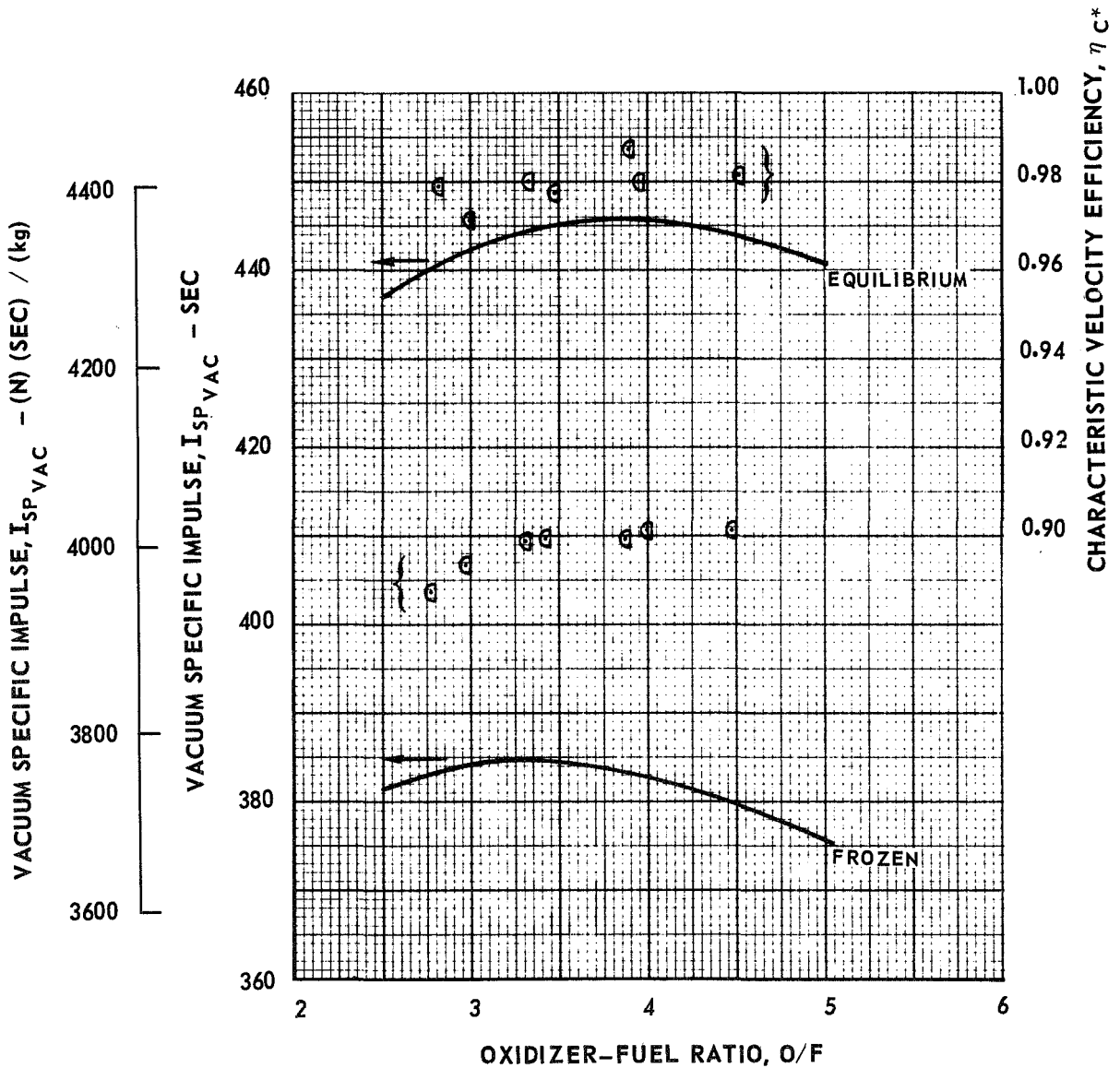


EFFECT OF OXIDIZER-FUEL RATIO ON DELIVERED VACUUM SPECIFIC IMPULSE AND CHARACTERISTIC VELOCITY EFFICIENCY FOR 70 PERCENT BELL CONTOUR EMPLOYED IN ROCKETDYNE ENGINE FIRINGS



$P_c = 100 \text{ PSIA } (6.895 \times 10^5 \text{ N/m}^2) \quad (A/A_{MIN})_{EXIT} = 60$

$(r_c/r_t)_{DOWNSTREAM \ THROAT} = 0.391 \quad (r_c/r_t)_{UPSTREAM \ THROAT} = 1.5 \quad r_t = 0.175 \text{ FT } (0.053 \text{ m})$

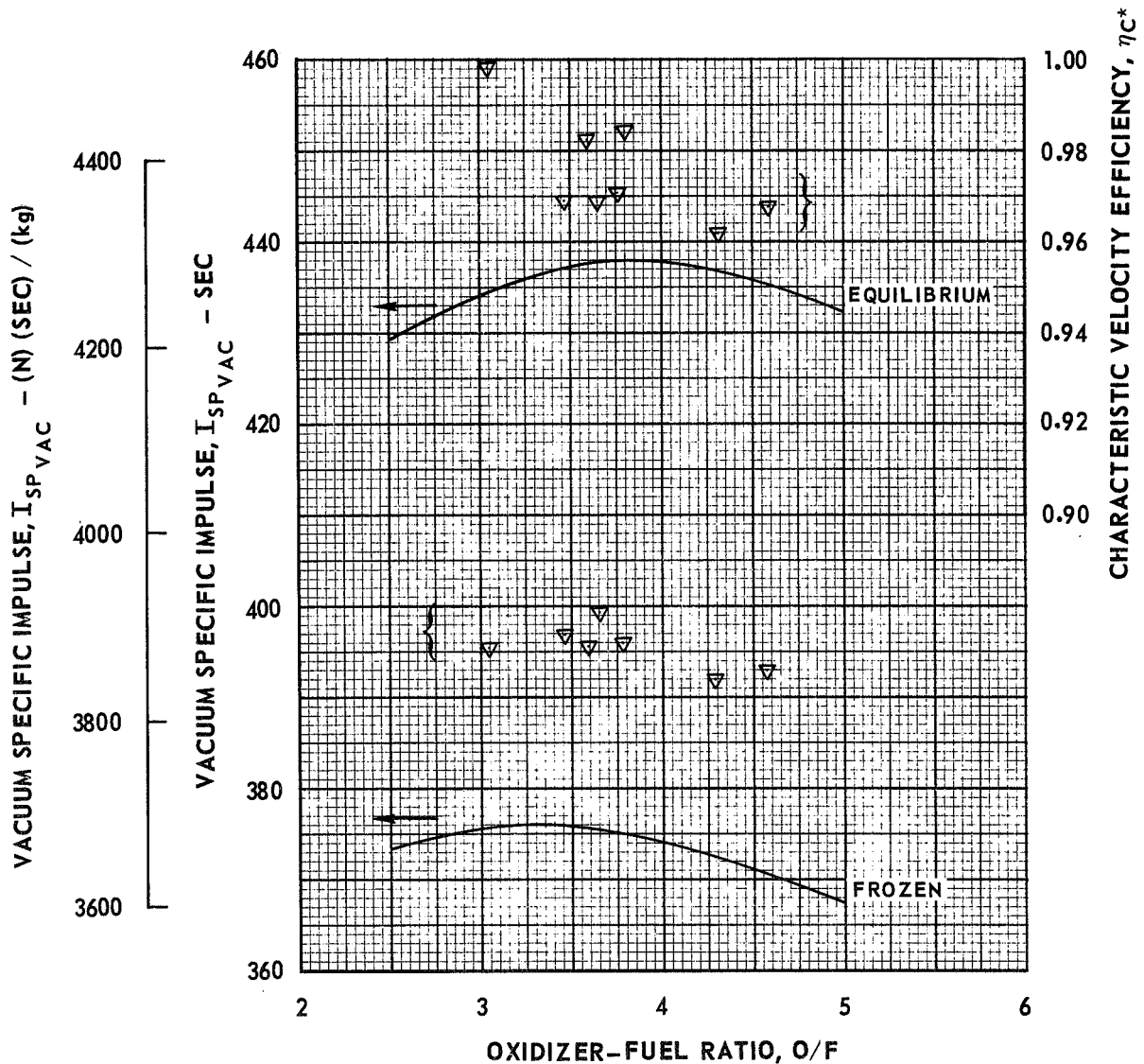


EFFECT OF OXIDIZER-FUEL RATIO ON DELIVERED VACUUM SPECIFIC AND CHARACTERISTIC VELOCITY EFFICIENCY FOR 15 DEGREE CONICAL NOZZLE EMPLOYED IN ROCKETDYNE ENGINE FIRINGS

$B_2 H_6 (g) - FLOX (70.4\% F_2)$

$P_C = 50 \text{ PSIA } (3.448 \times 10^5 \text{ N/m}^2) \quad (A/A_{MIN})_{EXIT} = 60$

$(r_c/r_t)_{DOWNSTREAM \ THROAT} = 3.635 \quad (r_c/r_t)_{UPSTREAM \ THROAT} = 1.5 \quad r_t = 0.175 \text{ FT } (0.053 \text{ m})$

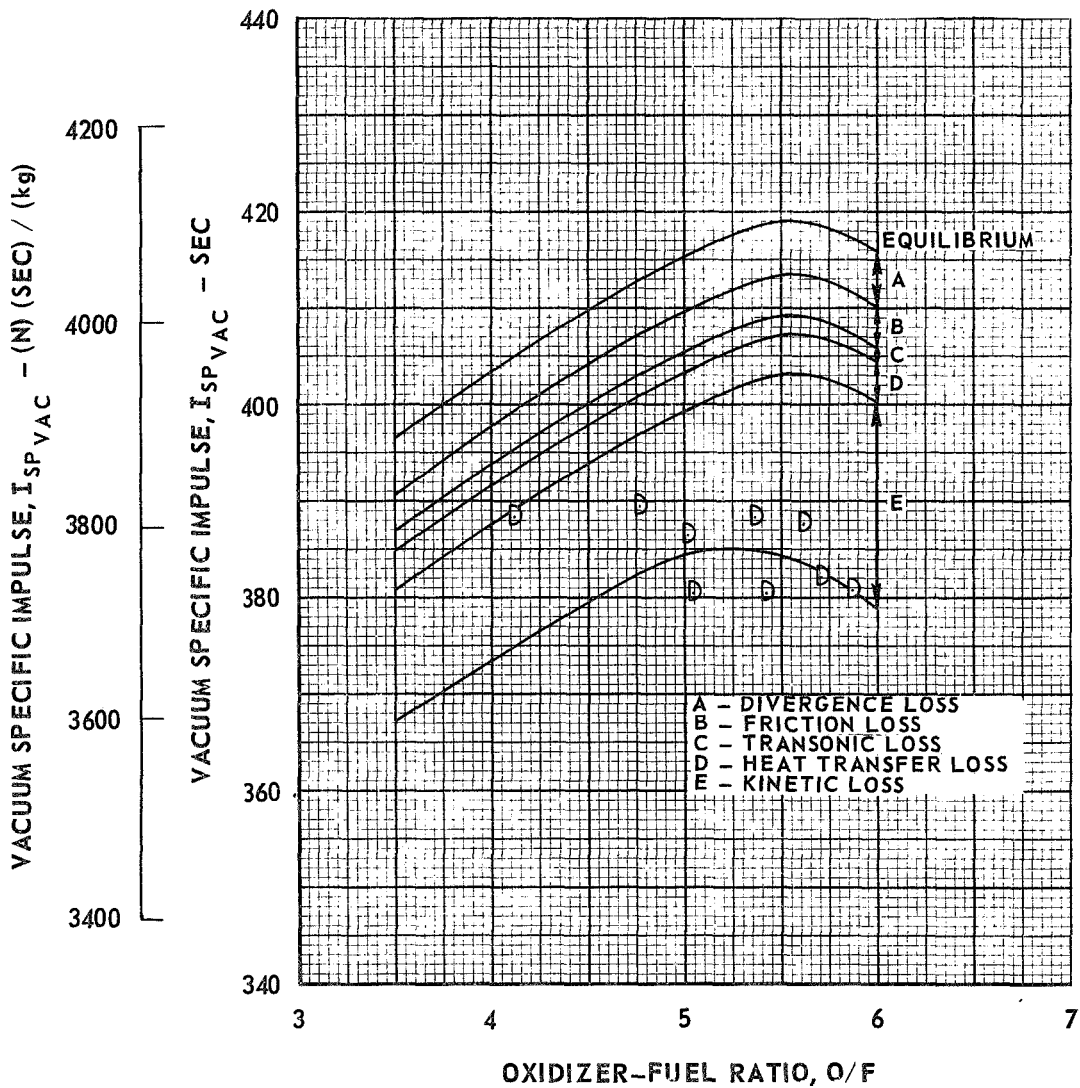


COMPARISON OF ANALYTICAL AND EXPERIMENTAL PERFORMANCE FOR 15 DEGREE CONICAL NOZZLE/TRIPLET INJECTOR

CH_4 (g) - FLOX (82.6% F_2)

$P_c = 100 \text{ PSIA } (6.895 \times 10^5 \text{ N/m}^2) \quad (A/A_{\text{MIN}})_{\text{EXIT}} = 40$
 $r_t = 0.249 \text{ FT } (0.076 \text{ m}) \quad (r_c/r_t) \approx 0$

NOTE: KINETIC IMPULSE LOSS CALCULATED USING MECHANISM AND RATES OF TABLE I
 COMBUSTION EFFICIENCY BASED ON C^* CORRELATION
 SYMBOLS REPRESENT DATA ADJUSTED BY EFFECTIVE C^* EFFICIENCY



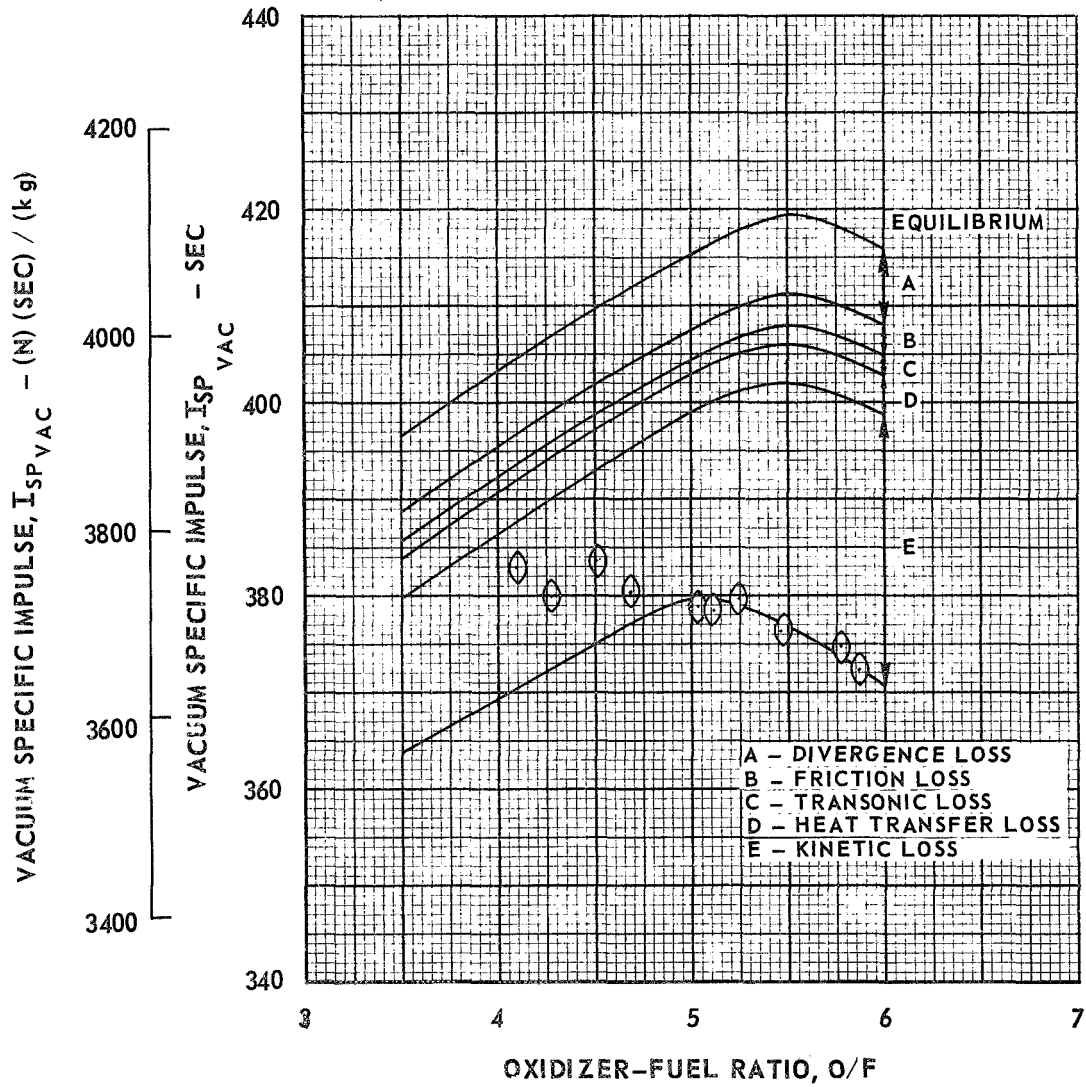
COMPARISON OF ANALYTICAL AND EXPERIMENTAL PERFORMANCE FOR RL-10 NOZZLE /TRIPLET INJECTOR

CH_4 (g) - FLOX (82.6% F_2)

$P_C = 100$ PSIA (6.895×10^5 N/m²) $(A/A_{\text{MIN}})_{\text{EXIT}} = 40$

$r_t = 0.249$ FT (0.076 m) $(r_c/r_t) \approx 0$

NOTE: KINETIC IMPULSE LOSS CALCULATED USING MECHANISM AND RATES OF TABLE I
COMBUSTION EFFICIENCY BASED ON C* CORRELATION
SYMBOLS REPRESENT DATA ADJUSTED BY EFFECTIVE C* EFFICIENCY



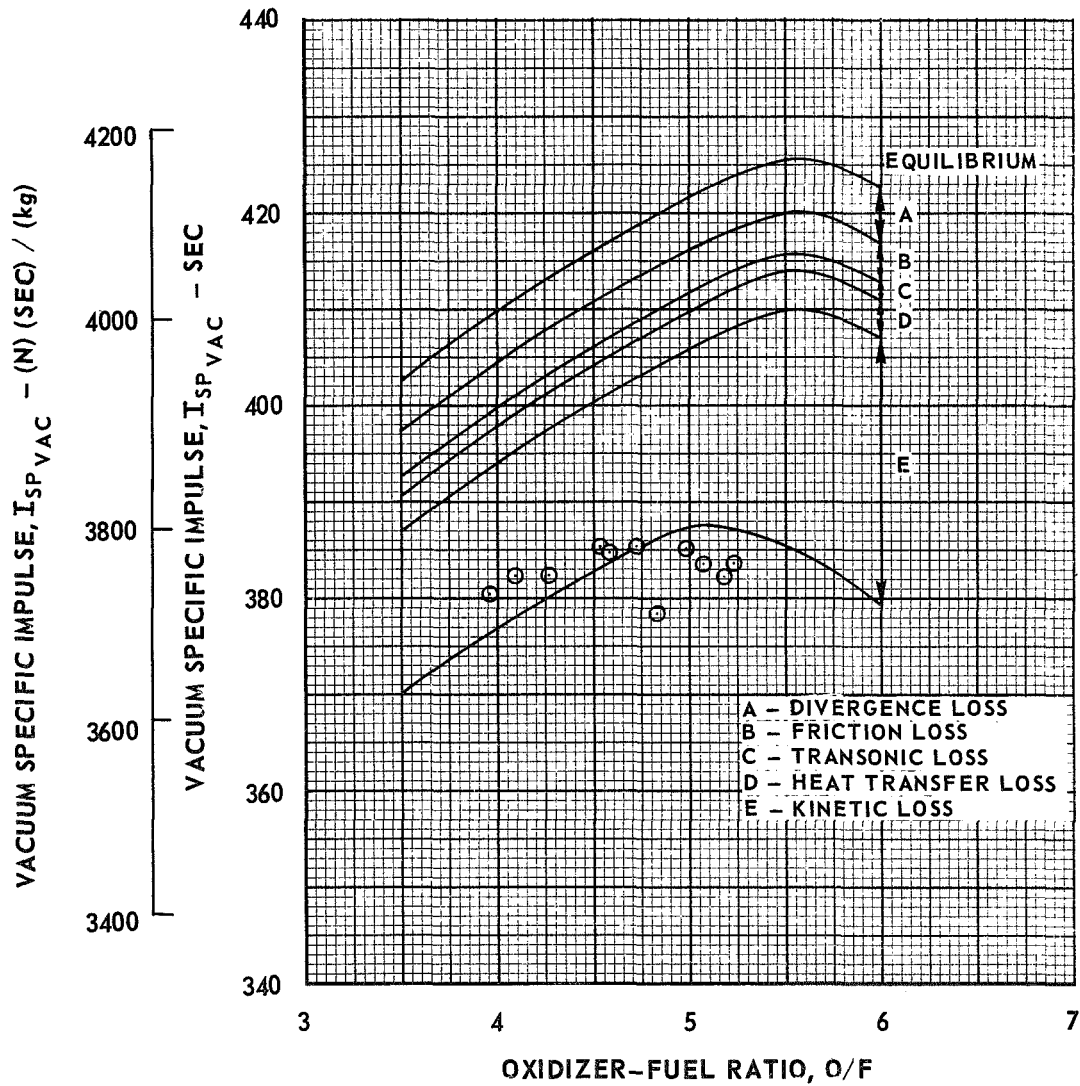
COMPARISON OF ANALYTICAL AND EXPERIMENTAL PERFORMANCE FOR ROCKETDYNE 15 DEGREE CONICAL NOZZLE

CH_4 (g) - FLOX (82.6% F_2)

$P_C = 100 \text{ PSIA } (6.895 \times 10^5 \text{ N/m}^2) \quad (A/A_{\text{MIN}})_{\text{EXIT}} = 60$

$(r_c/r_t)_{\text{DOWNSTREAM THROAT}} = 3.635 \quad (r_c/r_t)_{\text{UPSTREAM THROAT}} = 1.5 \quad r_t = 0.175 \text{ FT } (0.053 \text{ m})$

NOTE: KINETIC IMPULSE LOSS CALCULATED USING MECHANISM AND RATES OF TABLE I
COMBUSTION EFFICIENCY BASED ON C^* CORRELATION SYMBOLS REPRESENT
DATA ADJUSTED BY EFFECTIVE C^* EFFICIENCY



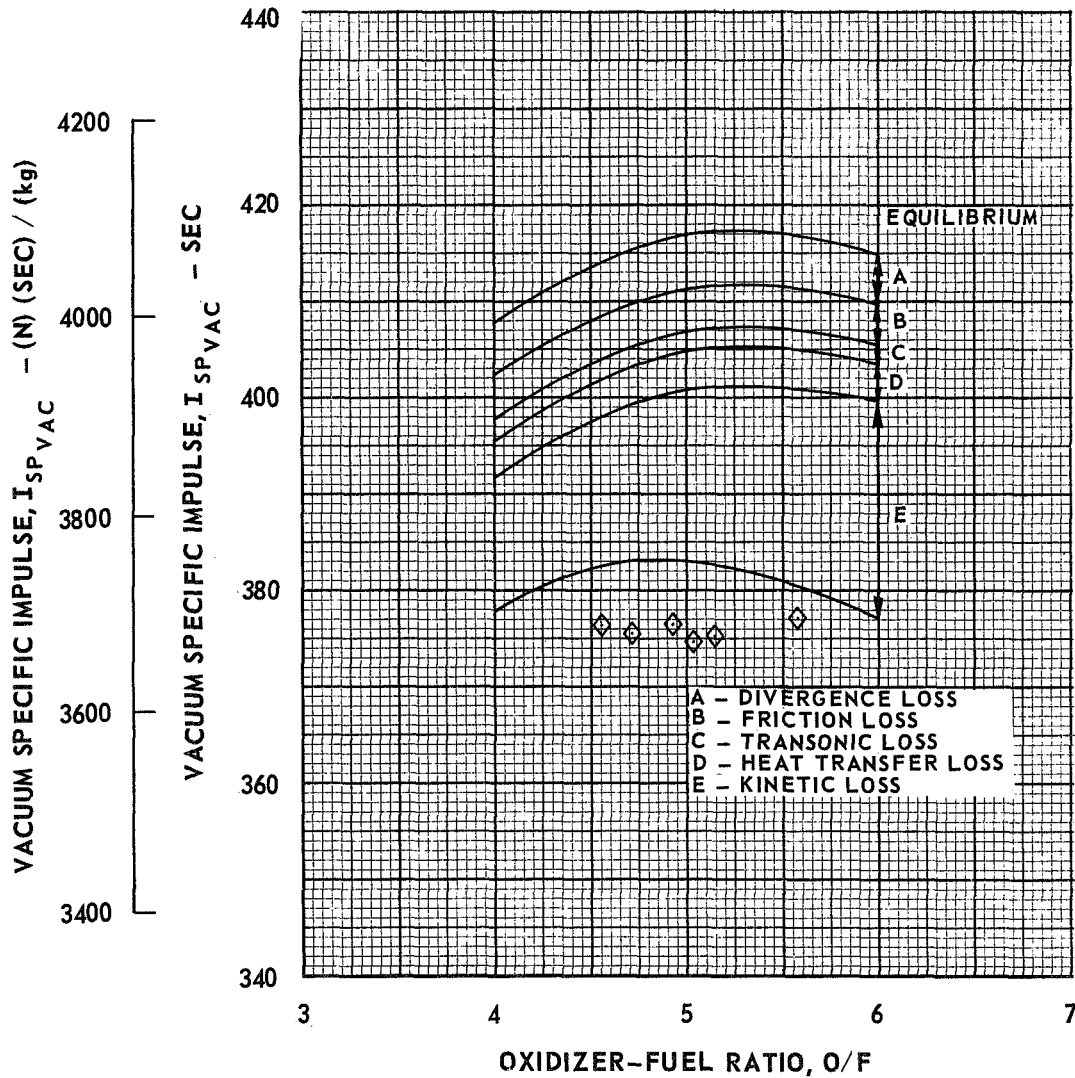
COMPARISON OF ANALYTICAL AND EXPERIMENTAL PERFORMANCE FOR ROCKETDYNE 15 DEGREE CONICAL NOZZLE

CH_4 (g) - FLOX (70.4% F_2)

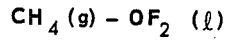
$P_c = 100 \text{ PSIA } (6.895 \times 10^5 \text{ N/m}^2) \quad (A/A_{\text{MIN}})_{\text{EXIT}} = 60$

$(r_c/r_t)_{\text{DOWNSTREAM THROAT}} = 3.635 \quad (r_c/r_t)_{\text{UPSTREAM THROAT}} = 1.5 \quad r_t = 0.175 \text{ FT } (0.053 \text{ m})$

NOTE: KINETIC IMPULSE LOSS CALCULATED USING MECHANISM AND RATES OF TABLE I
COMBUSTION EFFICIENCY BASED ON C^* CORRELATION
SYMBOLS REPRESENT DATA ADJUSTED BY EFFECTIVE C^* EFFICIENCY



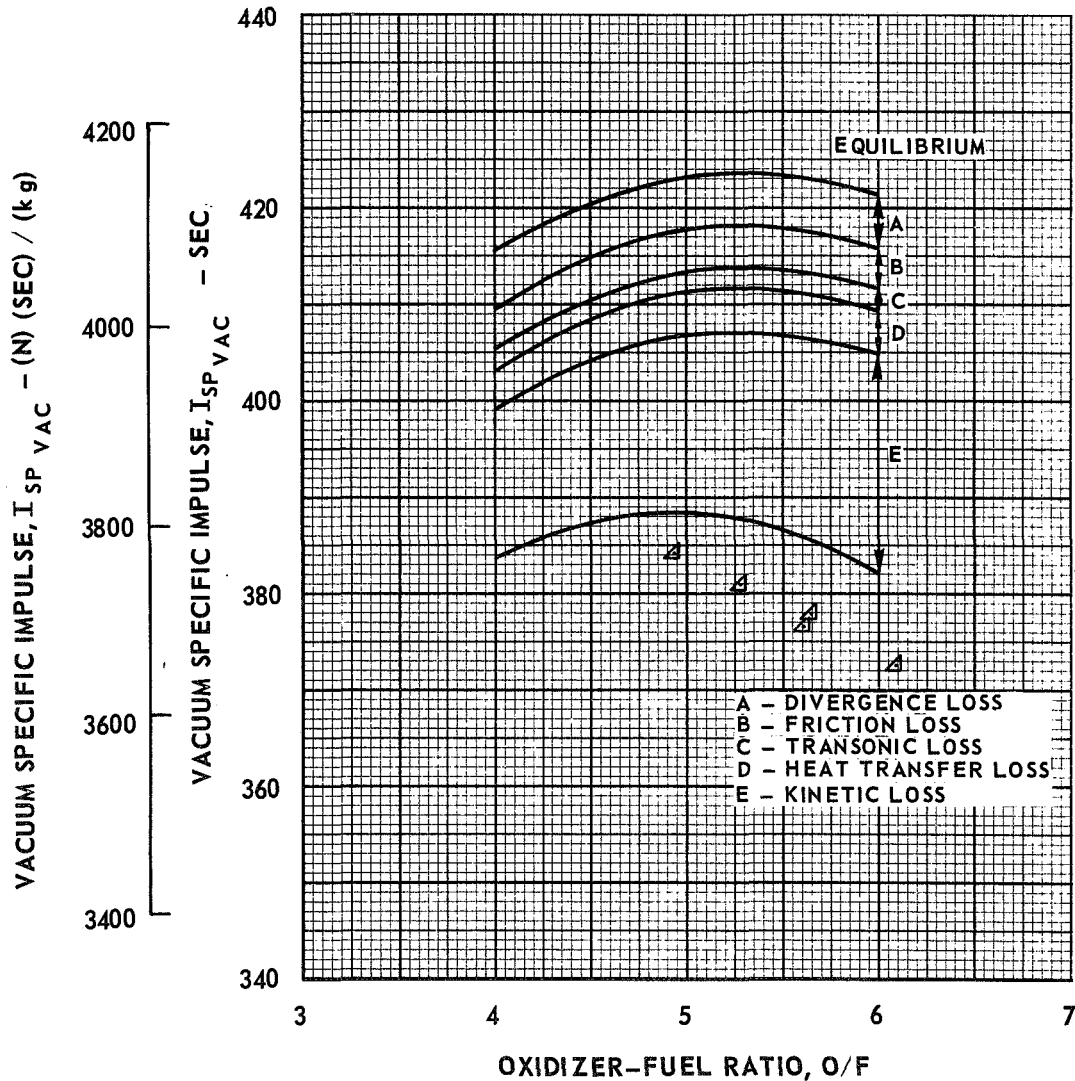
COMPARISON OF ANALYTICAL AND EXPERIMENTAL PERFORMANCE FOR ROCKETDYNE 15 DEGREE CONICAL NOZZLE



$P_C = 100 \text{ PSIA } (6.895 \times 10^5 \text{ N/m}^2) \quad (A/A_{\text{MIN}})_{\text{EXIT}} = 60$

$(r_c/r_t)_{\text{DOWNSTREAM THROAT}} = 3.635 \quad (r_c/r_t)_{\text{UPSTREAM THROAT}} = 1.5 \quad r_t = 0.175 \text{ FT } (0.053 \text{ m})$

NOTE: KINETIC IMPULSE LOSS CALCULATED USING MECHANISM AND RATES OF TABLE I
COMBUSTION EFFICIENCY BASED ON C* CORRELATION SYMBOLS REPRESENT
DATA ADJUSTED BY EFFECTIVE C* EFFICIENCY



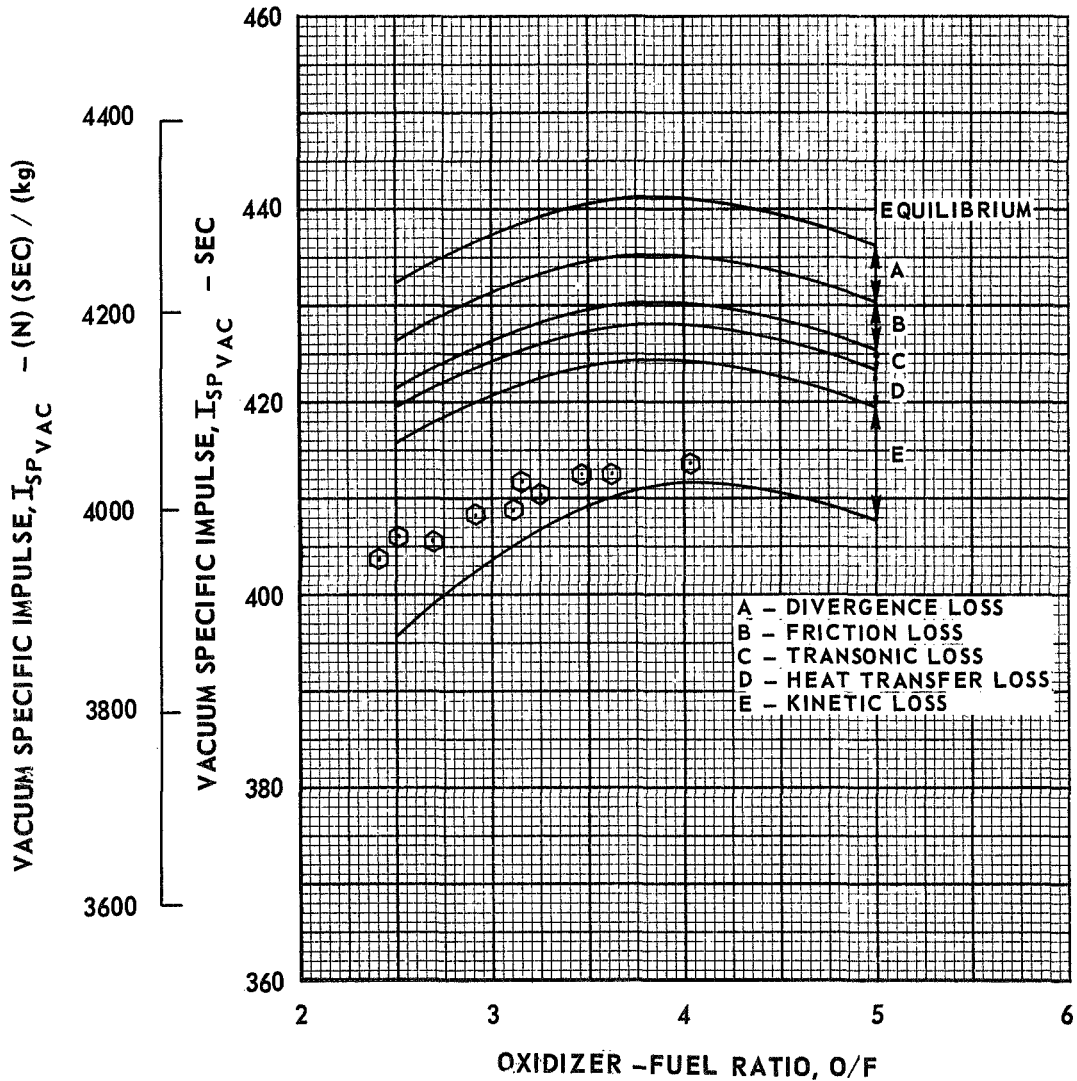
COMPARISON OF ANALYTICAL AND EXPERIMENTAL PERFORMANCE FOR ROCKETDYNE 15 DEGREE CONICAL NOZZLE

$B_2 H_6$ (g) - FLOX (70.4% F_2)

$P_C = 100$ PSIA (6.895×10^5 N/m²) $(A/A_{MIN})_{EXIT} = 60$

$(r_c/r_t)_{DOWNSTREAM THROAT} = 3.635$ $(r_c/r_t)_{UPSTREAM THROAT} = 1.5$ $r_t = 0.175$ FT (0.053 m)

NOTE: KINETIC IMPULSE LOSS CALCULATED USING MECHANISM AND RATES OF TABLE I
 COMBUSTION EFFICIENCY BASED ON C* CORRELATION
 SYMBOLS REPRESENT DATA ADJUSTED BY EFFECTIVE C* EFFICIENCY



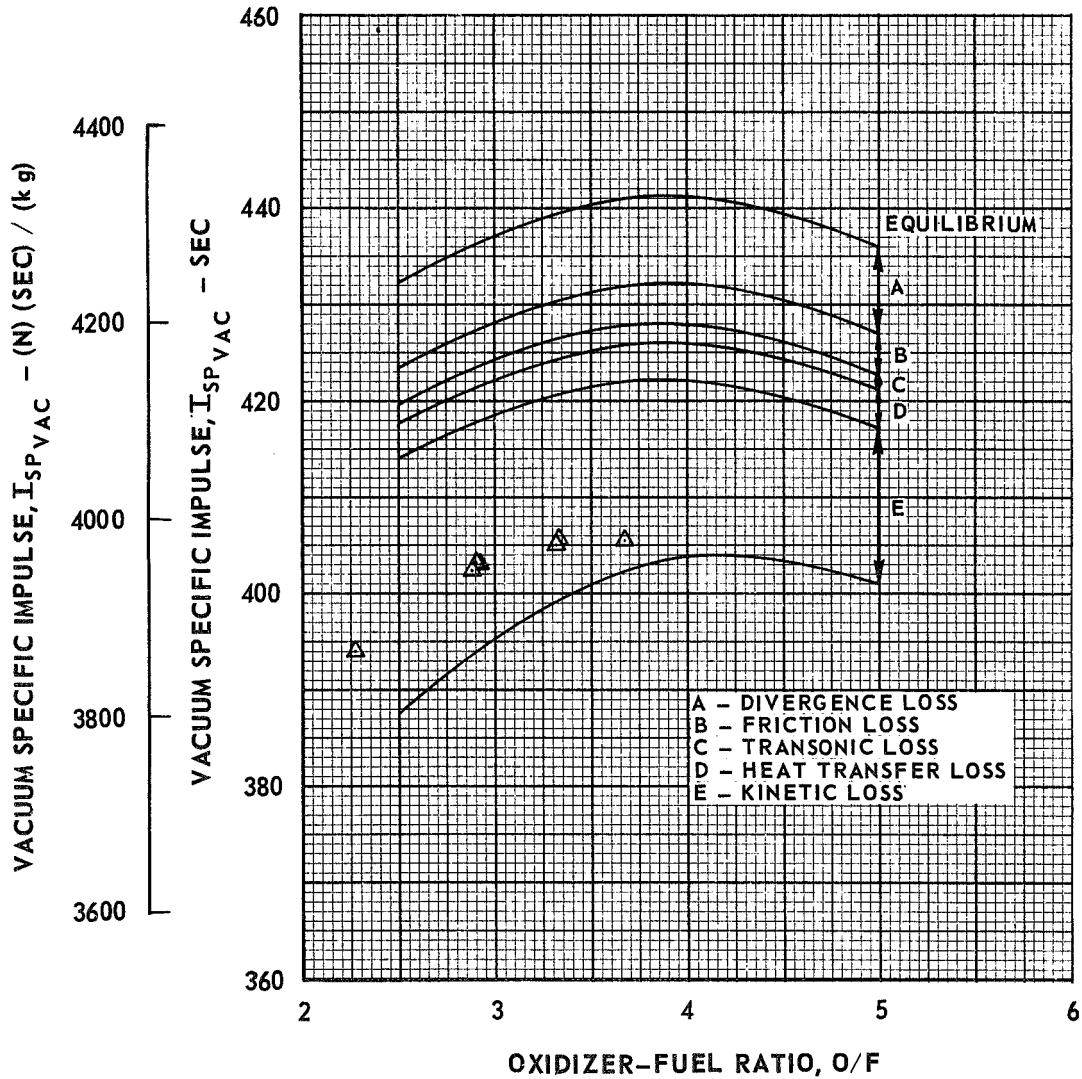
COMPARISON OF ANALYTICAL AND EXPERIMENTAL PERFORMANCE FOR ROCKETDYNE 70 PERCENT BELL CONTOUR

$B_2 H_6 (g) - FLOX (70.4\% F_2)$

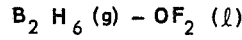
$P_C = 100 \text{ PSIA } (6.895 \times 10^5 \text{ N/m}^2) \quad (A/A_{MIN})_{EXIT} = 60$

$(r_c/r_t)_{DOWNSTREAM \ THROAT} = 0.391 \quad (r_c/r_t)_{UPSTREAM \ THROAT} = 1.5 \quad r_t = 0.175 \text{ FT } (0.053 \text{ m})$

NOTE: KINETIC IMPULSE LOSS CALCULATED USING MECHANISM AND RATES OF TABLE I
COMBUSTION EFFICIENCY BASED ON C* CORRELATION
SYMBOLS REPRESENT DATA ADJUSTED BY EFFECTIVE C* EFFICIENCY



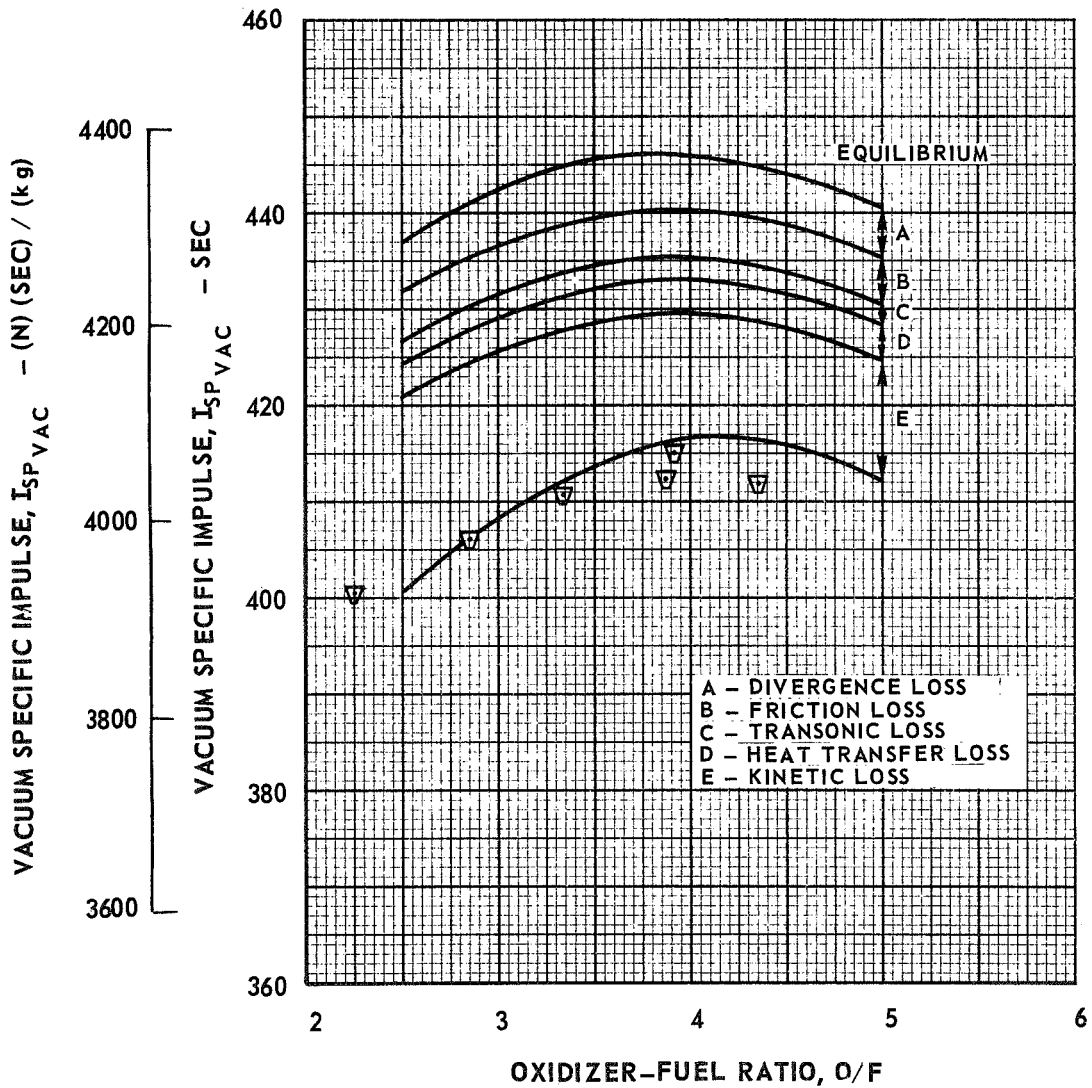
COMPARISON OF ANALYTICAL AND EXPERIMENTAL PERFORMANCE
FOR ROCKETDYNE 15 DEGREE CONICAL NOZZLE



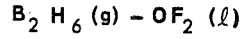
$P_C = 100 \text{ PSIA } (6.895 \times 10^5 \text{ N/m}^2) \quad (A/A_{MIN})_{EXIT} = 60$

$(r_c/r_t)_{DOWNSTREAM \ THROAT} = 3.635 \quad (r_c/r_t)_{UPSTREAM \ THROAT} = 1.5 \quad r_t = 0.175 \text{ FT } (0.053 \text{ m})$

NOTE: KINETIC IMPULSE LOSS CALCULATED USING MECHANISM AND RATES OF TABLE I
COMBUSTION EFFICIENCY BASED ON C* CORRELATION
SYMBOLS REPRESENT DATA ADJUSTED BY EFFECTIVE C* EFFICIENCY



COMPARISON OF ANALYTICAL AND EXPERIMENTAL PERFORMANCE
FOR ROCKETDYNE 70 PERCENT BELL CONTOUR



$P_C = 100 \text{ PSIA } (6.895 \times 10^5 \text{ N/m}^2)$

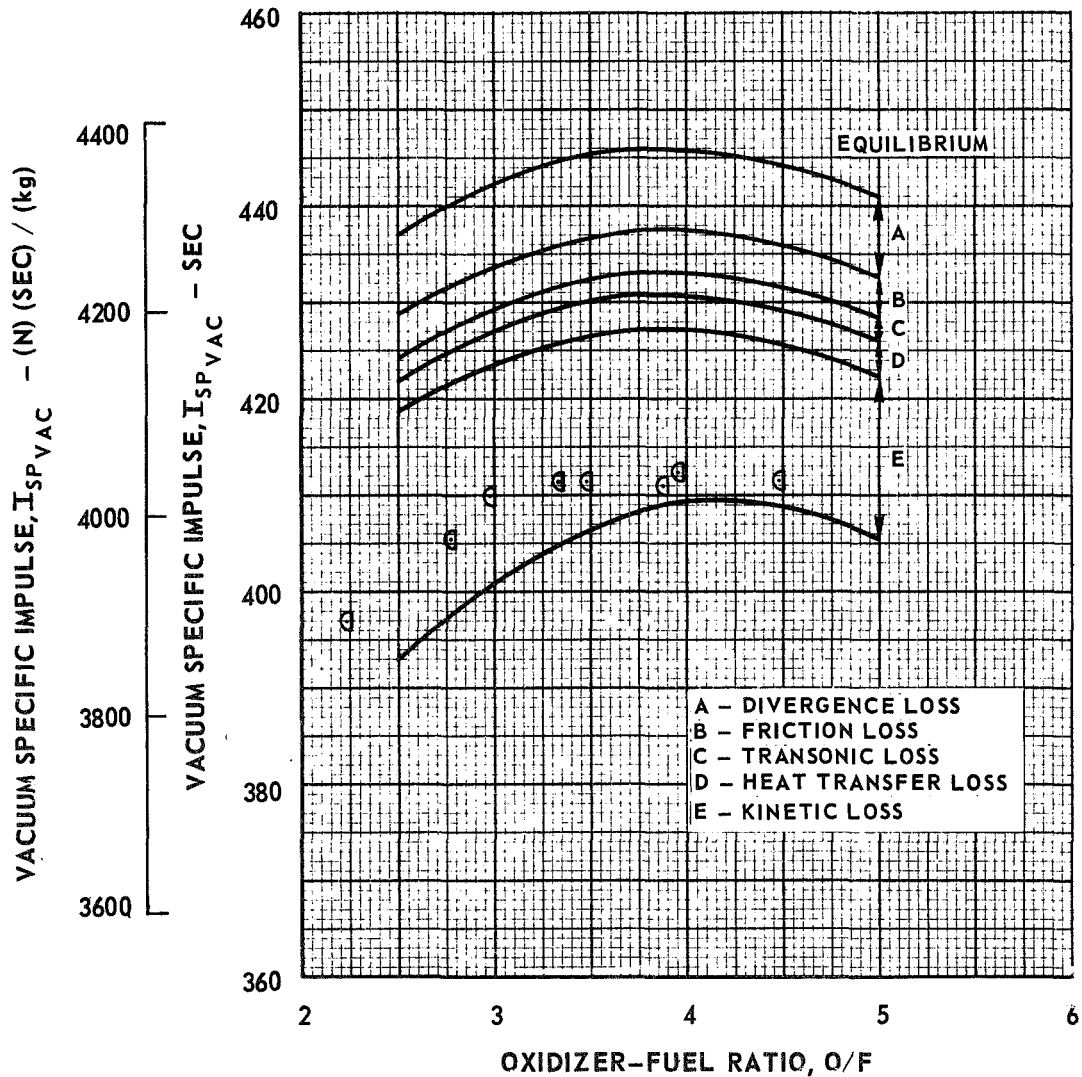
$(A/A_{MIN})_{EXIT} = 60$

$(r_c/r_t)_{DOWNSTREAM \ THROAT} = 0.391$

$(r_c/r_t)_{UPSTREAM \ THROAT} = 1.5$

$r_t = 0.175 \text{ FT } (0.053 \text{ m})$

NOTE: KINETIC IMPULSE LOSS CALCULATED USING MECHANISM AND RATES OF TABLE I
COMBUSTION EFFICIENCY BASED ON C* CORRELATION
SYMBOLS REPRESENT DATA ADJUSTED BY EFFECTIVE C* EFFICIENCY



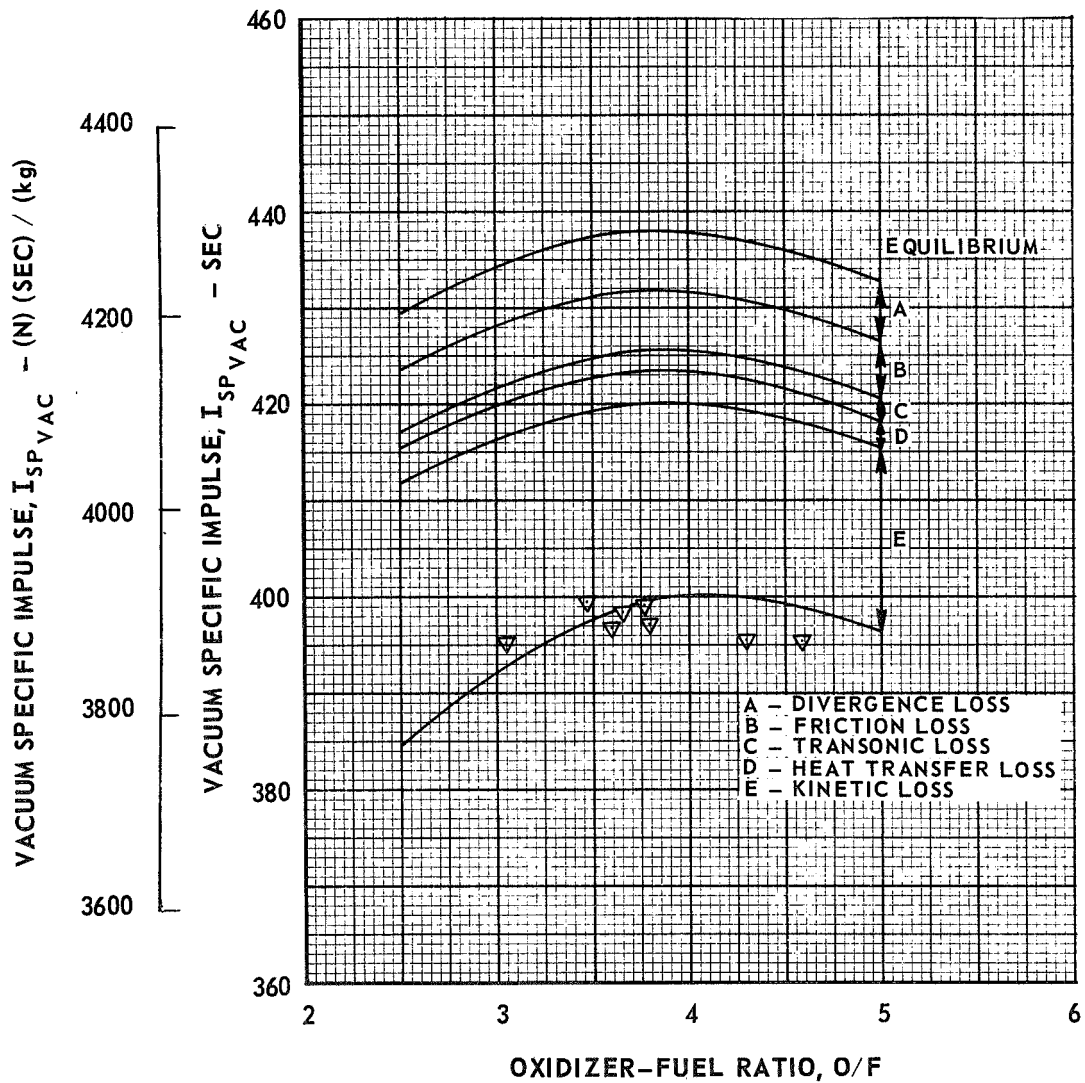
COMPARISON OF ANALYTICAL AND EXPERIMENTAL PERFORMANCE FOR ROCKETDYNE 15 DEGREE CONICAL NOZZLE

$B_2 H_6 (g) - FLOX (70.4\% F_2)$

$P_C = 50 \text{ PSIA } (3.448 \times 10^5 \text{ N/m}^2) \quad (A/A_{MIN})_{EXIT} = 60$

$(r_c/r_t)_{DOWNSTREAM \ THROAT} = 3.635 \quad (r_c/r_t)_{UPSTREAM \ THROAT} = 1.5 \quad r_t = 0.175 \text{ FT } (0.053 \text{ m})$

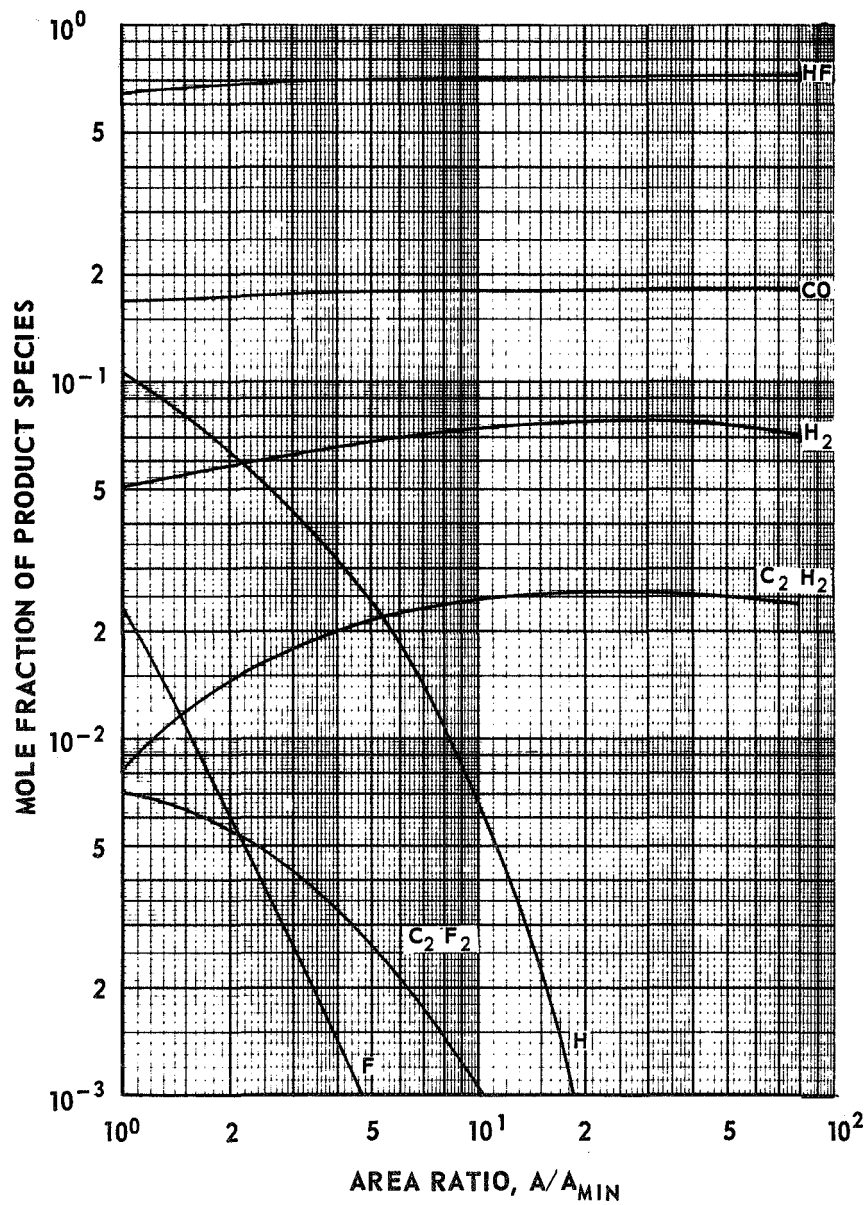
NOTE: KINETIC IMPULSE LOSS CALCULATED USING MECHANISM AND RATES OF TABLE I
COMBUSTION EFFICIENCY BASED ON C* CORRELATION
SYMBOLS REPRESENT DATA ADJUSTED BY EFFECTIVE C* EFFICIENCY



TYPICAL VARIATIONS OF EQUILIBRIUM PRODUCT SPECIES MOLE FRACTIONS WITH AREA RATIO IN CH₄-FLOX (82.6% F₂) PROPELLANT SYSTEM

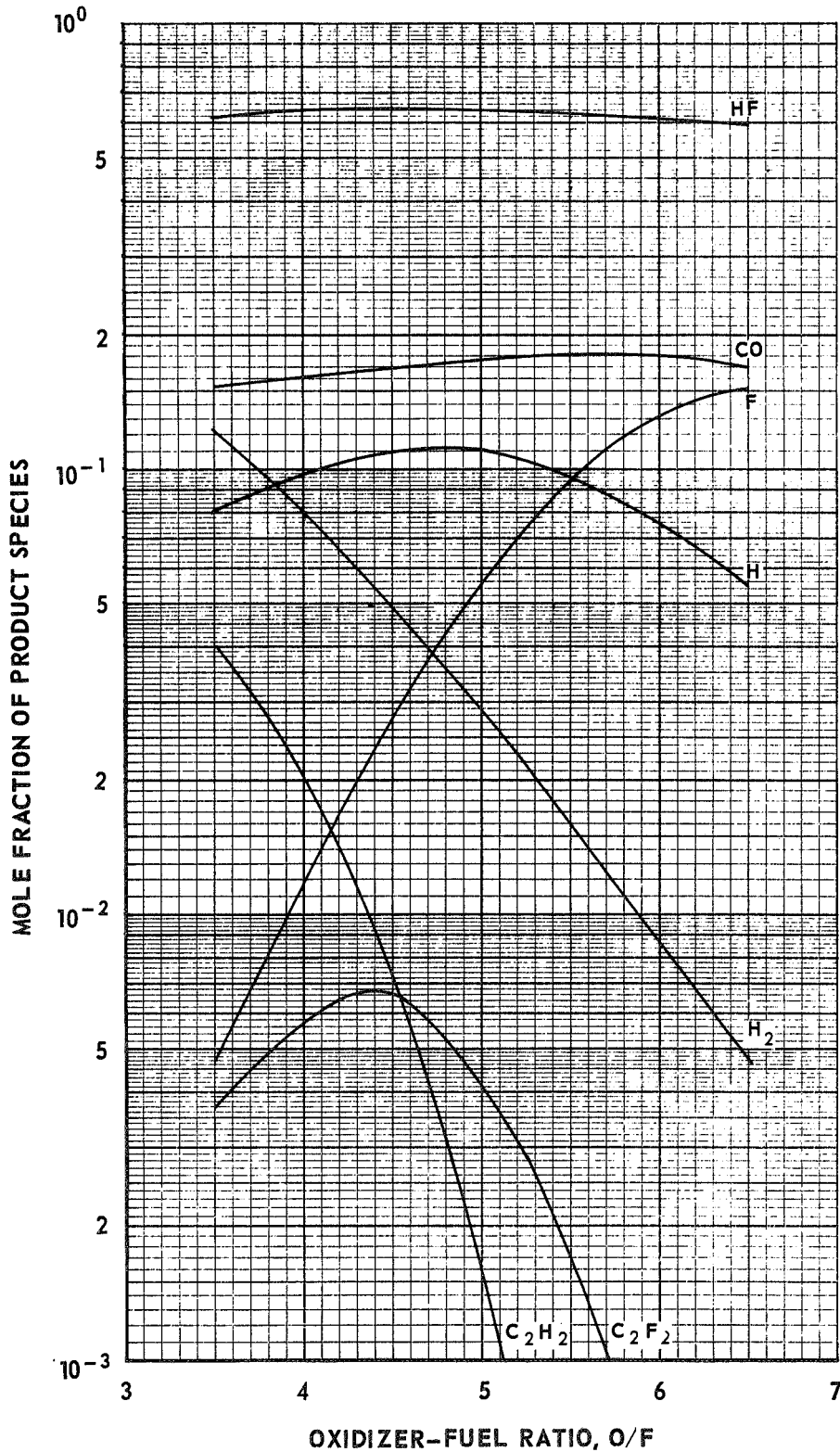
$$P_c = 100 \text{ PSIA } (6.895 \times 10^5 \text{ N/m}^2)$$

$$O/F = 4.5$$



EFFECT OF OXIDIZER-FUEL RATIO ON EQUILIBRIUM PRODUCT SPECIES MOLE FRACTION IN NOZZLE THROAT FOR CH₄-FLOX (82.6% F₂) PROPELLANT SYSTEM

$P_c = 100 \text{ PSIA } (6.895 \times 10^5 \text{ N/m}^2)$

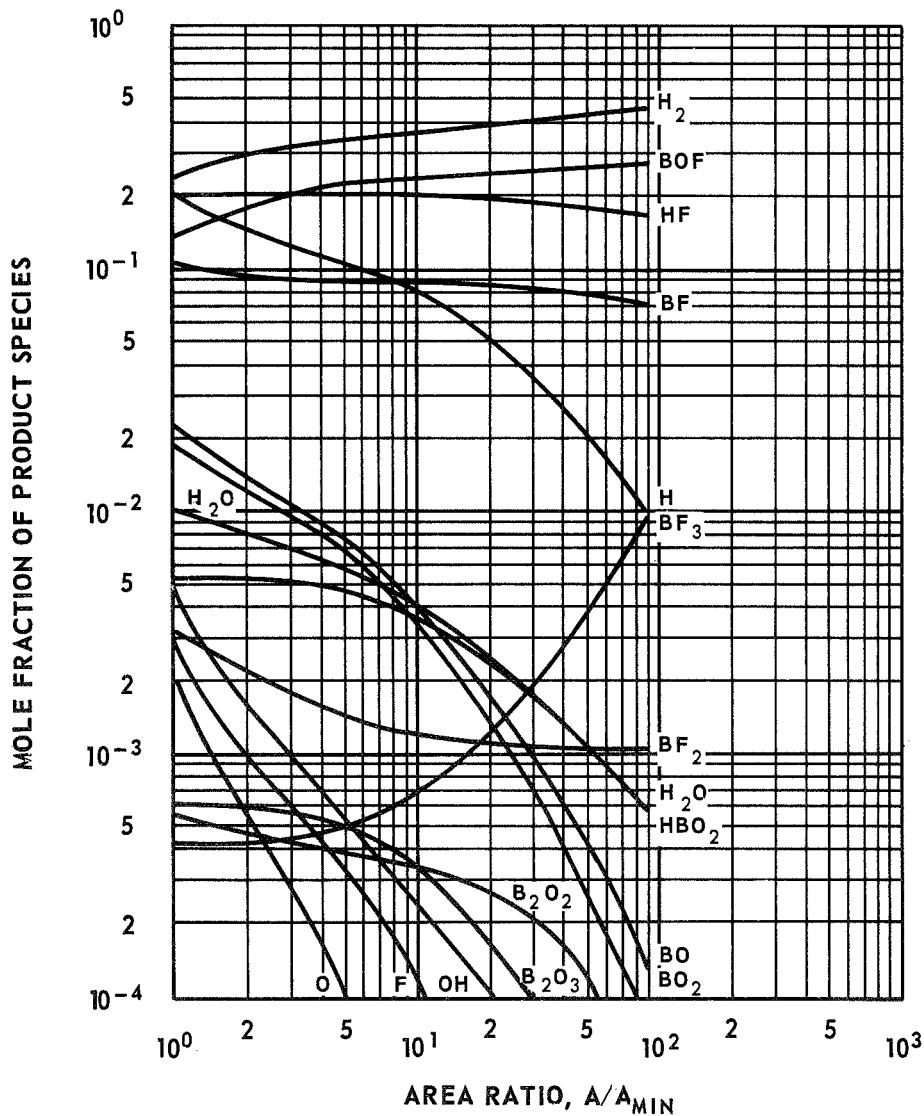


TYPICAL VARIATIONS OF EQUILIBRIUM PRODUCT SPECIES MOLE FRACTIONS WITH AREA RATIO IN B₂H₆-OF₂ PROPELLANT SYSTEM

$P_c = 100 \text{ PSIA } (6.895 \times 10^5 \text{ N/m}^2)$

$O/F = 3.0$

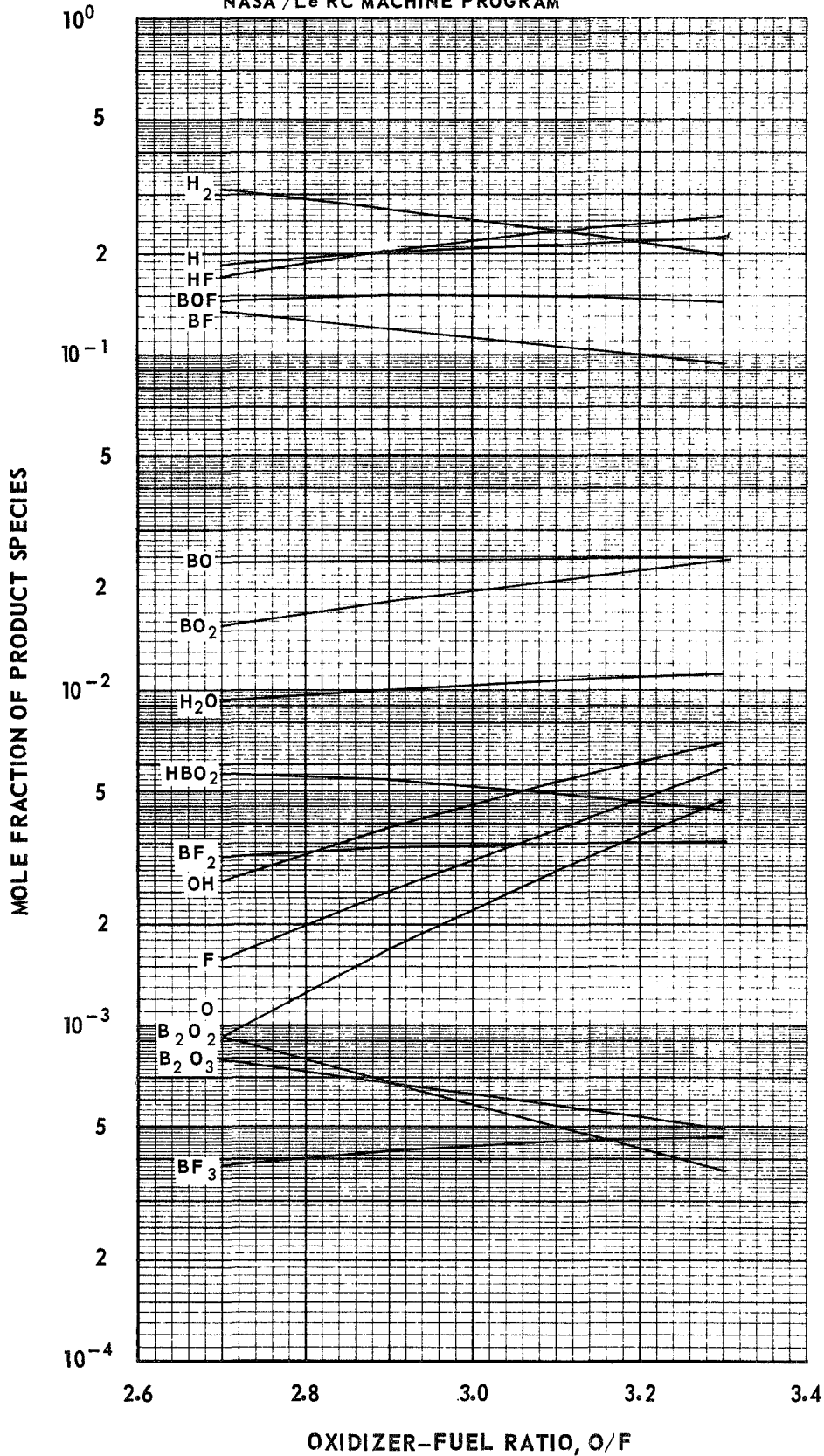
NOTE: EQUILIBRIUM RESULTS CALCULATED USING NASA/LeRC MACHINE PROGRAM



EFFECT OF OXIDIZER-FUEL RATIO ON EQUILIBRIUM PRODUCT SPECIES MOLE FRACTIONS IN NOZZLE THROAT FOR B₂H₆-OF₂ PROPELLANT SYSTEM

P_C = 100 PSIA (6.895 X 10⁵ N/m²)

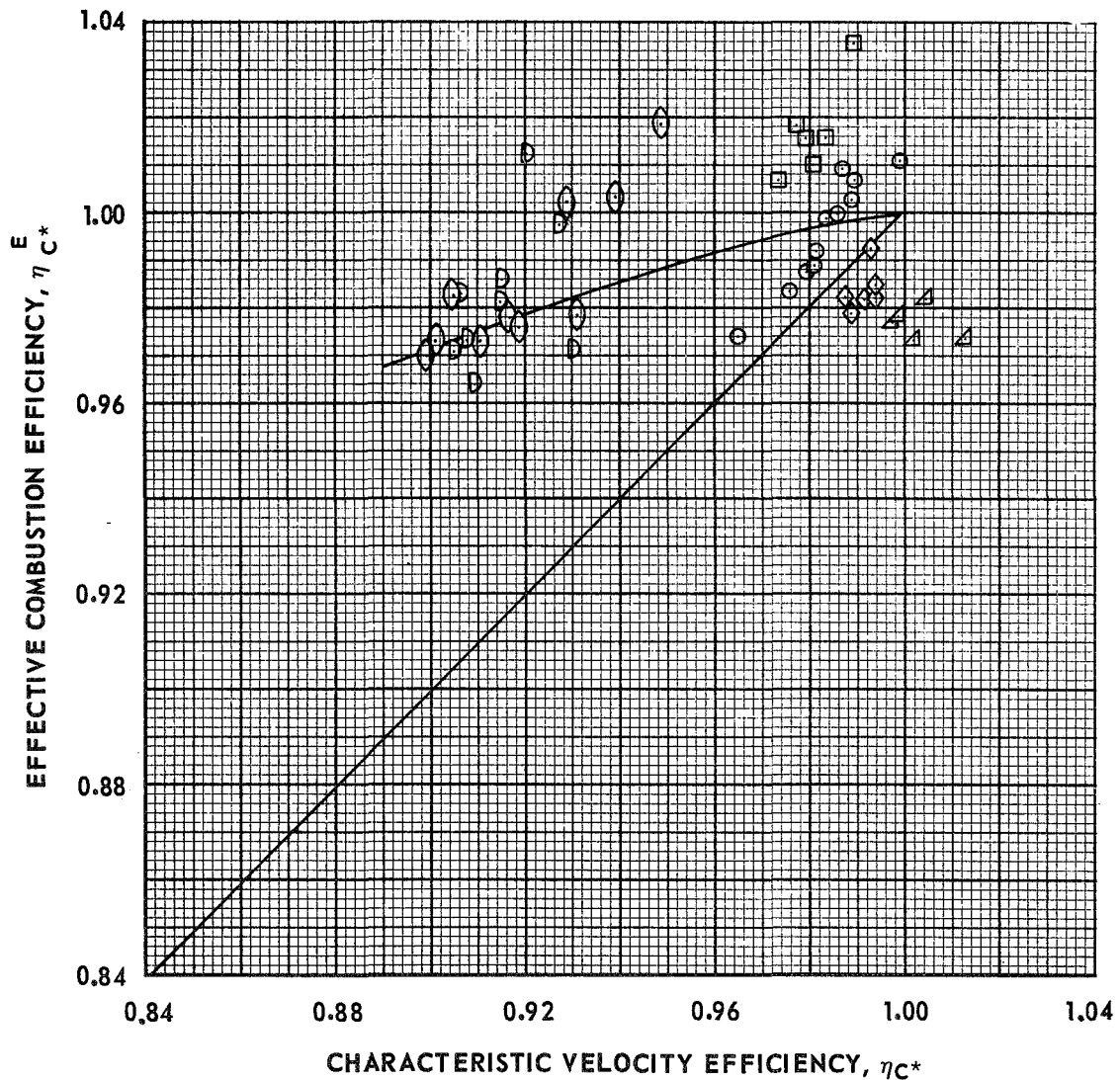
NOTE: EQUILIBRIUM RESULTS CALCULATED USING NASA /Le RC MACHINE PROGRAM



COMPARISON OF EFFECTIVE COMBUSTION EFFICIENCY AND MEASURED CHARACTERISTIC VELOCITY EFFICIENCY

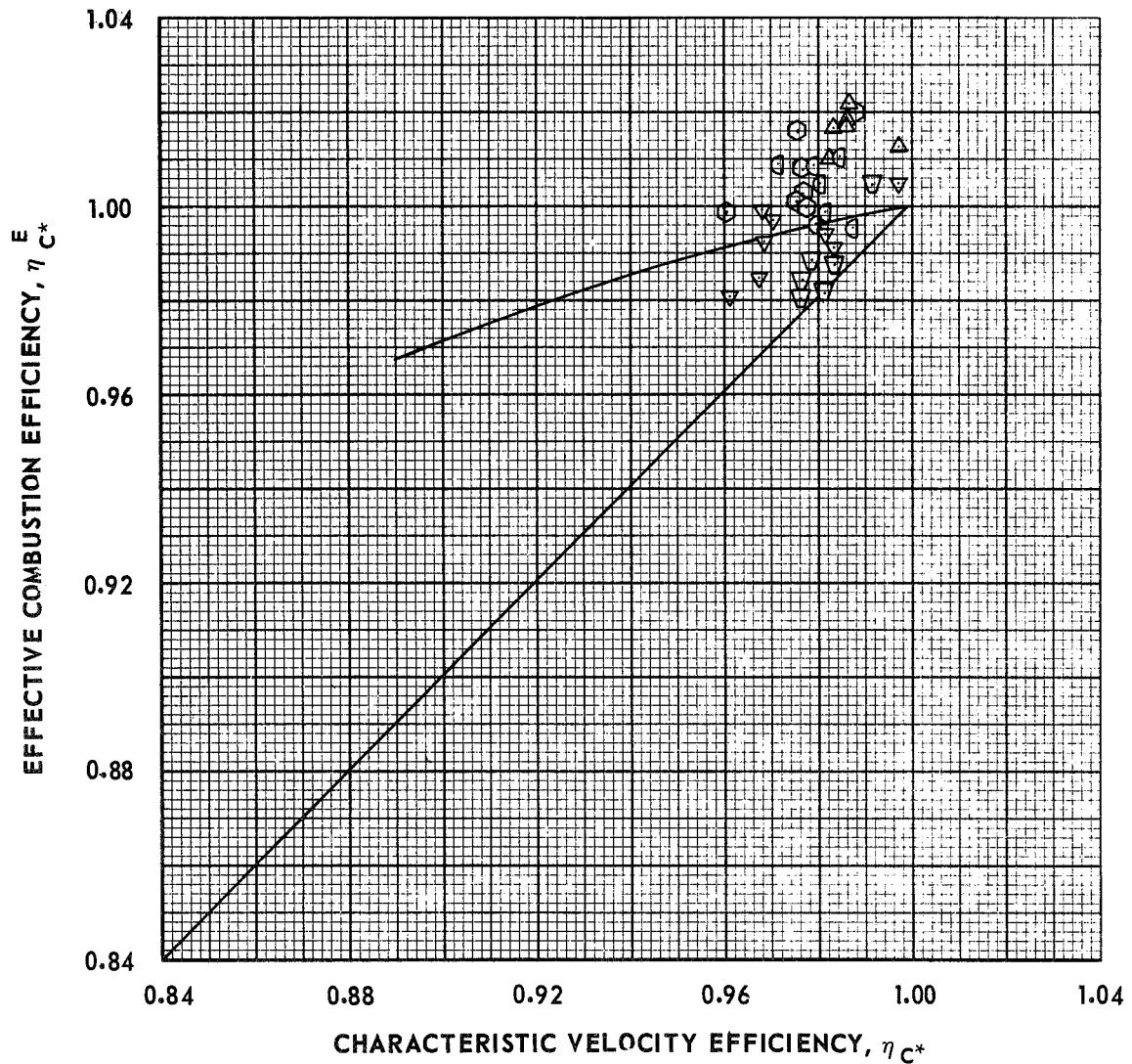
$$P_c = 100 \text{ PSIA } (6.895 \times 10^5 \text{ N/m}^2)$$

SYM	NOZZLE	PROPELLANT
○	ROCKETDYNE 15 DEG CONE	CH ₄ (g) - FLOX (82.6% F ₂)
◻	ROCKETDYNE 70 % BELL	
⊖	FRDC 15 DEG CONE	
⊕	FRDC RL-10	
◇	ROCKETDYNE 15 DEG CONE	CH ₄ (g) - FLOX (70.4% F ₂)
△	ROCKETDYNE 15 DEG CONE	CH ₄ (g) - OF ₂ (l)



COMPARISON OF EFFECTIVE COMBUSTION EFFICIENCY AND MEASURED CHARACTERISTIC VELOCITY EFFICIENCY

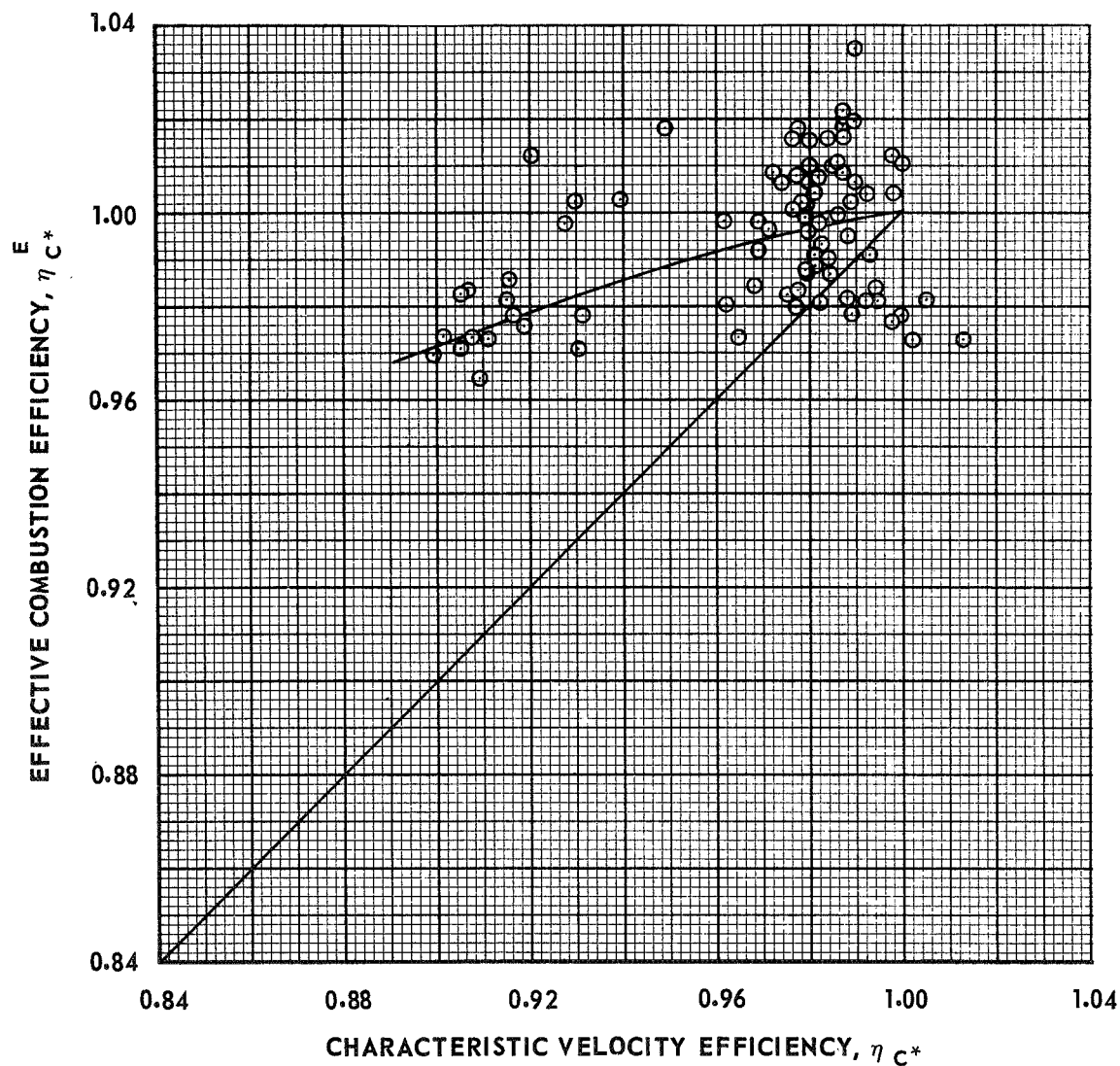
SYM	P_C		NOZZLE	PROPELLANT
	N/m^2	PSIA		
▽	6.895×10^5	100	ROCKETDYNE 15 DEG CONE	$B_2 H_6 (g) - OF_2 (l)$
⊙	↓	↓	70 % BELL	↓
▽	3.448×10^5	50	15 DEG CONE	$B_2 H_6 (g) - FLOX (70.4\% F_2)$
⊙	6.895×10^5	100	↓	↓
△	↓	↓	70 % BELL	↓



COMPARISON OF EFFECTIVE COMBUSTION EFFICIENCY AND MEASURED CHARACTERISTIC VELOCITY EFFICIENCY

$$P_C = 100 \text{ PSIA } (6.895 \times 10^5 \text{ N/m}^2)$$

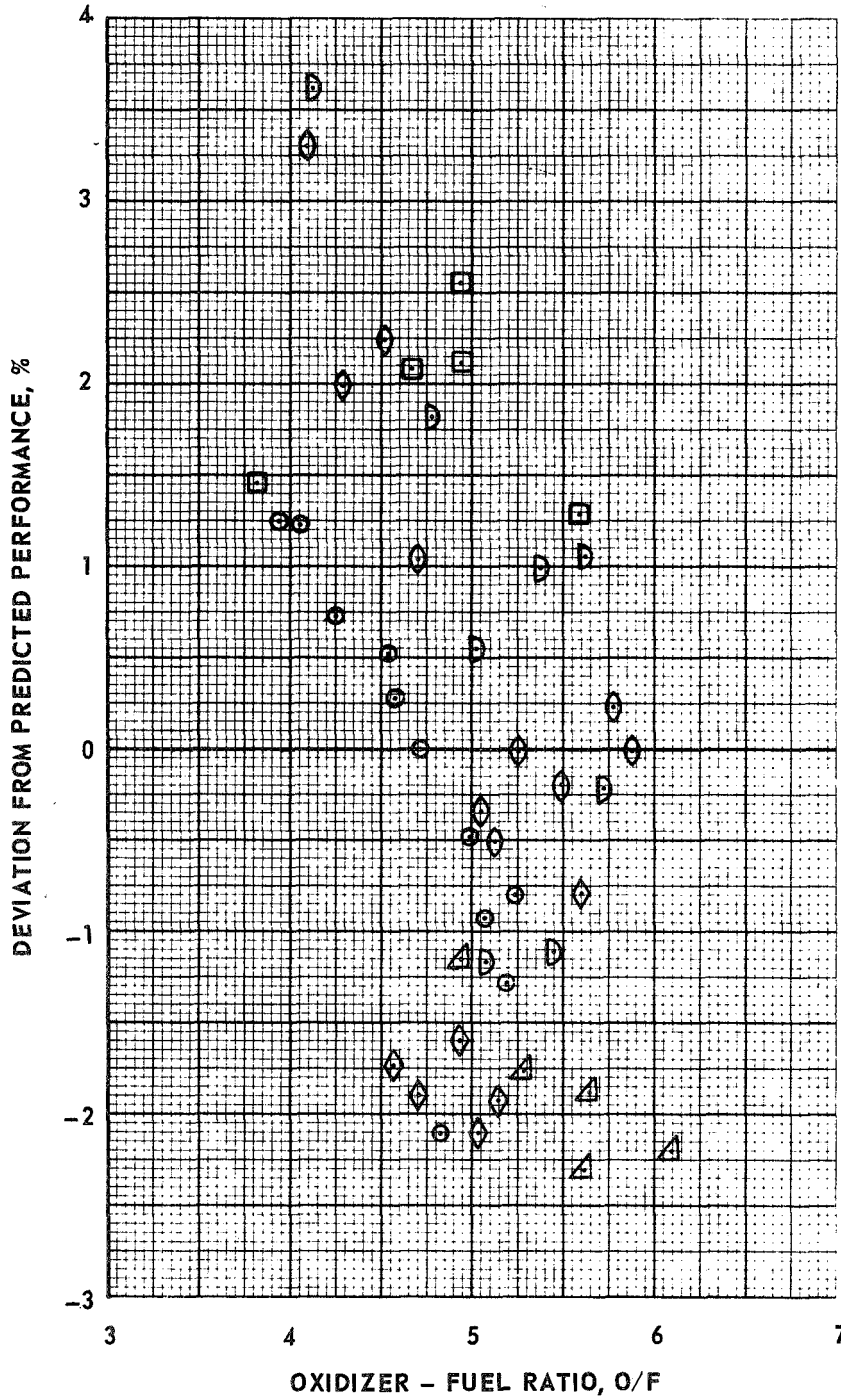
PROPELLANTS
CH ₄ (g) - FLOX (82.6% F ₂)
CH ₄ (g) - FLOX (70.4% F ₂)
B ₂ H ₆ (g) - FLOX (70.4% F ₂)
CH ₄ (g) - OF ₂ (l)
B ₂ H ₆ (g) - OF ₂ (l)



DEVIATION OF ANALYTICAL AND EXPERIMENTAL ENGINE PERFORMANCE FOR FRDC AND ROCKETDYNE NOZZLE CONFIGURATIONS

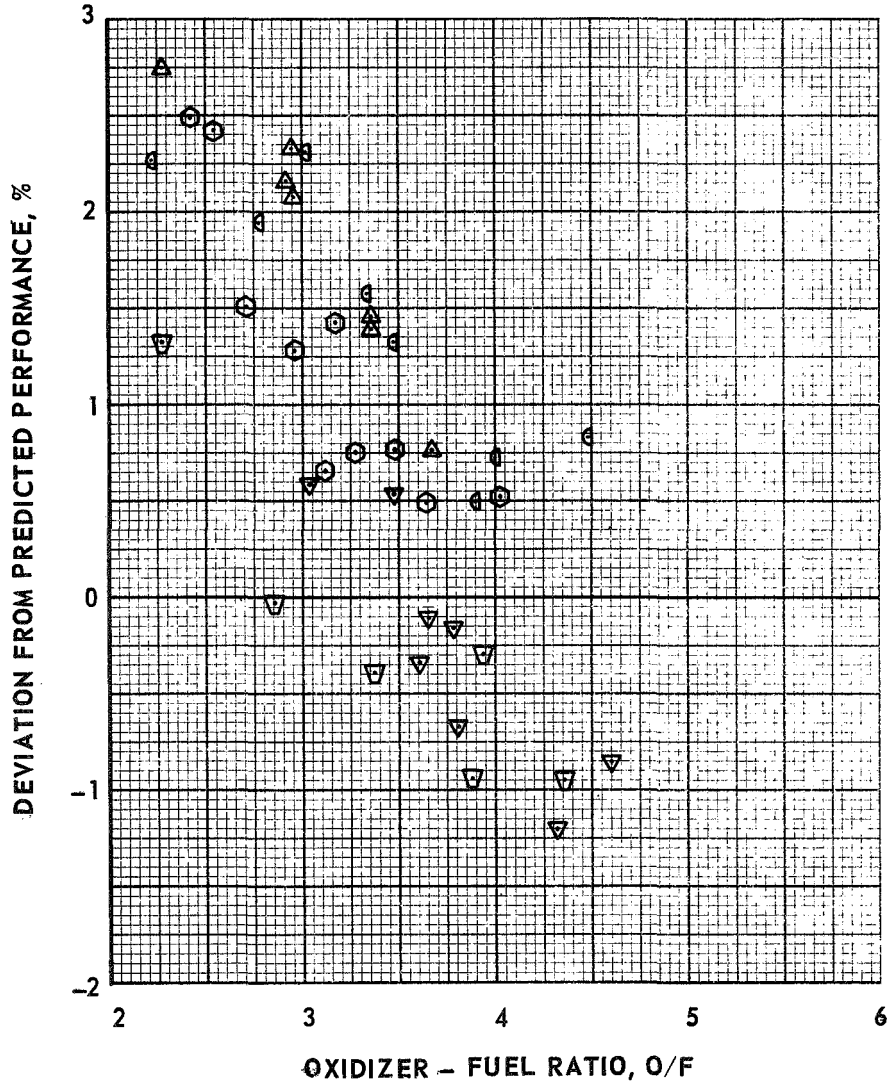
$$P_C = 100 \text{ PSIA } (6.895 \times 10^5 \text{ N/m}^2)$$

SYM	NOZZLE	PROPELLANT
⊙	ROCKETDYNE 15 DEG CONE	CH ₄ (g) - FLOX (82.6% F ₂)
⊠	ROCKETDYNE 70 % BELL	
⊞	FRDC 15 DEG CONE	
⊕	FRDC RL-10	
◇	ROCKETDYNE 15 DEG CONE	CH ₄ (g) - FLOX (70.4% F ₂)
△		CH ₄ (g) - O F ₂ (l)



DEVIATION OF ANALYTICAL AND EXPERIMENTAL ENGINE PERFORMANCE FOR ROCKETDYNE NOZZLE CONFIGURATIONS

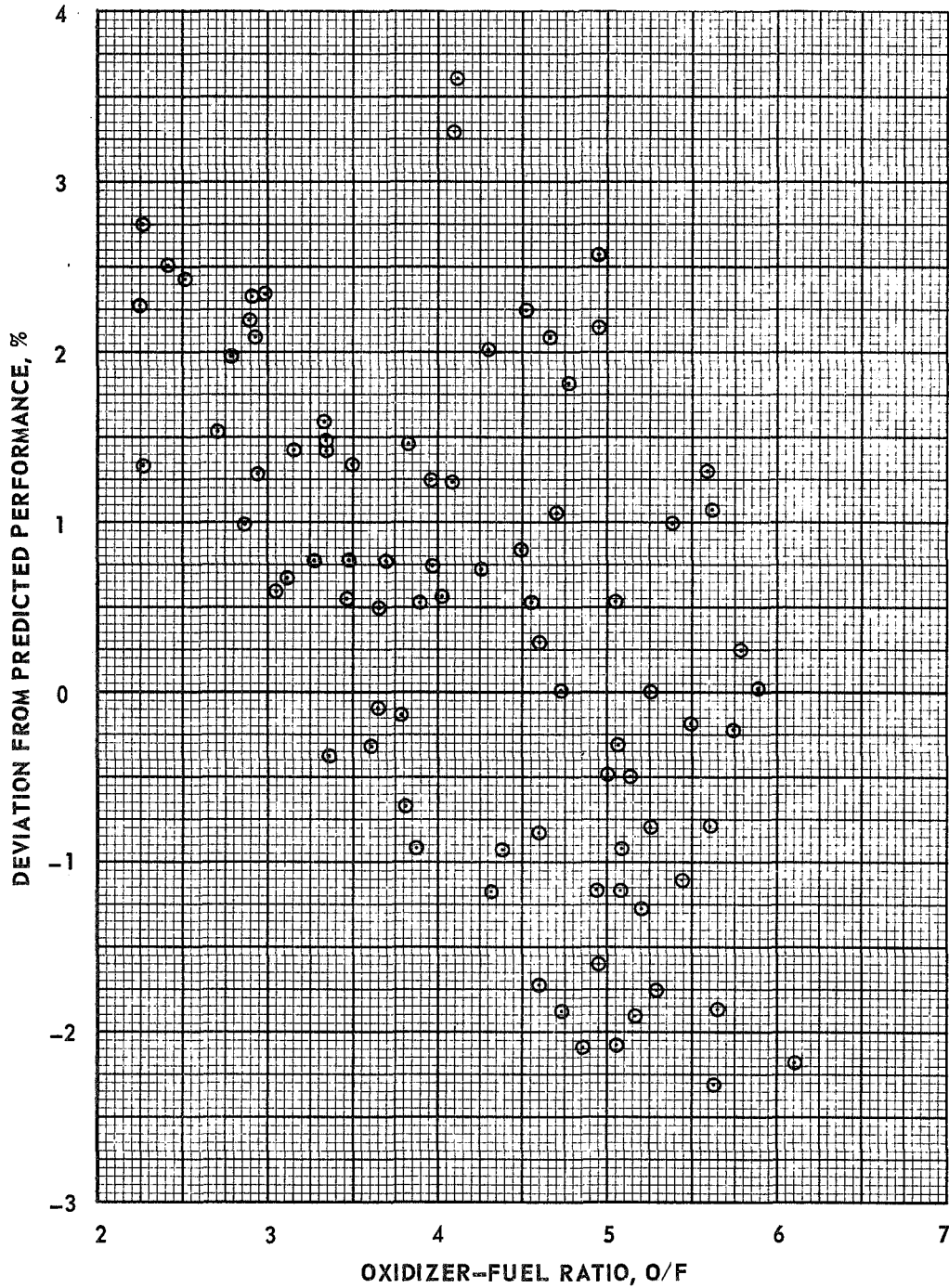
SYM	P_c		NOZZLE	PROPELLANT
	PSIA	N/m^2		
▽	100	6.895×10^5	ROCKETDYNE 15 DEG CONE	$B_2 H_6 (g) - OF_2 (l)$
◻	↓	↓	ROCKETDYNE 70 % BELL	↓
▽	50	3.448×10^5	ROCKETDYNE 15 DEG CONE	$B_2 H_6 (g) - FLOX (70.4\% F_2)$
○	100	6.895×10^5	↓	↓
△	↓	↓	ROCKETDYNE 70 % BELL	↓



DEVIATION OF ANALYTICAL AND EXPERIMENTAL ENGINE PERFORMANCE FOR FRDC AND ROCKETDYNE NOZZLE CONFIGURATIONS

$P_C = 100 \text{ PSIA } (6.895 \times 10^5 \text{ N/m}^2)$

PROPELLANTS
$\text{CH}_4 \text{ (g) - FLOX (82.6\% F}_2\text{)}$
$\text{CH}_4 \text{ (g) - FLOX (70.4\% F}_2\text{)}$
$\text{B}_2\text{H}_6 \text{ (g) - FLOX (70.4\% F}_2\text{)}$
$\text{CH}_4 \text{ (g) - OF}_2\text{ (l)}$
$\text{B}_2\text{H}_6 \text{ (g) - OF}_2\text{ (l)}$

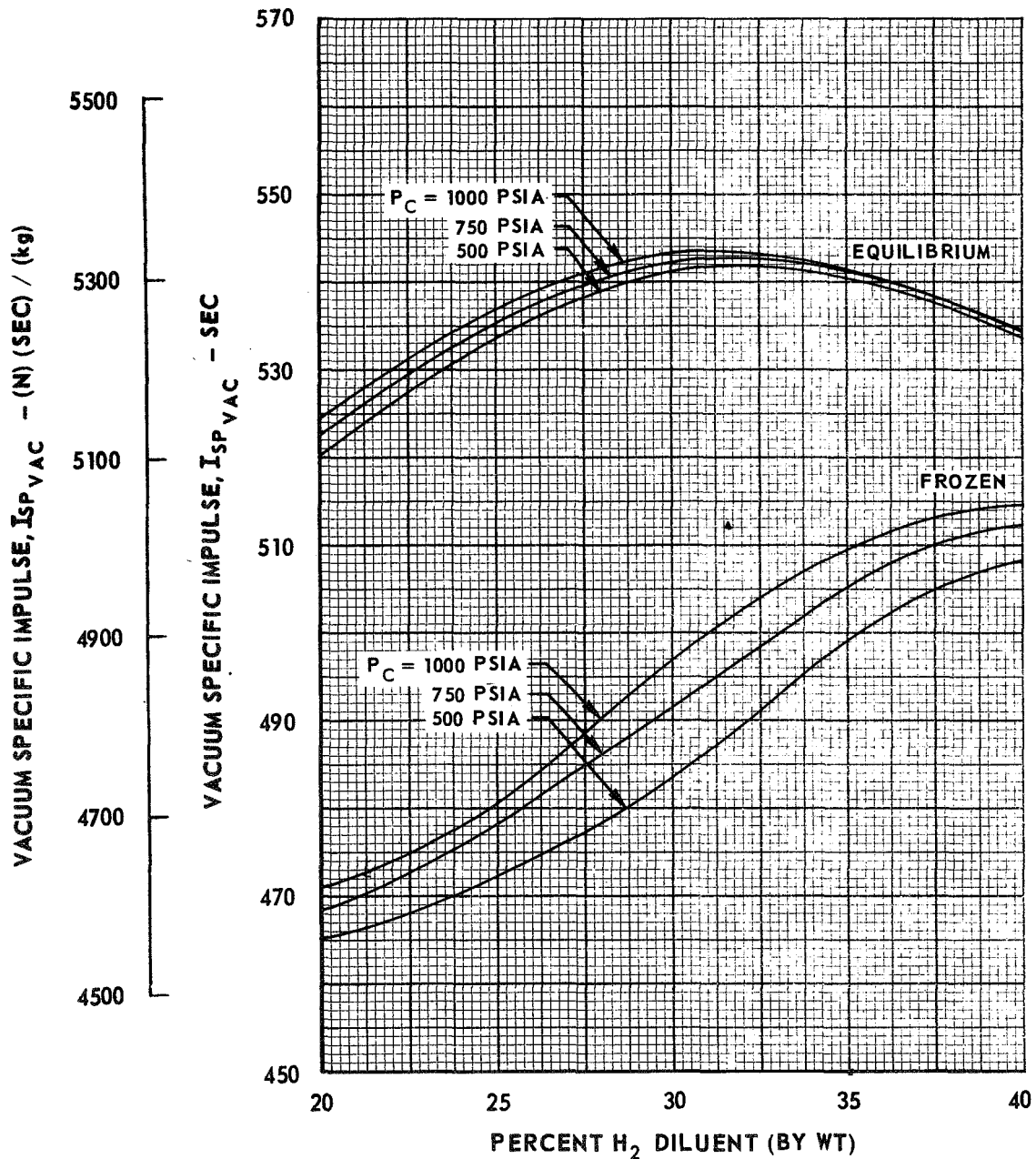


EFFECT OF PERCENT H₂ DILUENT ON EQUILIBRIUM AND FROZEN PERFORMANCE
 OF Li(l) - F₂(l) - H₂(g) PROPELLANT SYSTEM

STOICHIOMETRIC Li-F₂ MIXTURE

$$(A/A_{MIN})_{EXIT} = 60$$

P_C
500 PSIA (3.448×10^6 N/m ²)
750 PSIA (5.171×10^6 N/m ²)
1000 PSIA (6.895×10^6 N/m ²)

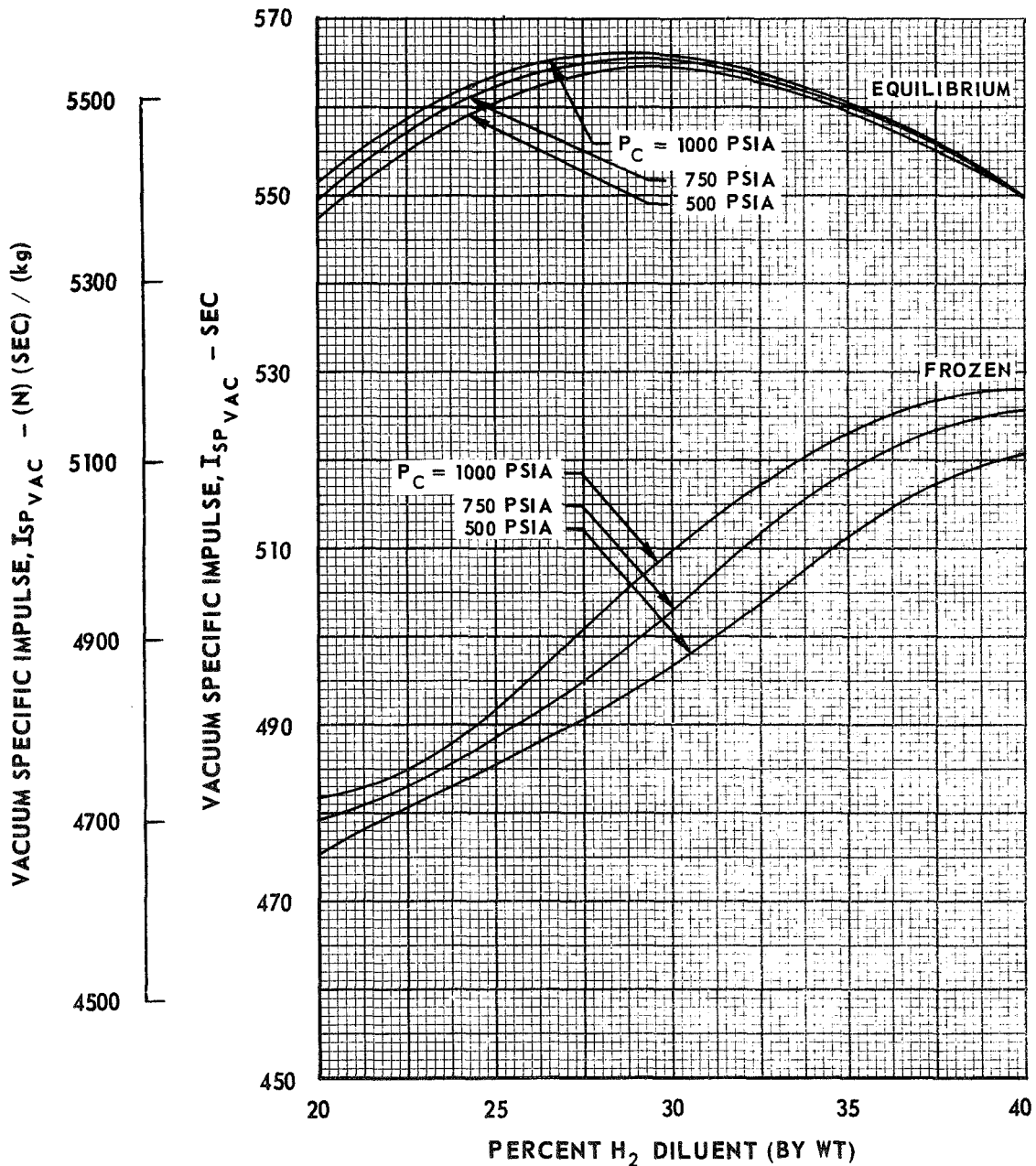


EFFECT OF PERCENT H₂ DILUENT ON EQUILIBRIUM AND FROZEN PERFORMANCE
 OF Li(l) - F₂(l) - H₂(g) PROPELLANT SYSTEM

STOICHIOMETRIC Li-F₂ MIXTURE

$$(A/A_{MIN})_{EXIT} = 200$$

P_C
500 PSIA (3.448×10^6 N/m ²)
750 PSIA (5.171×10^6 N/m ²)
1000 PSIA (6.895×10^6 N/m ²)

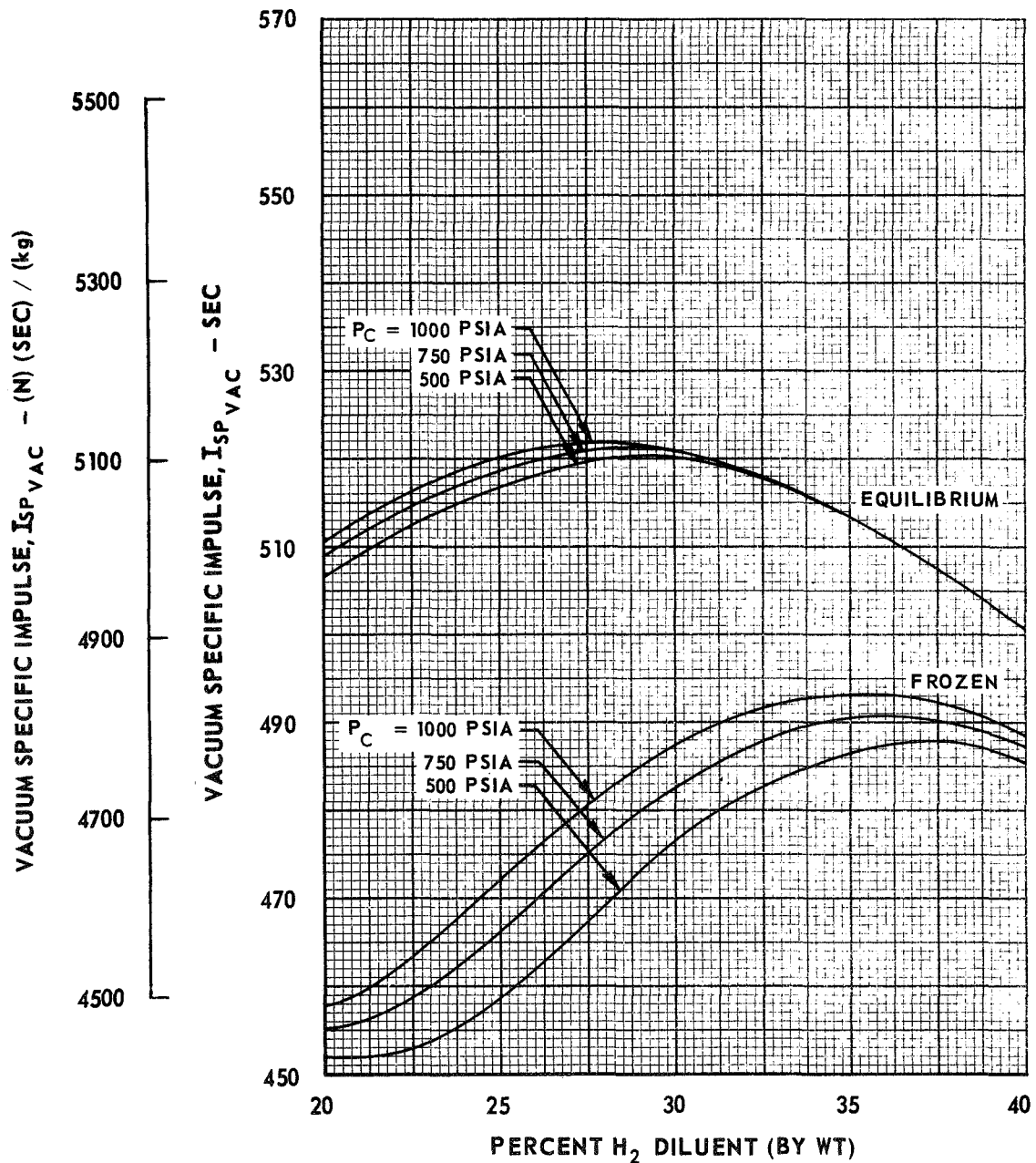


EFFECT OF PERCENT H₂ DILUENT ON EQUILIBRIUM AND FROZEN PERFORMANCE OF Li(s) - F₂(l) - H₂(l) PROPELLANT SYSTEM

STOICHIOMETRIC Li-F₂ MIXTURE

$$(A/A_{MIN})_{EXIT} = 60$$

P_C
500 PSIA (3.448×10^6 N/m ²)
750 PSIA (5.171×10^6 N/m ²)
1000 PSIA (6.895×10^6 N/m ²)

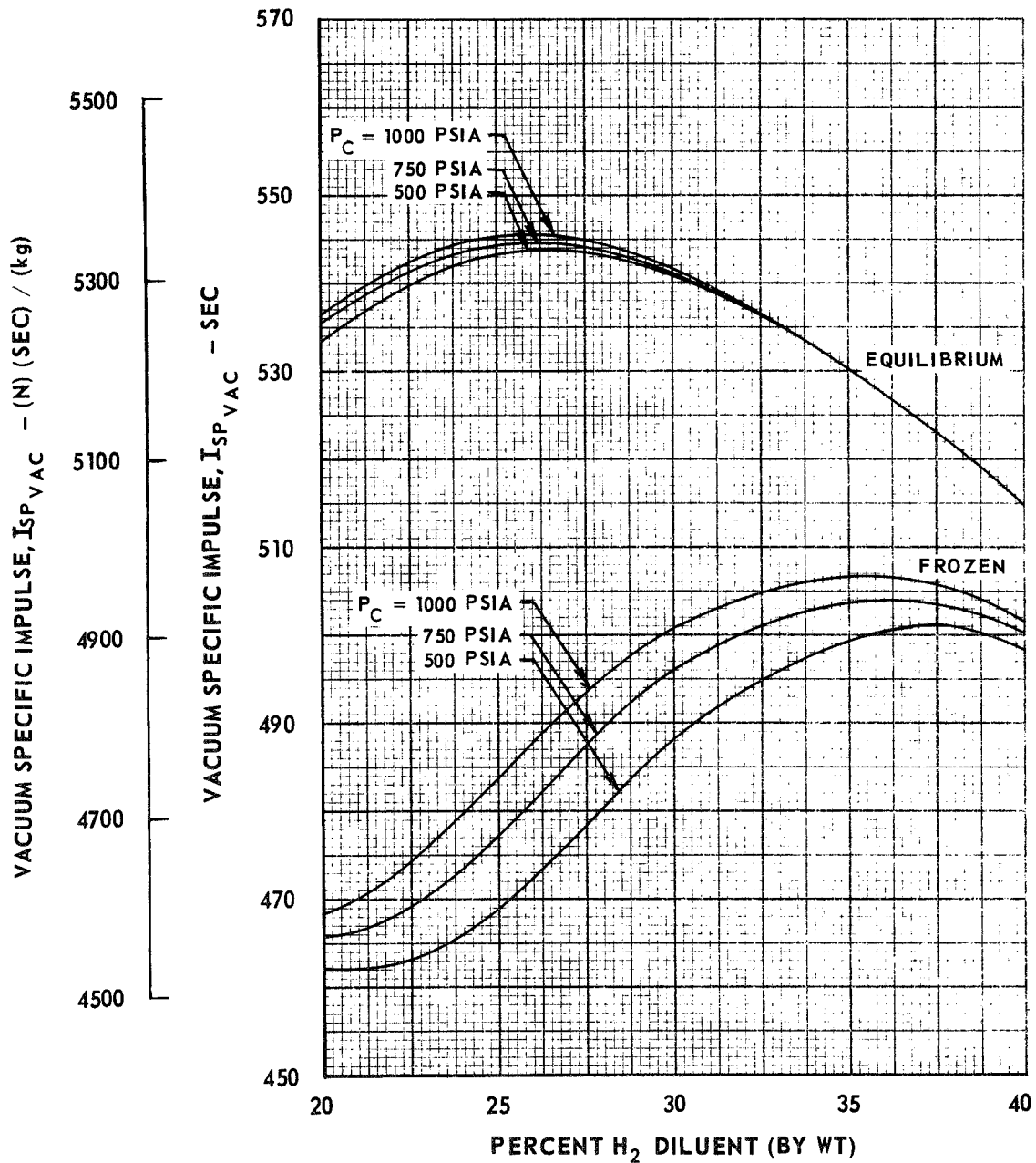


EFFECT OF PERCENT H₂ DILUENT ON EQUILIBRIUM AND FROZEN PERFORMANCE OF Li(s) - F₂(ℓ) - H₂(ℓ) PROPELLANT SYSTEM

STOICHIOMETRIC Li-F₂ MIXTURE

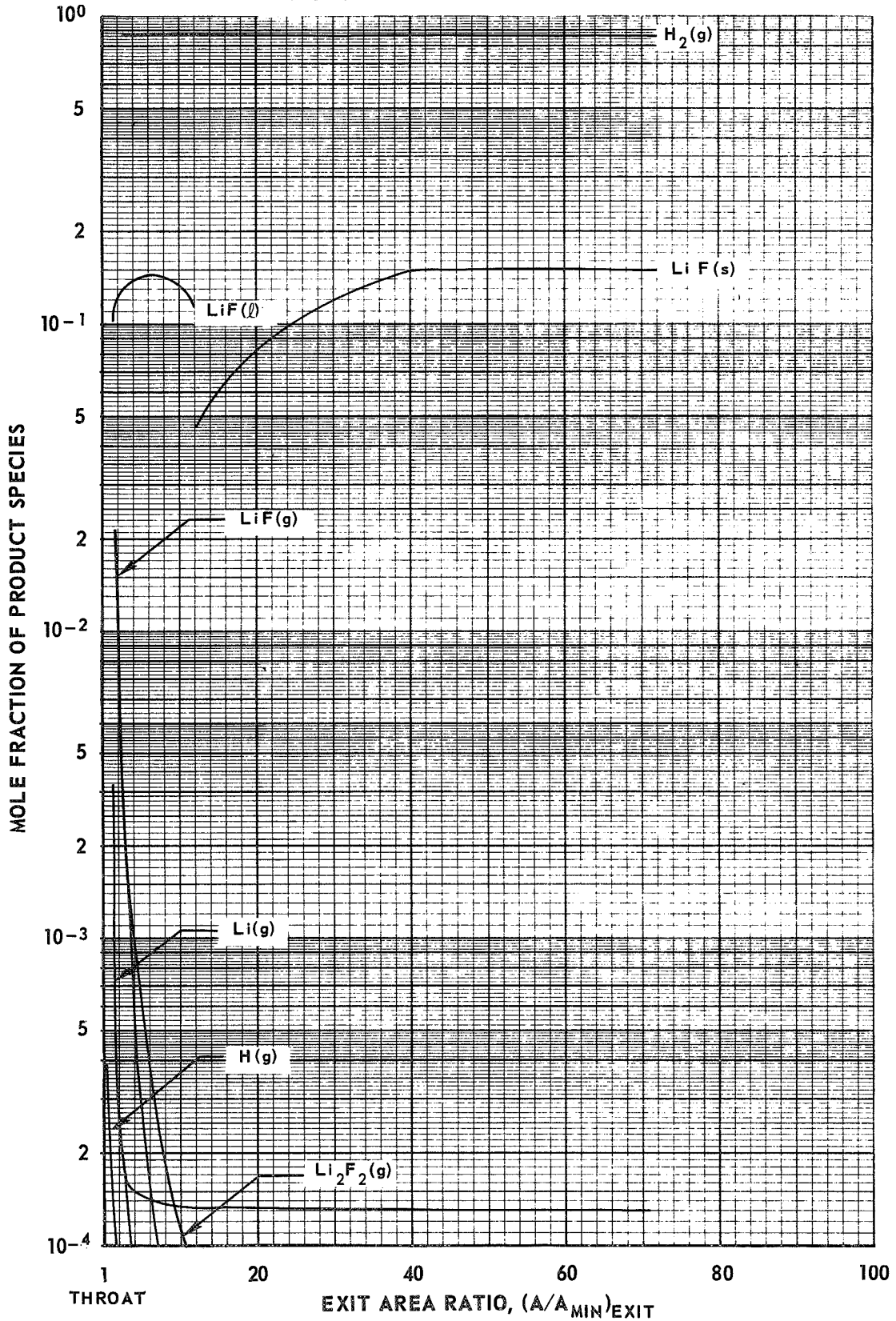
$$(A/A_{MIN})_{EXIT} = 200$$

P_C
500 PSIA (3.448×10^6 N/m ²)
750 PSIA (5.171×10^6 N/m ²)
1000 PSIA (6.895×10^6 N/m ²)



VARIATION OF EQUILIBRIUM PRODUCT MOLE FRACTIONS WITH AREA RATIO
 FOR $\text{Li(s)} - \text{F}_2(\ell) - \text{H}_2(\ell)$ PROPELLANT SYSTEM

$P_C = 1000 \text{ PSIA}$ 30% H_2 DILUENT
 STOICHIOMETRIC Li-F MIXTURE

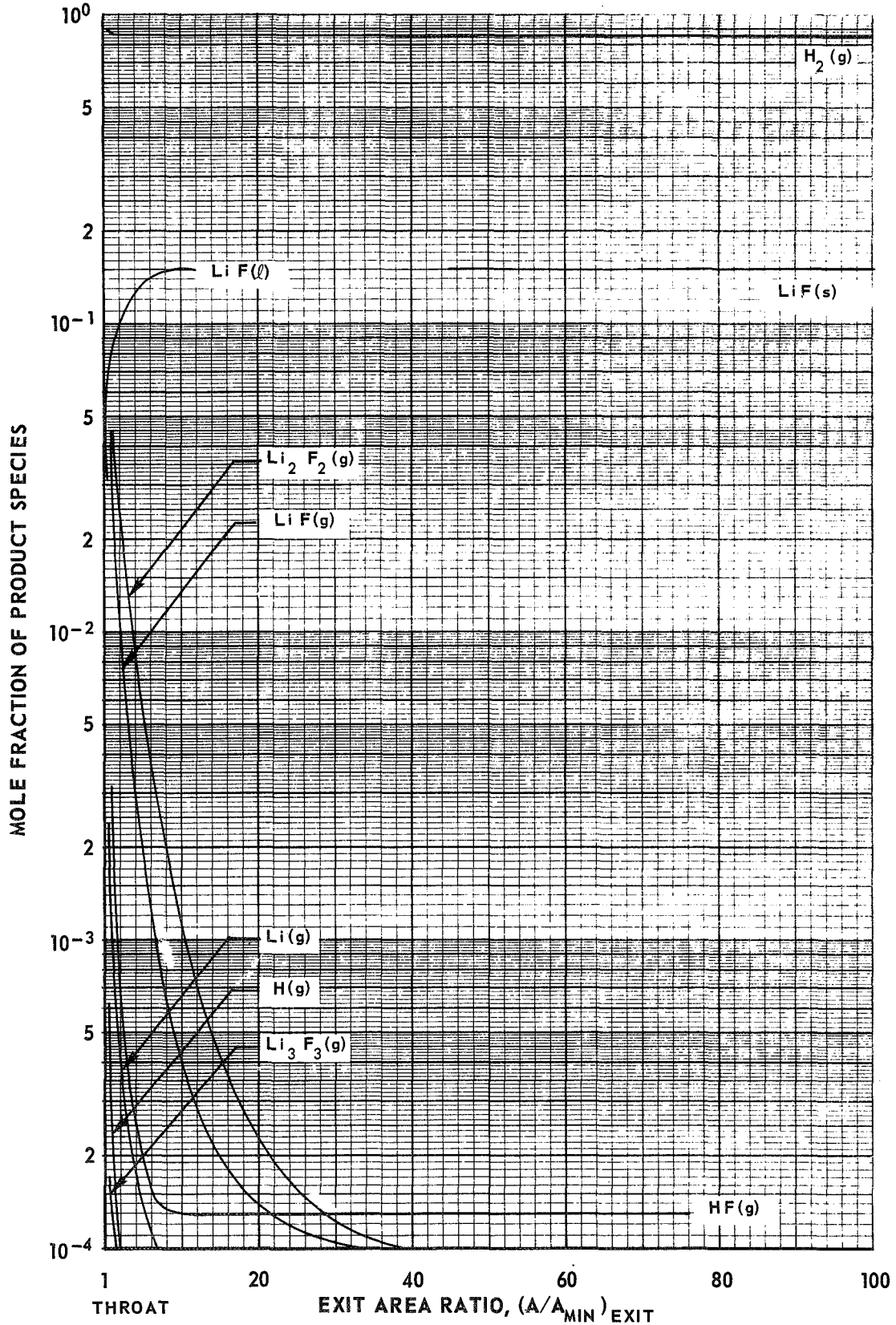


VARIATION OF EQUILIBRIUM PRODUCT MOLE FRACTIONS WITH AREA RATIO
 FOR $\text{Li}(\text{s}) - \text{F}_2(\ell) - \text{H}_2(\ell)$ PROPELLANT SYSTEM

$P_C = 500 \text{ PSIA} (3.448 \times 10^6 \text{ N/m}^2)$

30% H_2 DILUENT

STOICHIOMETRIC $\text{Li}-\text{F}_2$ MIXTURE



EFFECT OF FREEZING AREA RATIO ON NONEQUILIBRIUM PERFORMANCE FOR Li-F₂ - H₂ PROPELLANT SYSTEM

Li (ℓ) - F₂ (ℓ) - H₂ (g) H₂ : 20% BY WEIGHT, L_i/F : STOICHIOMETRIC

P_C = 500 PSIA (3.448 X 10⁶ N/m²) (A/A_{MIN})_{EXIT} = 200

NOTE: I _{SP VAC}	(EQUIL) = 547.7 SEC	WITH CONDENSATION	I _{SP VAC} (EQUIL) = 535.2 SEC	CONDENSATION SUPPRESSED
	(FROZ) = 475.8 SEC			

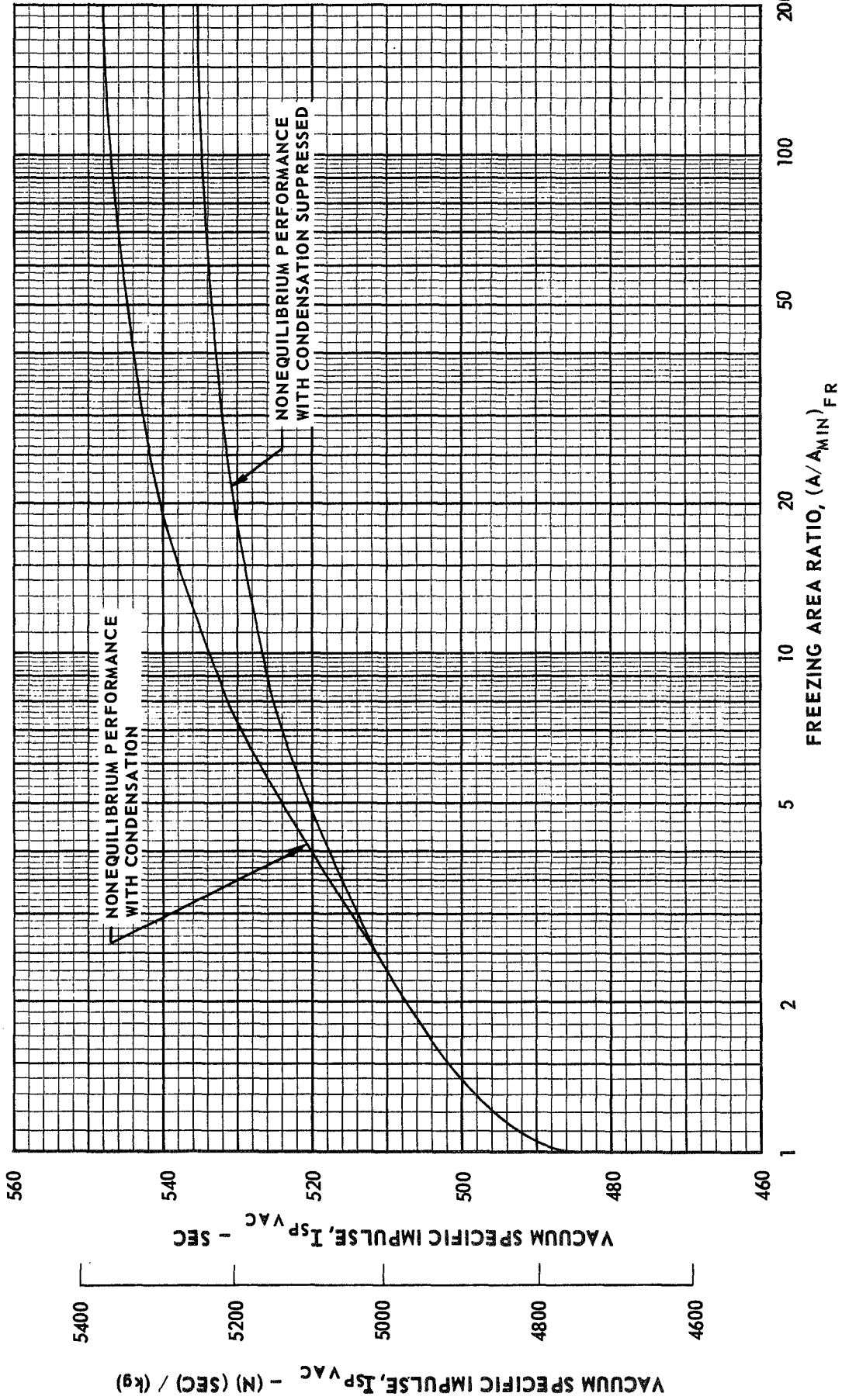


FIG. 39

EFFECT OF FREEZING AREA RATIO ON NONEQUILIBRIUM PERFORMANCE FOR Li-F₂ - H₂ PROPELLANT SYSTEM

Li (ℓ) - F₂ (ℓ) - H₂ (g) H₂ : 25% BY WEIGHT, L/I/F : STOICHIOMETRIC
 P_C = 500 PSIA (3.448 X 10⁶ N/m²) (A/A_{MIN})_{EXIT} = 200

NOTE: I_{SP VAC} (EQUIL) = 561.0 SEC I_{SP VAC} (EQUIL) = 536.3 SEC }
 I_{SP VAC} (FROZ) = 486.0 SEC I_{SP VAC} (FROZ) = 486.0 SEC }
 WITH CONDENSATION WITH CONDENSATION SUPPRESSED

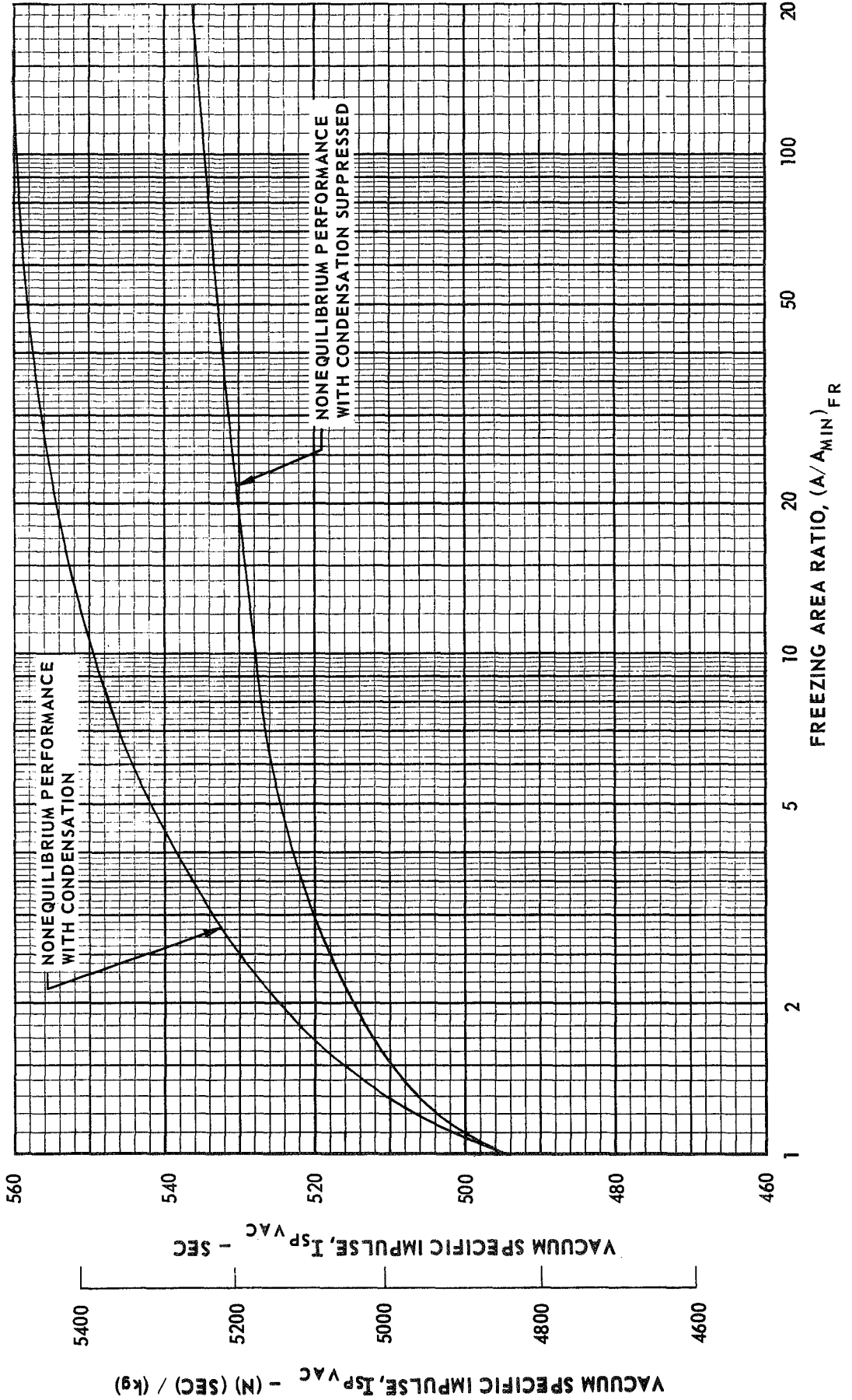
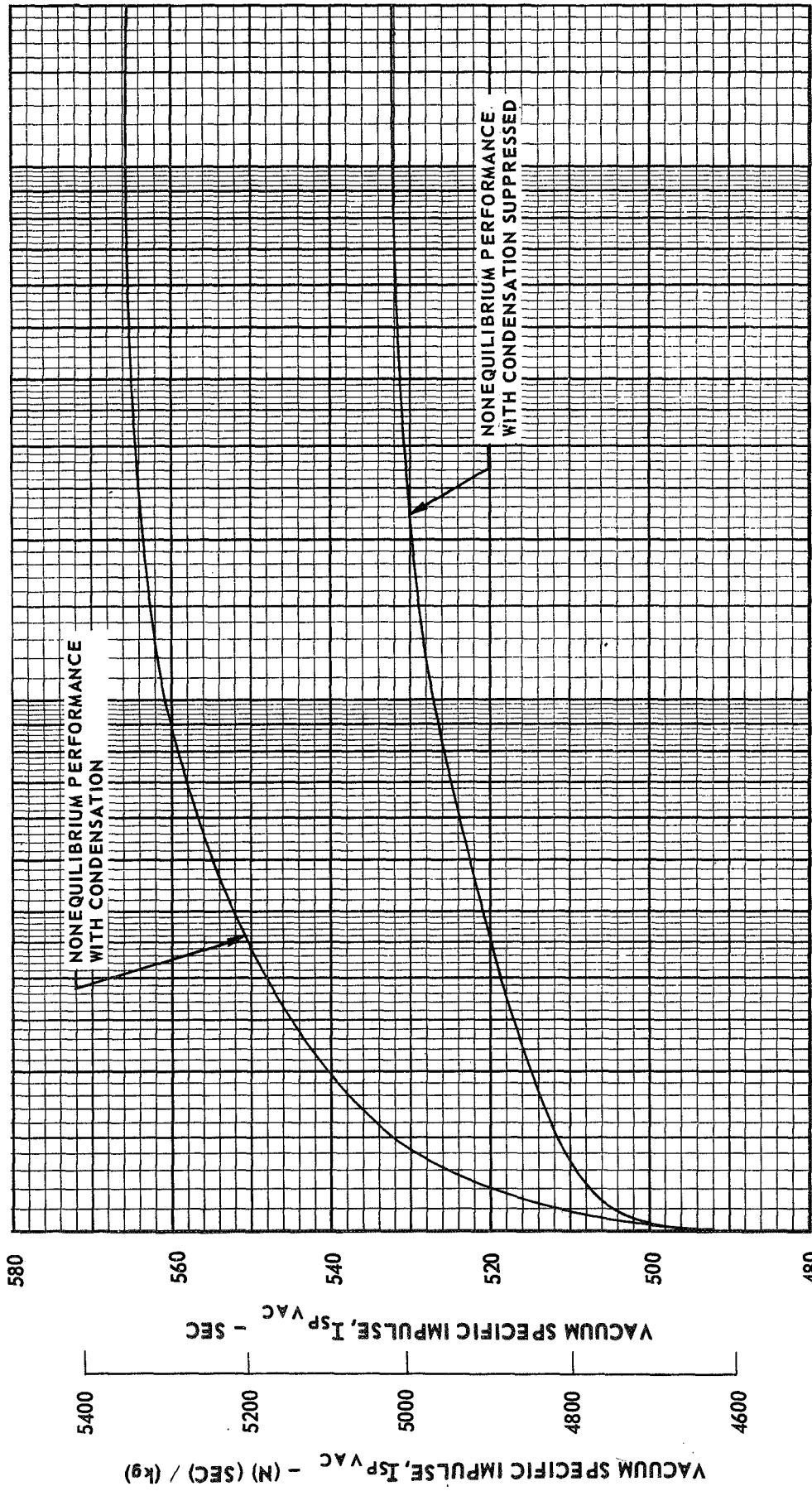


FIG. 40

EFFECT OF FREEZING AREA RATIO ON NONEQUILIBRIUM PERFORMANCE FOR Li-F₂-H₂ PROPELLANT SYSTEM

Li (ℓ) - F₂ (ℓ) - H₂ (g) H₂ : 30% BY WEIGHT, Li/F : STOICHIOMETRIC
 P_C = 500 PSIA (3.448 X 10⁶ N/m²) (A/A_{MIN})_{EXIT} = 200

NOTE: I _{SP VAC} (EQUIL) = 564.6 SEC	} WITH CONDENSATION	I _{SP VAC} (EQUIL) = 531.7 SEC	} CONDENSATION SUPPRESSED
I _{SP VAC} (FROZ) = 494.2 SEC			



EFFECT OF FREEZING AREA RATIO ON NONEQUILIBRIUM PERFORMANCE FOR Li-F₂-H₂ PROPELLANT SYSTEM

Li (s) - F₂ (ℓ) - H₂ (ℓ) H₂ : 25% BY WEIGHT, L_i/F : STOICHIOMETRIC
 P_C = 1000 PSIA (6.895 X 10⁶ N/m²) (A/A_{MIN})_{EXIT} = 60

NOTE: I _{SP VAC} (EQUIL) = 521.0 SEC	} WITH CONDENSATION	I _{SP VAC} (EQUIL) = 496.0 SEC	} CONDENSATION SUPPRESSED
I _{SP VAC} (FROZ) = 472.0 SEC			

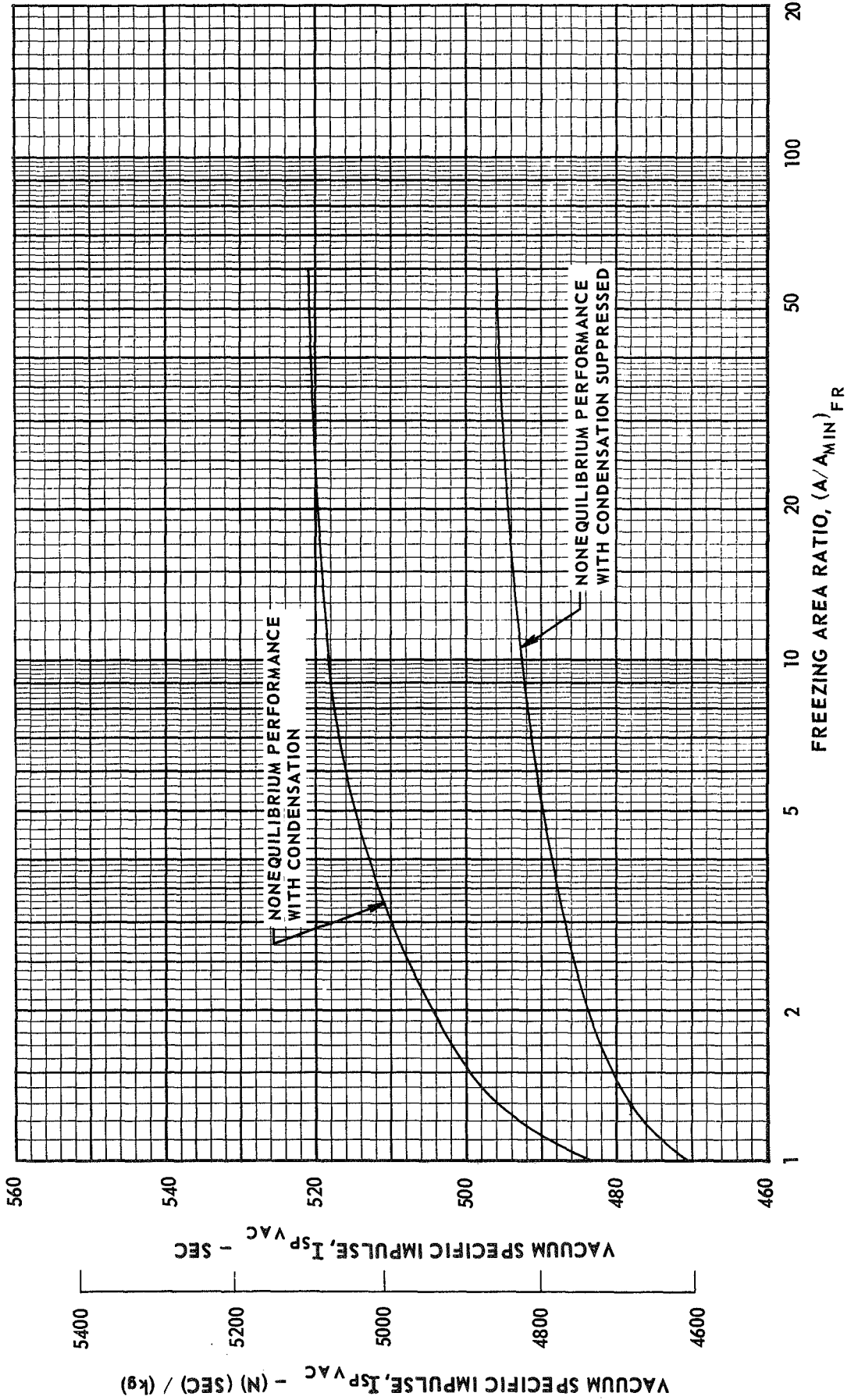


FIG. 42

EFFECT OF FREEZING AREA RATIO ON NONEQUILIBRIUM PERFORMANCE FOR Li-F₂ - H₂ PROPELLANT SYSTEM

Li (s) - F₂ (ℓ) - H₂ (ℓ) H₂ : 25% BY WEIGHT, L_i/F : STOICHIOMETRIC
 P_C = 1000 PSIA (6.895 X 10⁶ N/m²) (A/A_{MIN})_{EXIT} = 200

NOTE: I _{SP VAC}	(EQUIL) = 545.4 SEC	} WITH CONDENSATION	} CONDENSATION SUPPRESSED
I _{SP VAC}	(FROZ) = 484.0 SEC		
I _{SP VAC}	(EQUIL) = 514.0 SEC	} WITH CONDENSATION	} CONDENSATION SUPPRESSED
I _{SP VAC}	(FROZ) = 481.5 SEC		

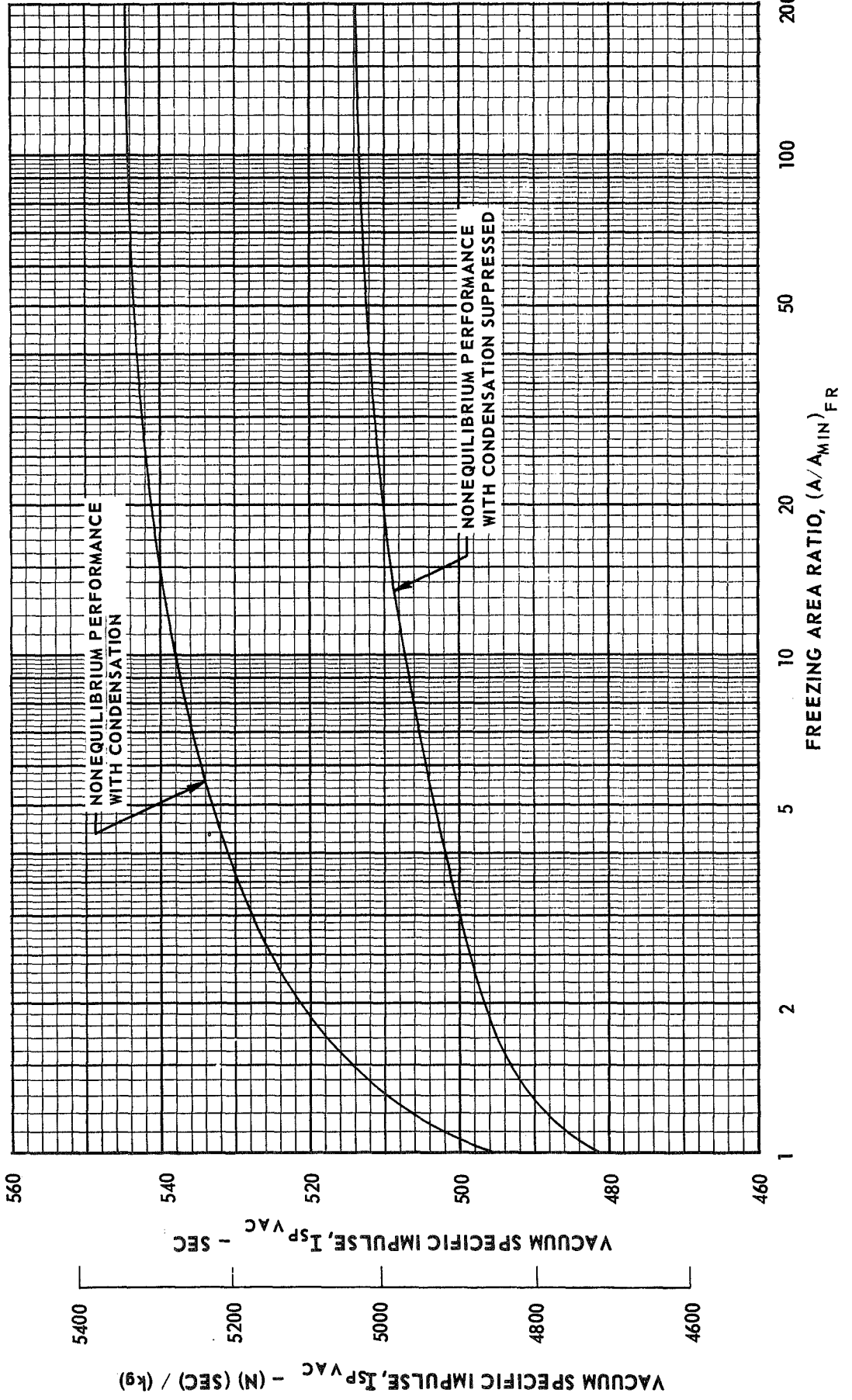


FIG. 43

EFFECT OF FREEZING AREA RATIO ON NONEQUILIBRIUM PERFORMANCE FOR Li-F₂-H₂ PROPELLANT SYSTEM

Li(l) - F₂(l) - H₂(g) H₂: 20% BY WEIGHT, L_i/F: STOICHIOMETRIC
 P_C = 500 PSIA (3.448 X 10⁶ N/m²) (A/A_{MIN})_{EXIT} = 60

NOTE: I _{SP VAC} (EQUIL) = 520.7 SEC	I _{SP VAC} (EQUIL) = 513.4 SEC	CONDENSATION SUPPRESSED
I _{SP VAC} (FROZ) = 465.5 SEC	I _{SP VAC} (FROZ) = 465.5 SEC	
		WITH CONDENSATION

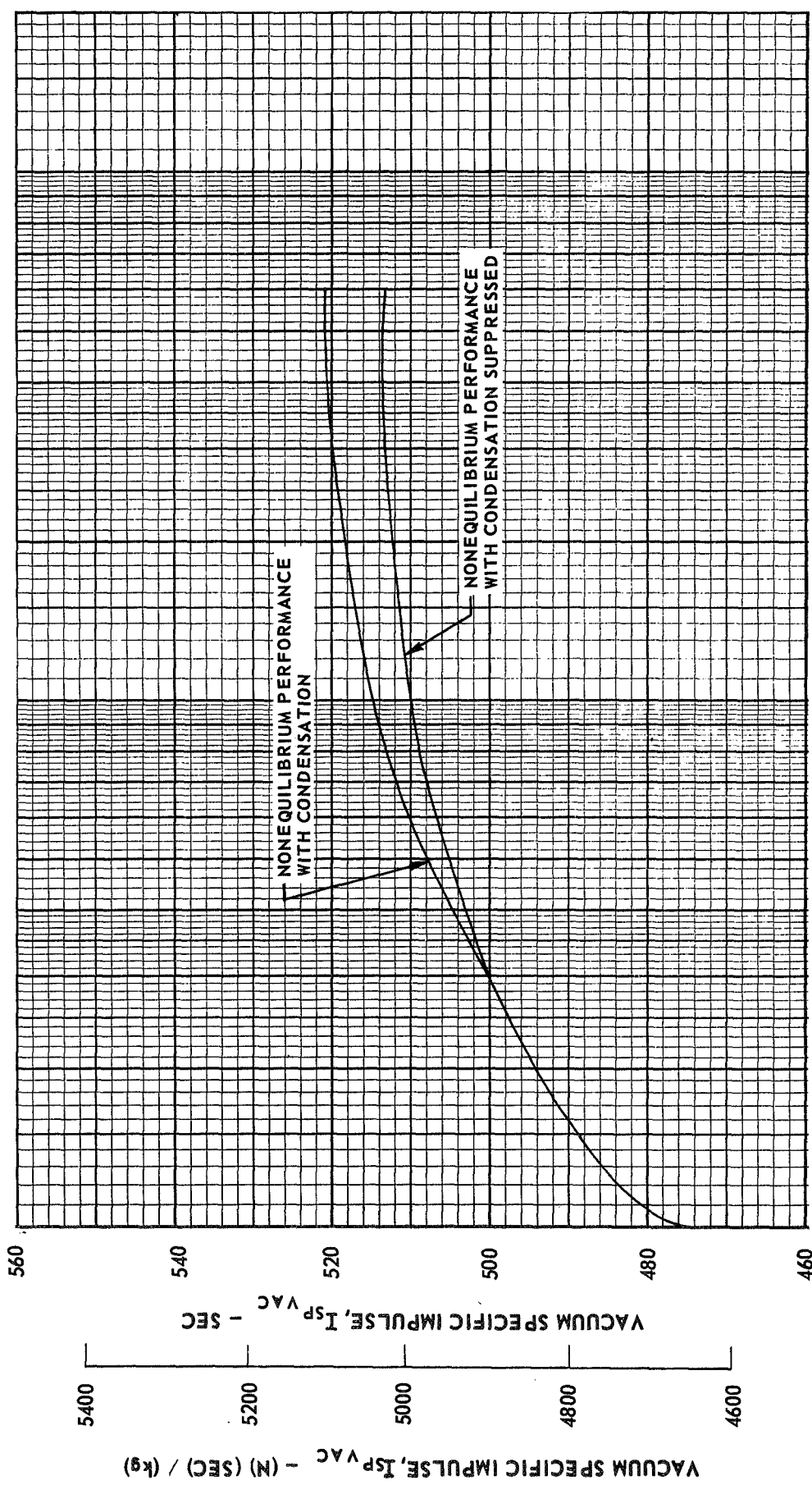


FIG. 44

EFFECT OF FREEZING AREA RATIO ON NONEQUILIBRIUM PERFORMANCE FOR Li-F₂-H₂ PROPELLANT SYSTEM

Li (ℓ) - F₂ (ℓ) - H₂ (g) H₂ : 30% BY WEIGHT, Li/F : STOICHIOMETRIC
 P_C = 500 PSIA (3.448 X 10⁶ N/m²) (A/A_{MIN})^{EXIT} = 60

NOTE: I_{SP VAC} (EQUIL) = 541.7 SEC WITH CONDENSATION I_{SP VAC} (EQUIL) = 515.2 SEC CONDENSATION SUPPRESSED
 I_{SP VAC} (FROZ) = 483.3 SEC WITH CONDENSATION I_{SP VAC} (FROZ) = 481.3 SEC CONDENSATION SUPPRESSED

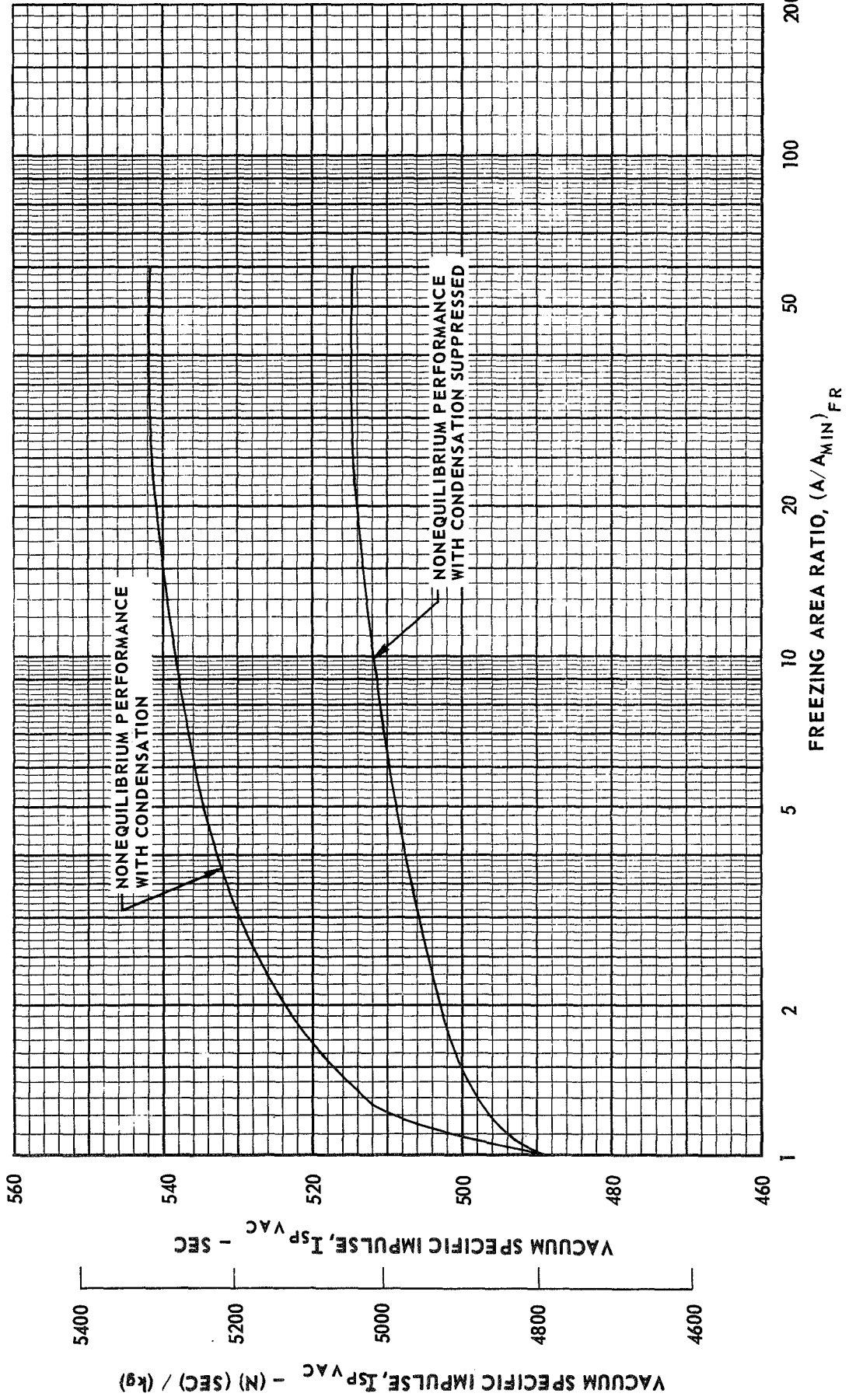


FIG. 45

EFFECT OF FREEZING AREA RATIO ON NONEQUILIBRIUM LOSS FOR Li - F₂ - H₂ PROPELLANT SYSTEM

Li (ℓ) - F₂ (ℓ) - H₂ (g) H₂: 20% BY WEIGHT, L/F: STOICHIOMETRIC

P_C = 500 PSIA (3.448 × 10⁶ N/m²) (A/A_{MIN})_{EXIT} = 60

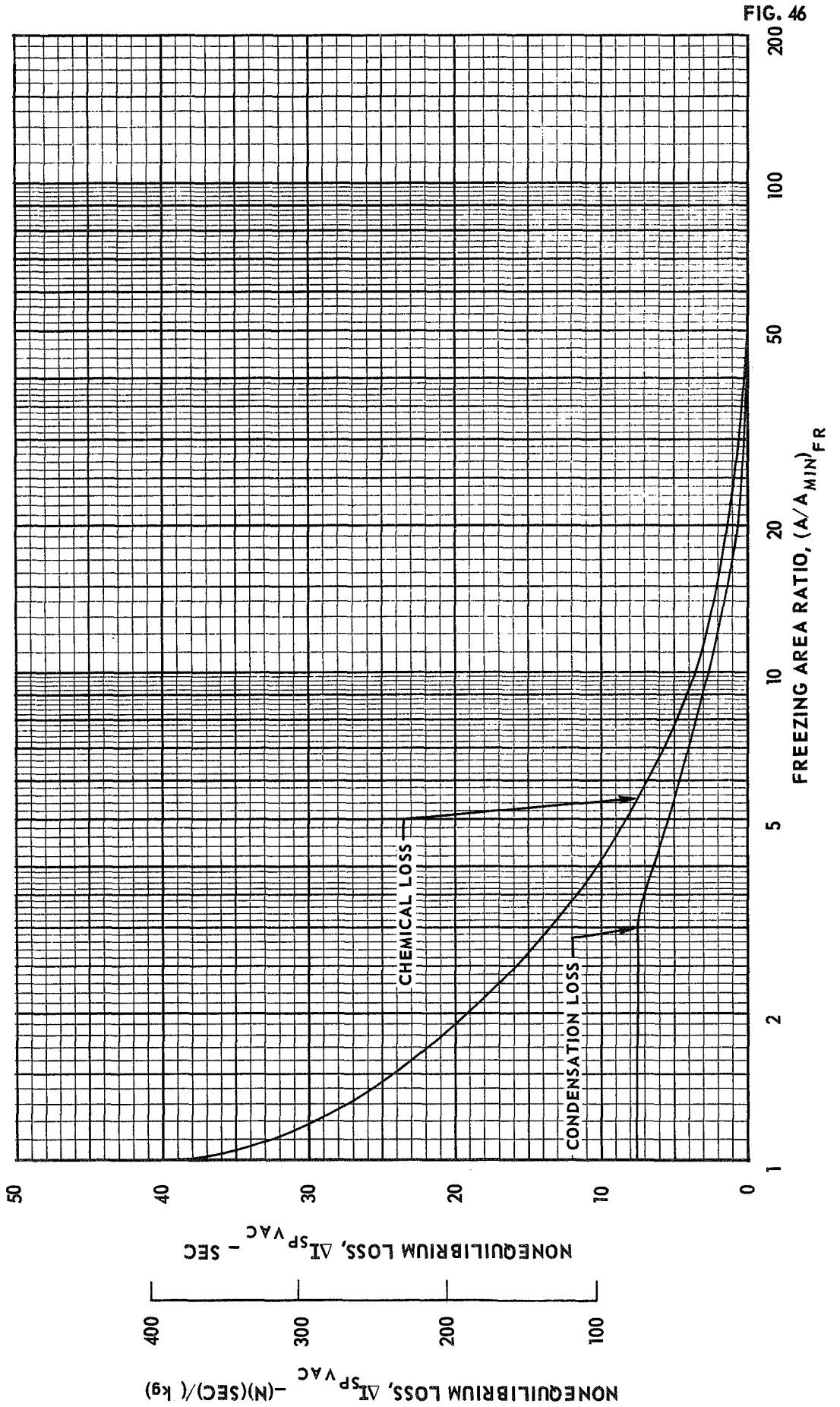


FIG. 46

EFFECT OF FREEZING AREA RATIO ON NONEQUILIBRIUM LOSS FOR Li - F₂-H₂ PROPELLANT SYSTEM

Li (ℓ) - F₂ (ℓ) - H₂ (g) H₂: 30% BY WEIGHT, Li/F: STOICHIOMETRIC

P_C = 500 PSIA (3.448 × 10⁶ N/m²) (A/A_{MIN})_{EXIT} = 60

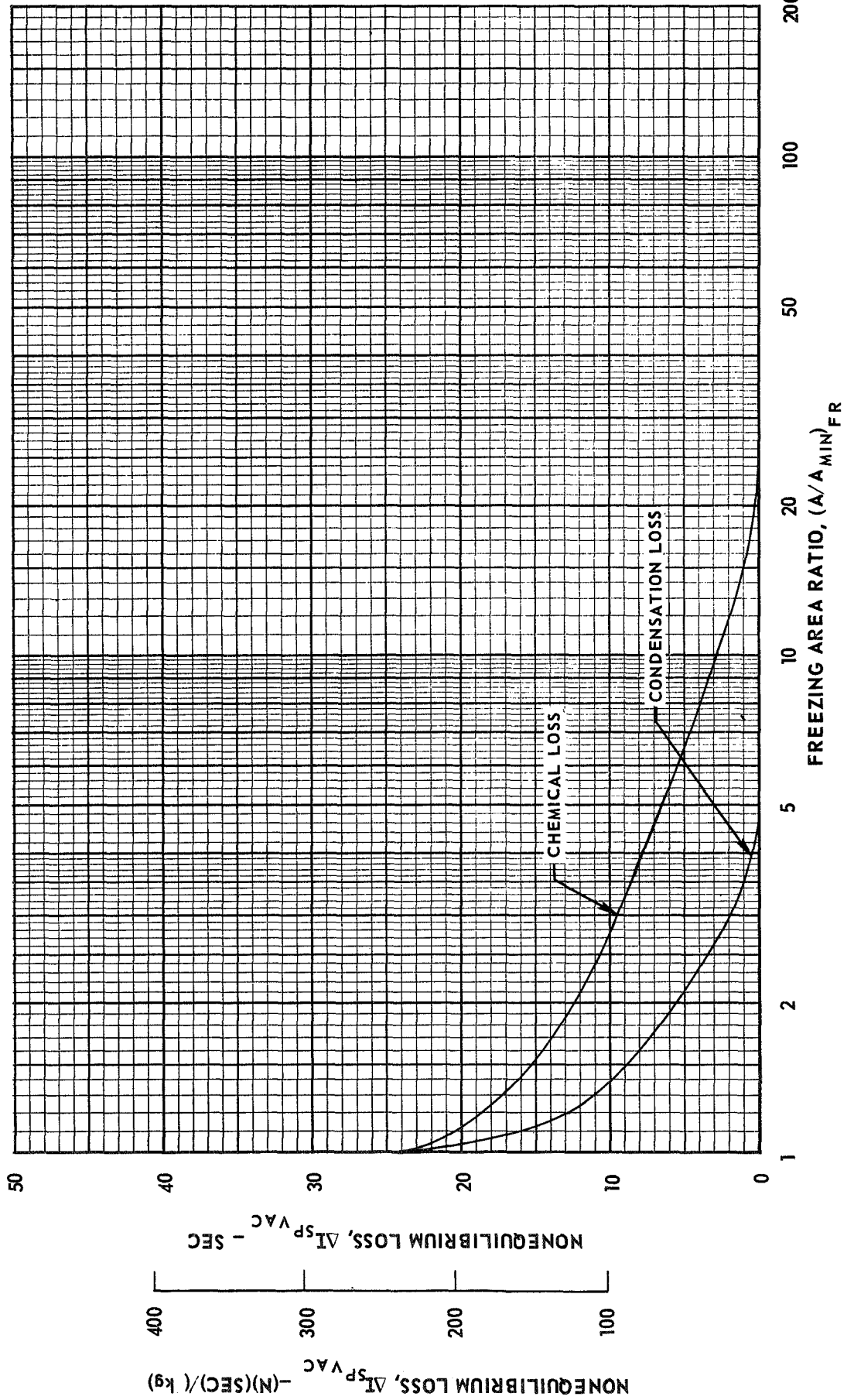


FIG. 47

EFFECT OF FREEZING AREA RATIO ON NONEQUILIBRIUM LOSS FOR Li - F₂ - H₂ PROPELLANT SYSTEM

Li (s) - F₂ (l) - H₂ (l) H₂: 25% BY WEIGHT, Li/F: STOICHIOMETRIC

P_C = 1000 PSIA (6.895 × 10⁶ N/m²) (A/A_{MIN})_{EXIT} = 60

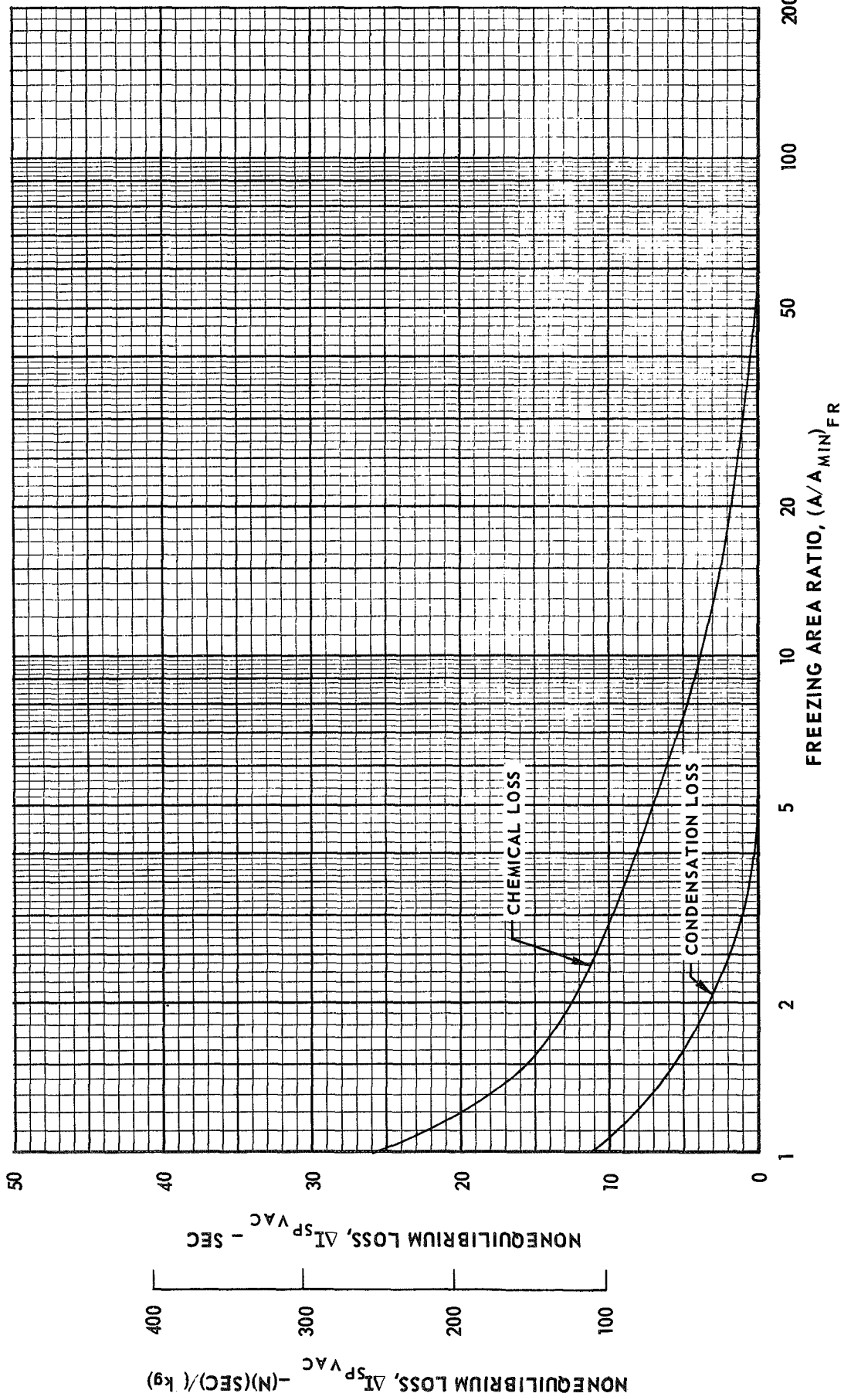


FIG. 48

EFFECT OF FREEZING AREA RATIO ON NONEQUILIBRIUM LOSS FOR Li - F₂ - H₂ PROPELLANT SYSTEM

Li(s) - F₂(g) - H₂(g) H₂: 25% BY WEIGHT, Li/F: STOICHIOMETRIC

P_C = 1000 PSIA (6.895 × 10⁶ N/m²) (A/A_{MIN})_{EXIT} = 200

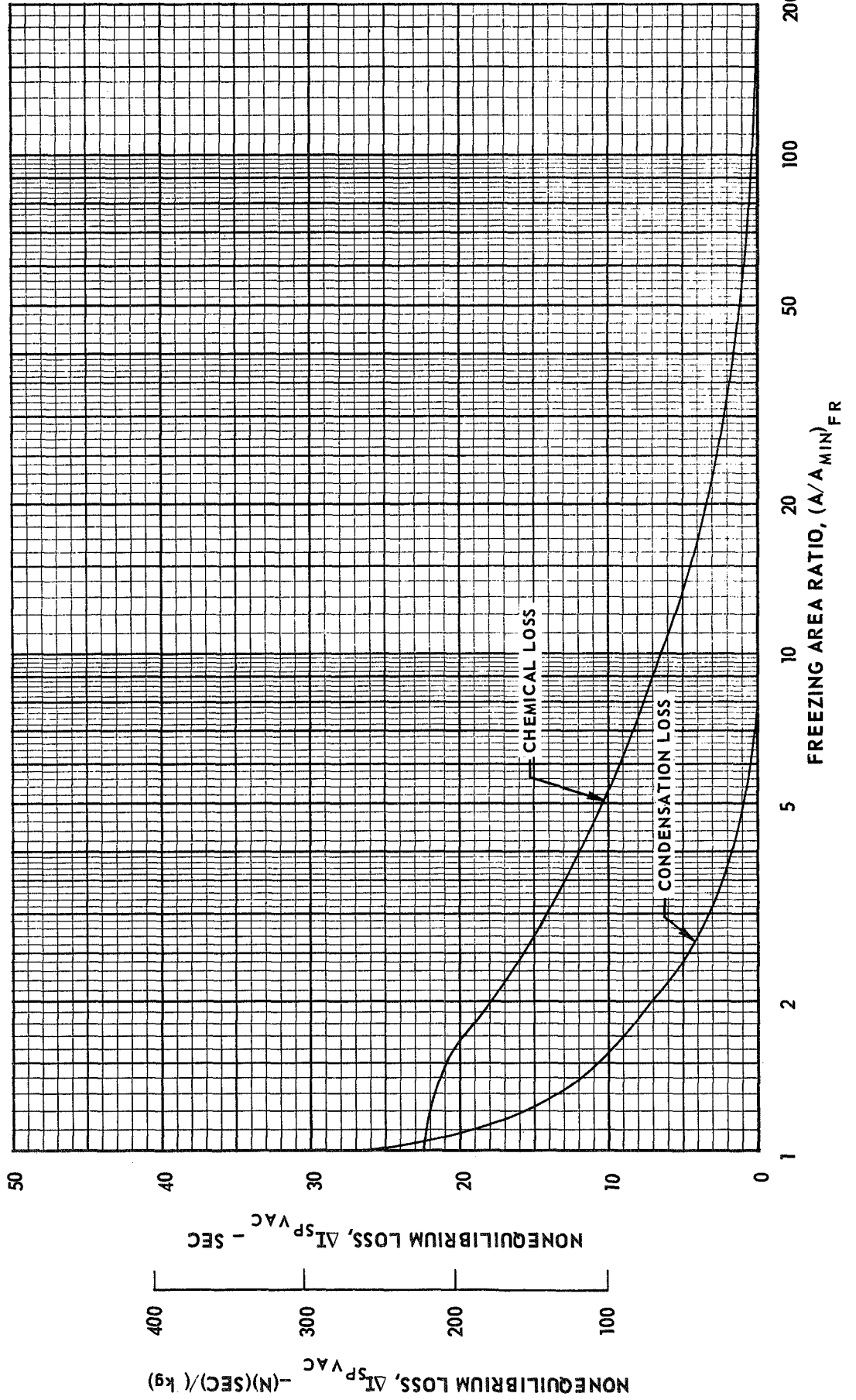


FIG. 49

EFFECT OF FREEZING AREA RATIO ON NONEQUILIBRIUM LOSS FOR Li - F₂ - H₂ PROPELLANT SYSTEM

Li (ℓ) - F₂ (ℓ) - H₂ (g) H₂: 20% BY WEIGHT, Li/F: STOICHIOMETRIC

P_C = 500 PSIA (3.448 × 10⁶ N/m²) (A/A_{MIN})_{EXIT} = 200

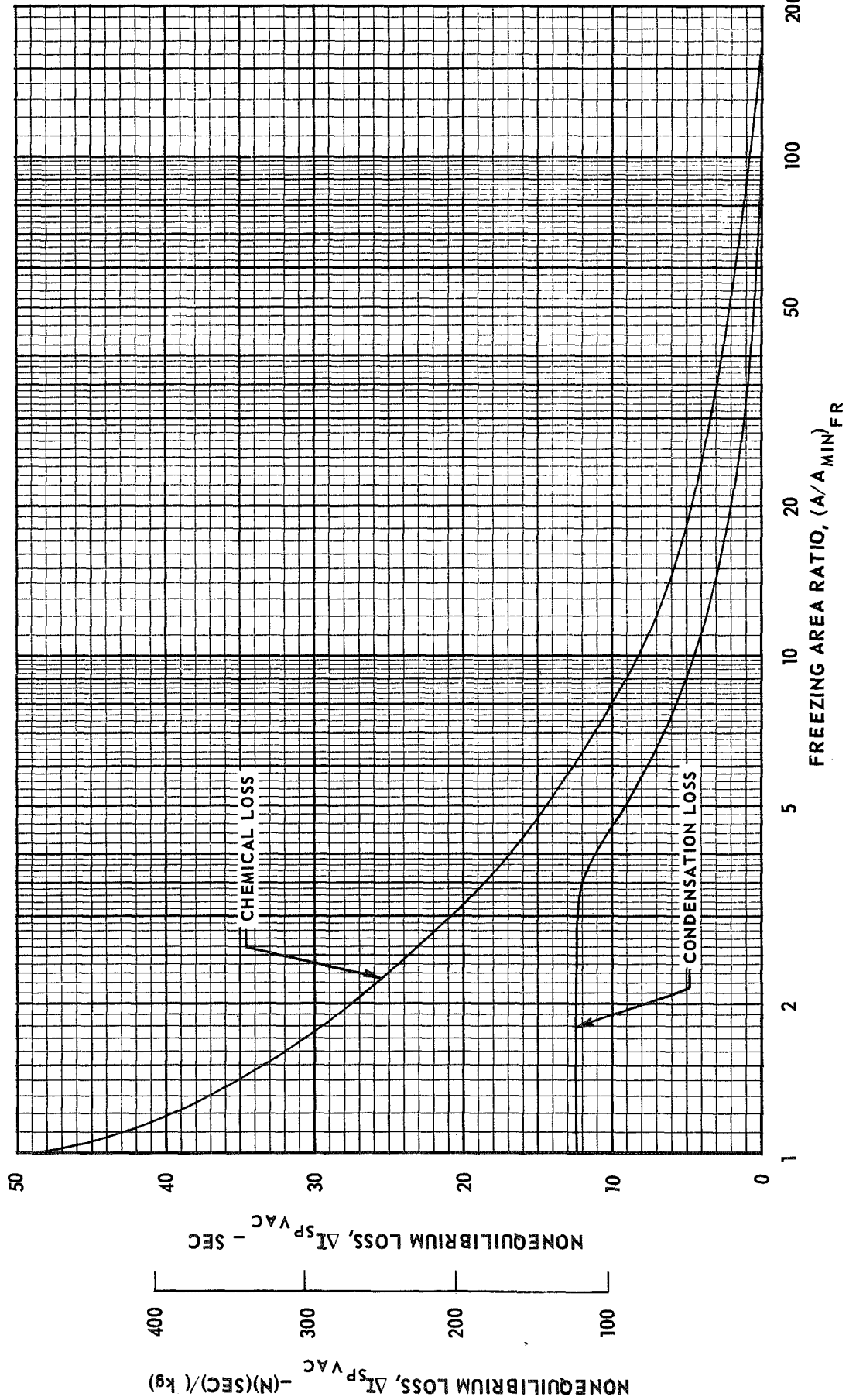


FIG. 50

EFFECT OF FREEZING AREA RATIO ON NONEQUILIBRIUM LOSS FOR Li - F₂ - H₂ PROPELLANT SYSTEM

Li(l) - F₂(l) - H₂(g) H₂: 25% BY WEIGHT, L/F: STOICHIOMETRIC

P_C = 500 PSIA (3.448 × 10⁶ N/m²) (A/A_{MIN})_{EXIT} = 200

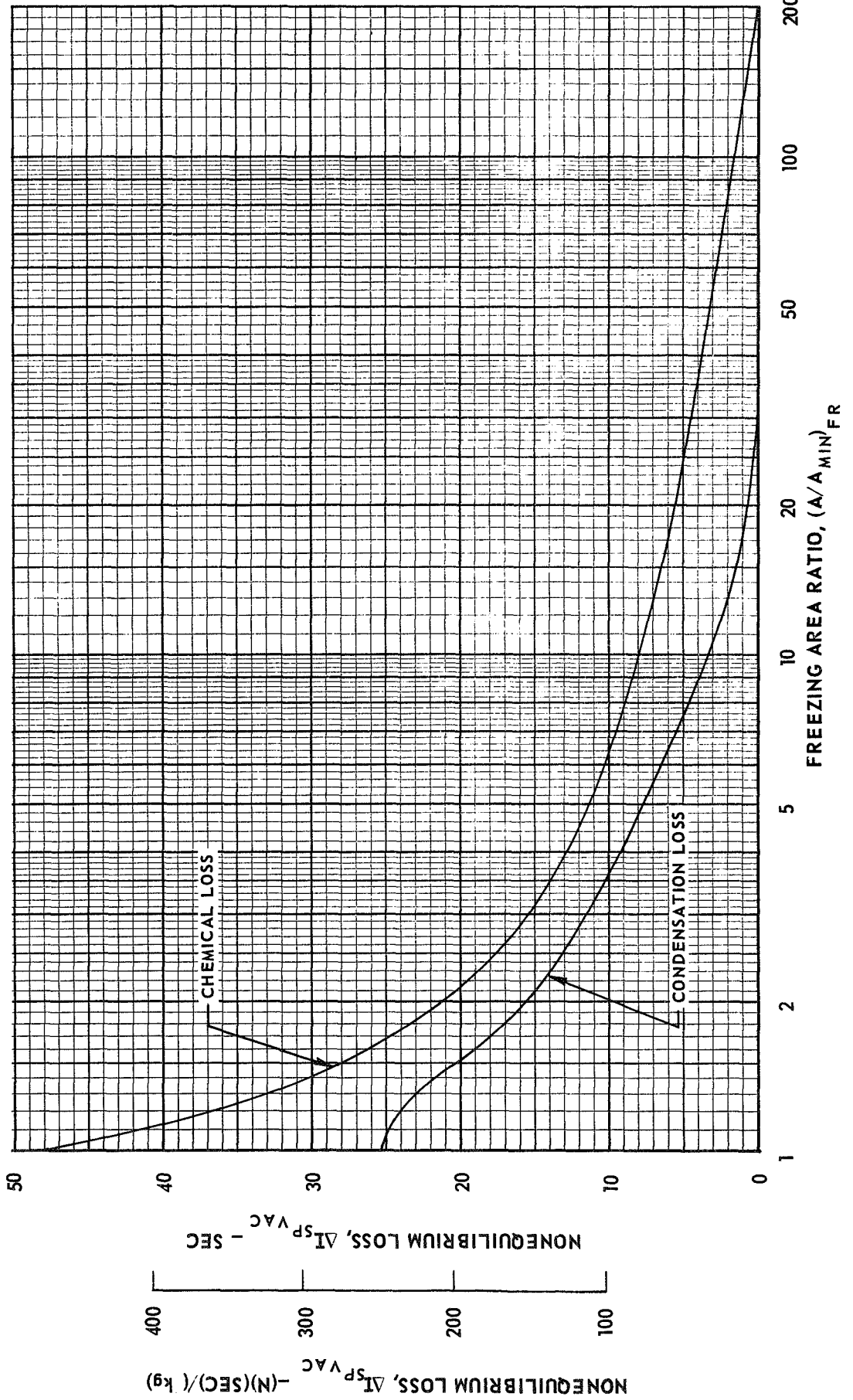


FIG. 51

EFFECT OF FREEZING AREA RATIO ON NONEQUILIBRIUM LOSS FOR Li-H₂ PROPELLANT SYSTEM

Li (ℓ) - F₂ (ℓ) - H₂ (g) H₂: 30% BY WEIGHT, Li/F: STOICHIOMETRIC

P_C = 500 PSIA (3.448 × 10⁶ N/m²) (A/A_{MIN})_{EXIT} = 200

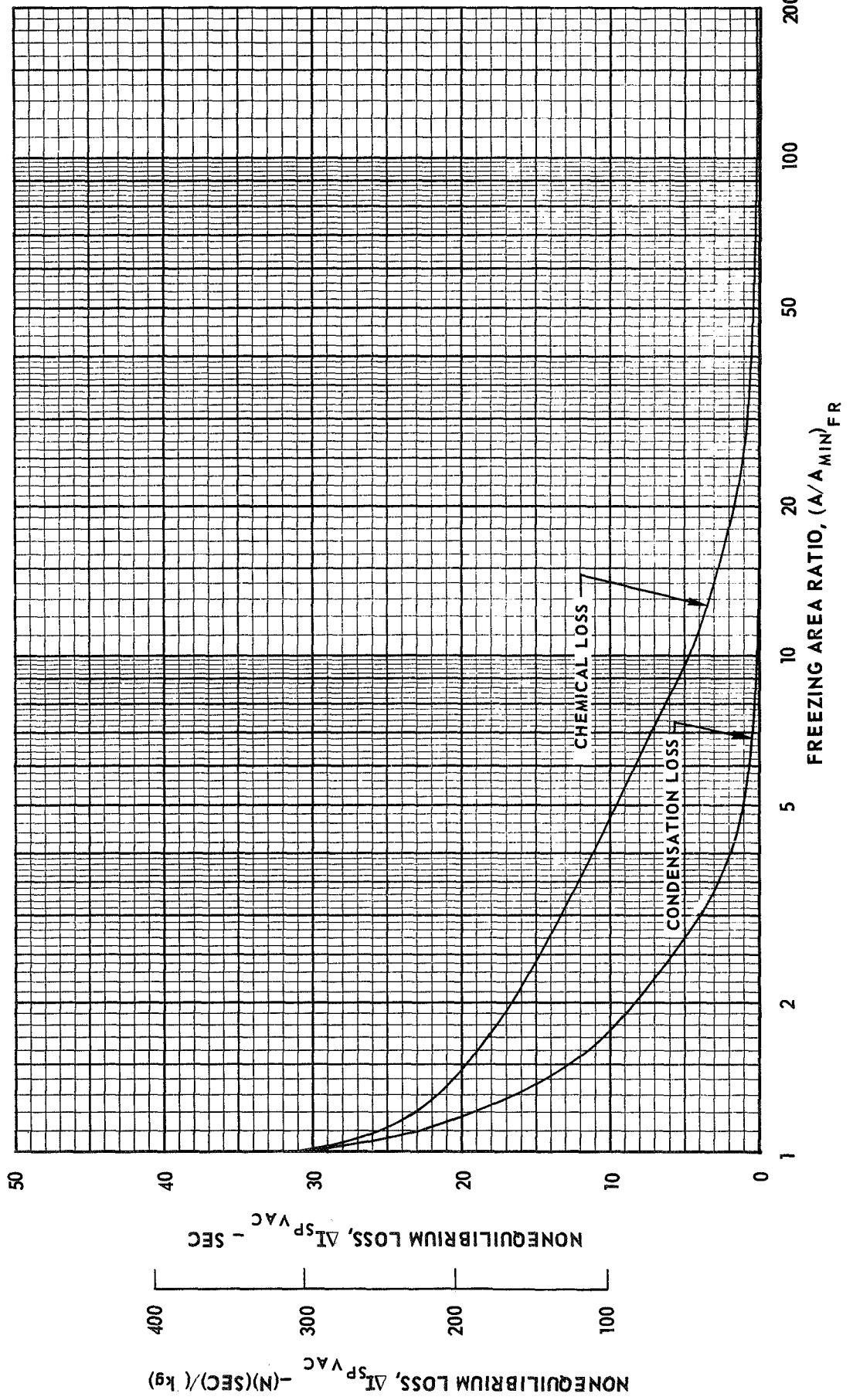
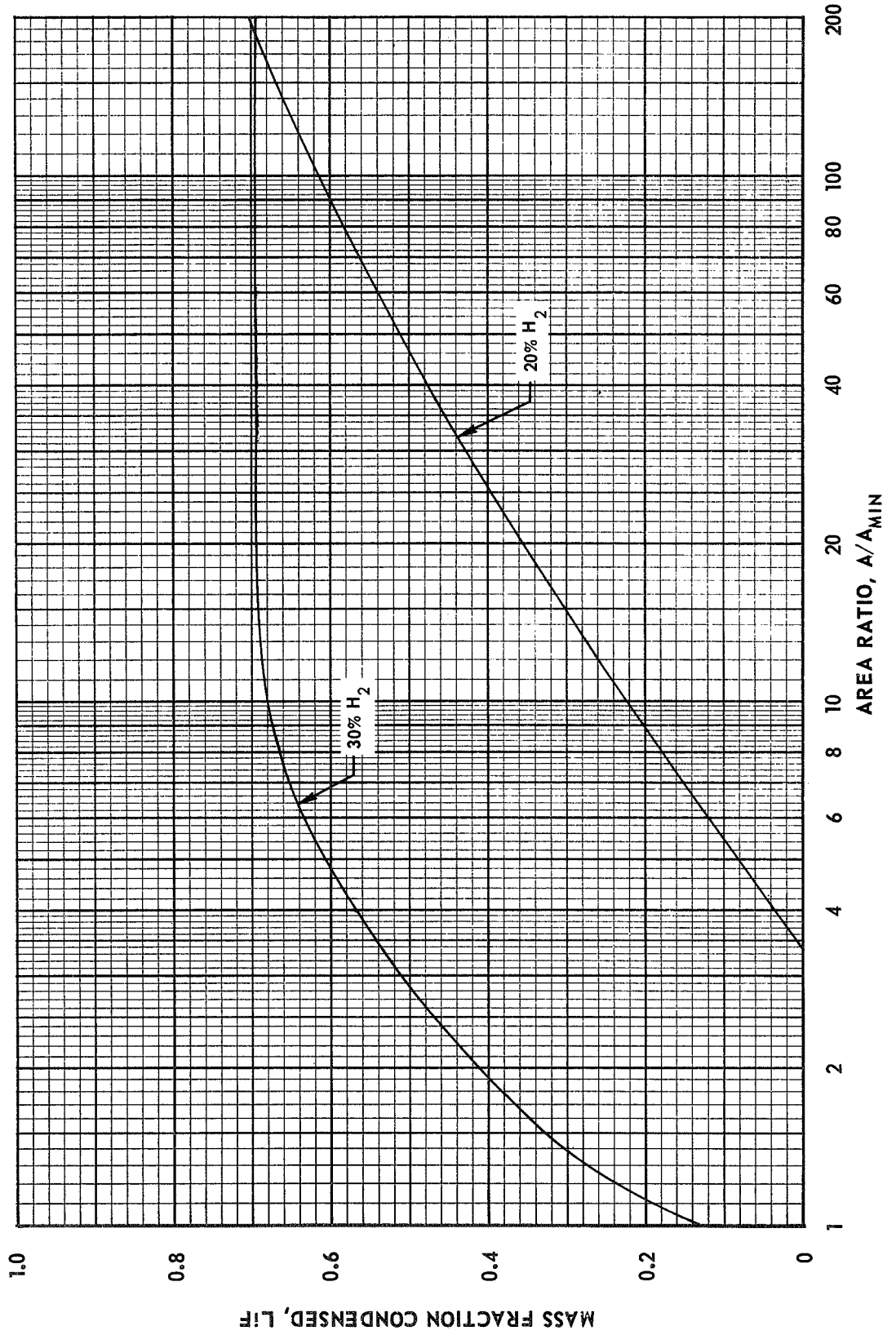


FIG. 52

EQUILIBRIUM MASS FRACTION OF CONDENSED LIF WITH AREA RATIO

$L_i(l) - F_2(l) - H_2(g)$ F/Li : STOICHIOMETRIC

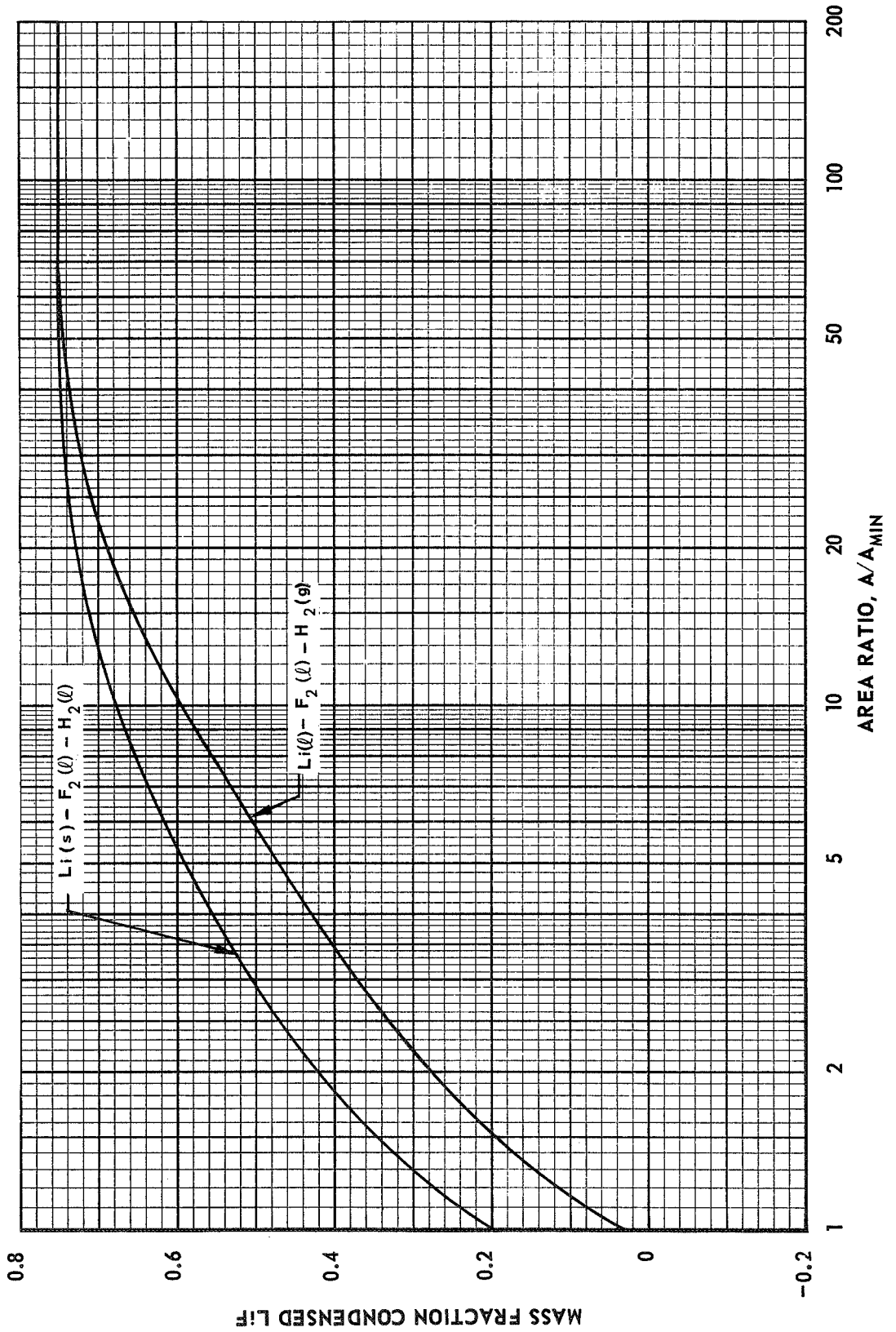
$P_C = 500$ PSIA (3.448×10^6 N/m²)



EQUILIBRIUM MASS FRACTION OF CONDENSED LIF WITH AREA RATIO

$H_2(l) - F_2(l) - Li(s) ; H_2(g) - F_2(l) - Li(l)$ $F/Li : \text{STOICHIOMETRIC}$

$P_C = 1000 \text{ PSIA} (6.895 \times 10^6 \text{ N/m}^2)$ $H_2 - 25\% \text{ BY WEIGHT}$



EFFECT OF ARBITRARY FREEZING AREA RATIO ON PARTICLE VELOCITY AND LAG LOSSES

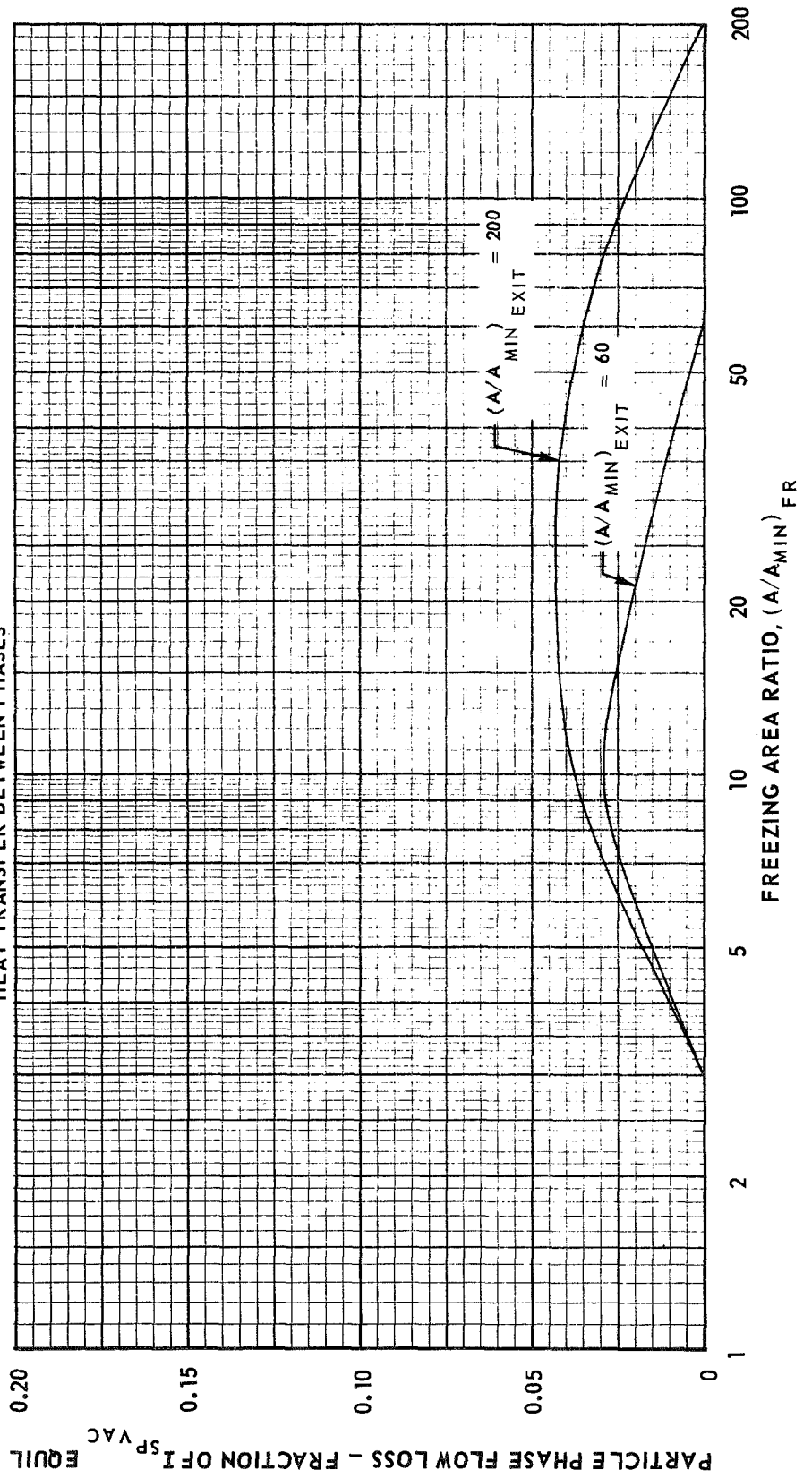
$$Li(l) - F_2(l) - H_2(g)$$

$$P_C = 500 \text{ PSIA } (3.448 \times 10^6 \text{ N/m}^2)$$

F_2/Li : STOICHIOMETRIC, H_2 : 30% BY WEIGHT

THRUST: 10,000 LBS ($4,448 \times 10^4 \text{ N}$) PARTICLE SIZE: 50 MICRONS

NOTE: ACTUAL LOSS IS NEGLIGIBLE FOR 50 MICRON PARTICLE CURVES SHOWN REPRESENT MAXIMUM POTENTIAL LOSS ASSUMING NO ACCELERATION OF PARTICLE AND NO HEAT TRANSFER BETWEEN PHASES



EFFECT OF ARBITRARY FREEZING AREA RATIO ON PARTICLE VELOCITY AND LAG LOSSES

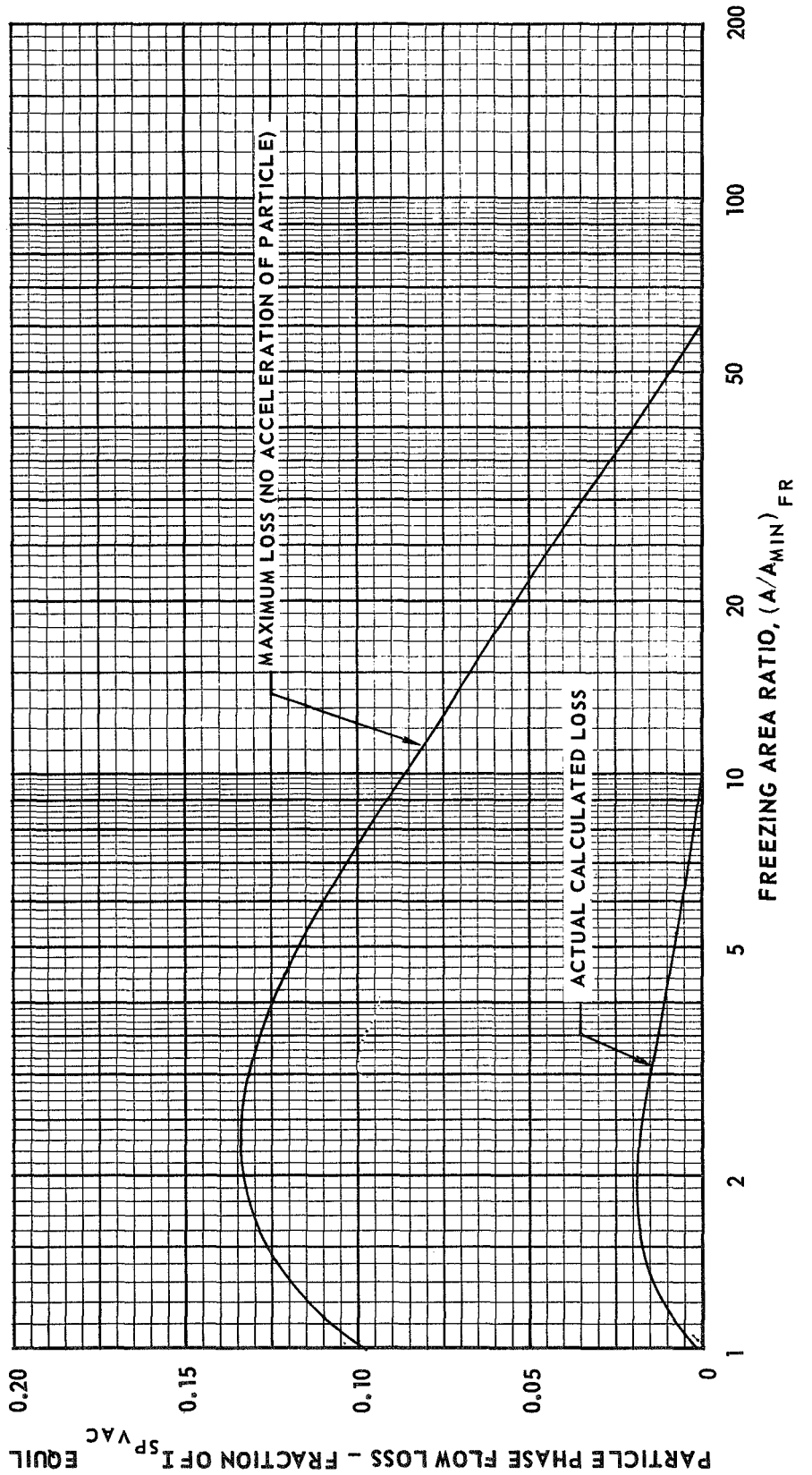
$$L_i(\ell) = F_2(\ell) - H_2(g)$$

$$P_C = 500 \text{ PSIA } (3.448 \times 10^6 \text{ N/m}^2) \quad (A/A_{\text{MIN}})_{\text{EXIT}} = 60$$

F₂/L_i: STOICHIOMETRIC, H₂: 30% BY WEIGHT

THRUST: 10,000 LBS (4.448 × 10⁴N) PARTICLE SIZE: 200 MICRONS

NOTE: ACTUAL LOSS IS NEGLIGIBLE FOR 50 MICRON PARTICLE



EFFECT OF ARBITRARY FREEZING AREA RATIO ON PARTICLE VELOCITY AND LAG LOSSES

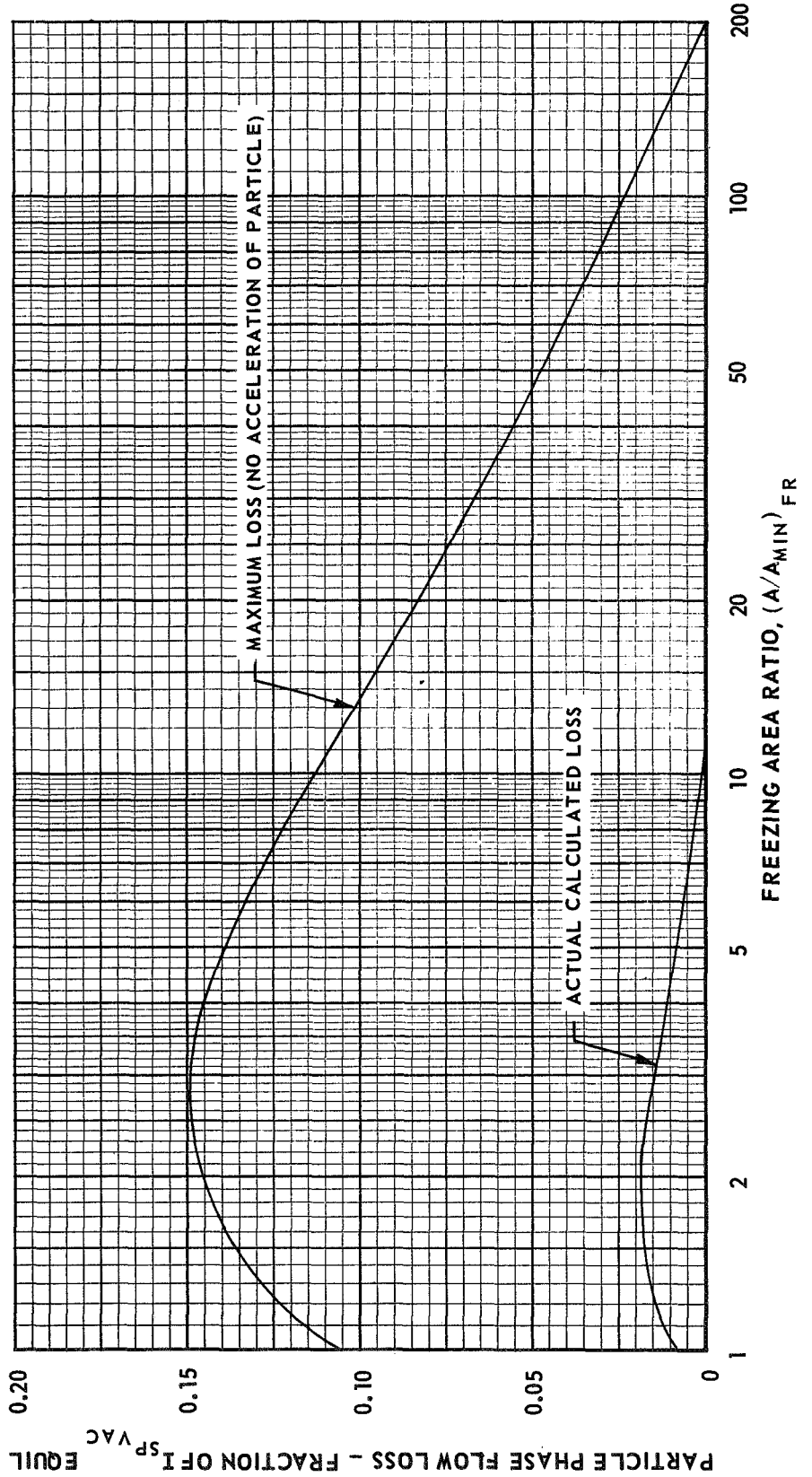
$$Li(\ell) - F_2(\ell) - H_2(g)$$

$$P_C = 500 \text{ PSIA } (3.448 \times 10^6 \text{ N/m}^2) \quad (A/A_{MIN})_{EXIT} = 200$$

$$F_2/Li: \text{ STOICHIOMETRIC, } H_2: 30\% \text{ BY WEIGHT}$$

THRUST: 10,000 LBS (4.448 x 10⁴ N) PARTICLE SIZE: 200 MICRONS

NOTE: ACTUAL LOSS IS NEGLIGIBLE FOR 50 MICRON PARTICLE



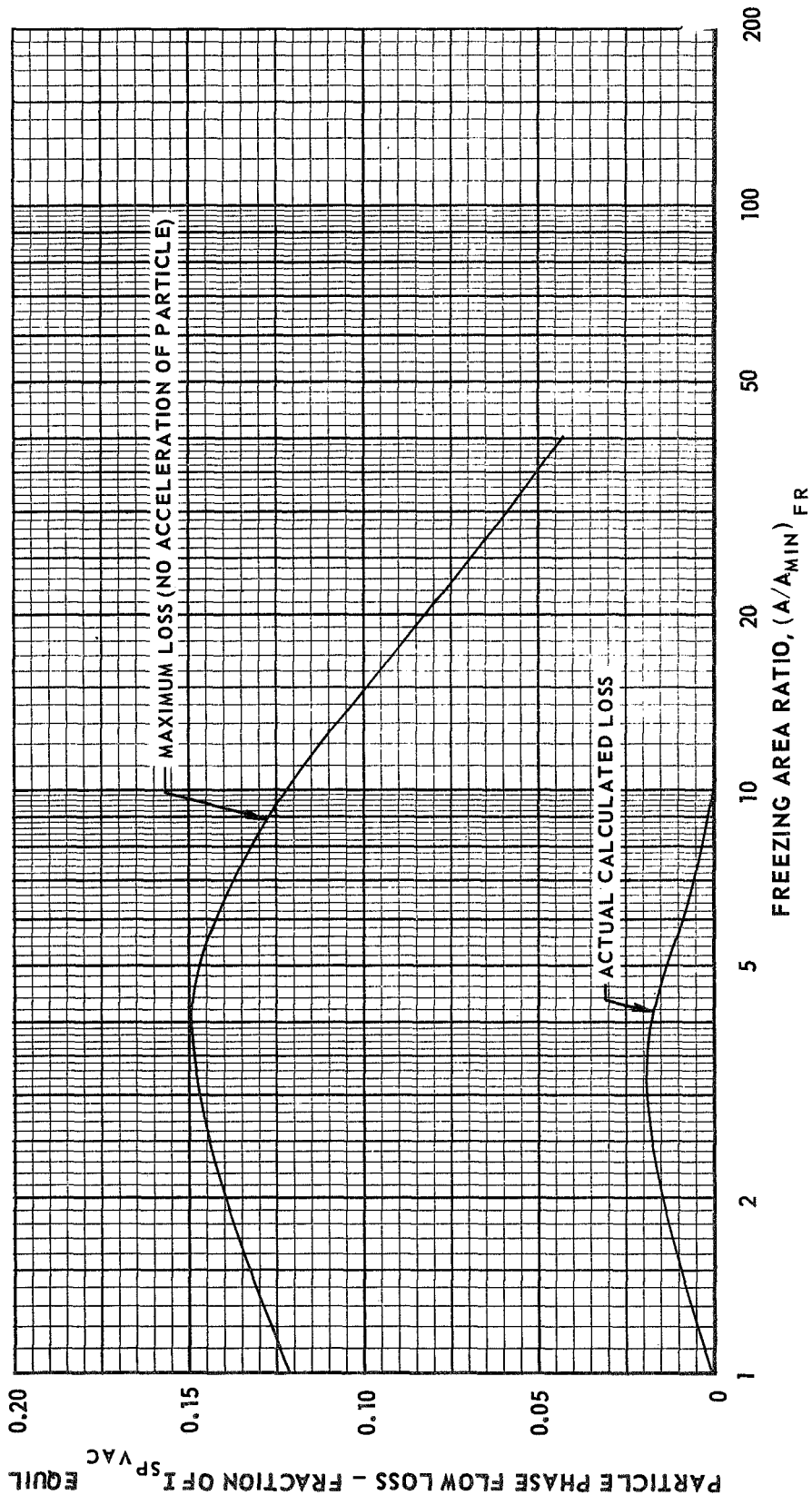
EFFECT OF ARBITRARY FREEZING AREA RATIO ON PARTICLE VELOCITY AND LAG LOSSES

$$L_i(\bar{s}) - F_2(\bar{L}) - H_2(\bar{L})$$

$$P_C = 1000 \text{ PSIA } (6.895 \times 10^6 \text{ N/m}^2) \quad (A/A_{\text{MIN}})_{\text{EXIT}} = 200$$

F_2/L_1 : STOICHIOMETRIC, H_2 : 25% BY WEIGHT

THRUST: 100 LBS ($4.448 \times 10^2 \text{ N}$) PARTICLE SIZE: 50 MICRONS



EFFECT OF ARBITRARY FREEZING AREA RATIO ON PARTICLE VELOCITY AND LAG LOSSES

$$Li(l) - F_2(l) - H_2(g)$$

$$P_C = 1000 \text{ PSIA } (6.895 \times 10^6 \text{ N/m}^2) \quad (A/A_{MIN})_{EXIT} = 200$$

F₂/Li: STOICHIOMETRIC, H₂: 25% BY WEIGHT

THRUST: 100 LBS (4.448 × 10²N) PARTICLE SIZE: 50 MICRONS

